universität wien

MASTERARBEIT

A brittle-ductile high- and low-angle fault system related to the Kea extensional detachment, Greece

Monika Rockenschaub Bakk.rer.nat.

Zur Erlangung des Akademischen Grades

Master of Science (MSc)

Wien, 2011

Studienkennzahl lt. Studienblatt:	A 066 815
Studienrichtung lt. Studienblatt:	Erdwissenschaften UG2002
Betreuerin/Betreuer:	Univ. Prof. Mag. Dr. Bernhard Grasemann

The following thesis was generated within the framework of the ACCEL-project.

Aegean **C**ore **C**omplexes along an **E**xtended **L**ithosphere
Western Cyclades, Greece

This project was funded by the Austrian Science Foundation (FWF) in 2005
P18823-N19
Principal investigator: B. Grasemann.

CONTENTS

ABSTRACT……6
ZUSAMMENFASSUNG……7
1. INTRODUCTION……8
2. METHODOLOGY……10
2.1. ArcGis and WinGeol……10
2.2. CL……10
2.3. SEM……10
2.4. Argon-argon dating……11
3. GEOLOGICAL FRAME – AEGEAN REGION……12
3.1. Geographic setting……12
3.2. The evolution of the Aegean region……13
Insertion: Subduction zones in relation to geodynamic processes……14
a) General overview……14
b) Subduction zones related extension……15
c) Low-angle normal faults (LANFs) and metamorphic core complexes (MCCs)……18
3.3. The Cycladic Blueschist Unit……23
3.4. Block rotations in the Aegean region……24
3.5. Recent and active extension……25
3.6. Comparison between Oligocene-Miocene and Recent extension……26
3.7. The Hellenic subduction zone……27
3.8. Kea……29
3.8.1. Previous geological researches……29
3.8.2. Lithological and structural overview……30
3.8.3. Research area……32
4. RESULTS……33
4. 1. Satellite image analyses……33
4. 2. Field data evaluation……34
4.2.1. Lithology and general structural inventory……34
4.2.2. Development of high- and low-angle fault systems……37
4.2.3. Displacement gradient and extension……42
4.2.3.1. Introduction……42
4.2.3.2. Displacement gradient……45
4.2.3.3. Extension……48
4.3. Micro-analyses……49
4.3.1. Mineral assemblage and deformation conditions……49
Insertion: Microstructures……50
4.3.2. Faults and fluids……55
Samples: KM3a……56
KM16……58
KM2b……61

KM6…………………………………………………………………… 68
KM7…………………………………………………………………….68
4.4. Age constraints……………………………………………………………………. 70
5. DISCUSSION…………………………………………………………………………71
6. CONCLUSION……………………………………………………………………...75
REFERENCES……………………………………………………………………………76
APPENDIX I – Mapping area with outcrop numbers……………………………………82
APPENDIX II – List of outcrop numbers for stereo plots…………………………….. 83
APPENDIX III – EDAX, chemical mappings…………………………………………84
ACKNOWLEDGEMENTS………………………………………………………………89

ABSTRACT

The island of Kea in the Western Cyclades, Greece, exposes a SW-directed extensional detachment, which formed as a result of Aegean back-arc extension since the Oligocene. Research on a conspicuous high-angled fault pattern and its relationship to the detachment were carried out in the western part of Kea (area north and south of Pisses), using remote sensing, field observations and thin-section analysis (optical microscope, CL, SEM).

The research area, which only exposes the footwall of the extensional shear zone, consists of greenschist-facies calcitic schists with interlayered blue-grey marbles. Deformation mechanisms in quartz and calcite constrain deformation conditions at around 300 to 450 °C.

Two dominant steeply-dipping conjugate high-angle fault systems cut the rocks: one NW-SE and one NE-SW striking. Remote sensing analysis of these lineaments, reflecting the high-angle fault systems, show that the angle between the two directions changes gradually from the north of Pisses southwards, from a rhombohedral (ca. 50°/130° angle between faults, with the acute angle facing westwards) to an orthogonal geometry.

Both fault systems show a coeval development but also a kinematic linkage to the SW-directed extensional detachment. Further, fault development of both the high- and low-angle fault systems show transitions from ductile to brittle deformation mechanisms, and vice-versa, and therefore indicate formation at the brittle-ductile transition zone. The conjugate pattern of the high-angle fault systems and the sub-vertical extension veins also present in the rocks indicate formation with an overall vertical maximum principal stress direction and suggest that the detachment was weak.

Measured offsets only reveal minor extension (~2–3 %) accommodated on this SW-directed high-angle faulting.

Faults reveal polyphase evolution characterised by numerous events of brittle deformation and cementation by SiO_2 and CO_3^{2-} fluids. The existence of veins which developed by cyclical variation in fluid pressures indicates that fault activity was strongly influenced by fluid pressures decreasing the critical level of failure.

Ar/Ar data from the Kea greenschists are considered to constrain the deformation age and indicate top-to-the SW extension occurred between 16 - 20 Ma.

ZUSAMMENFASSUNG

Kea (eine Insel der Westkykladen, Griechenland) repräsentiert eine nach SW gerichtete, flachwinkelige extensionelle Scherzone (Detachment), die sich durch die seit dem Oligozän im Ägäischen Raum herrschende Backarc-Extension gebildet hat. Untersuchungen an einem markanten, steilwinkeligen Störungsmuster und dessen Verhältnis zu dem Detachment wurden im Westen von Kea (nördlich und südlich von Pisses) mittels Fernerkundung, Geländearbeit und Dünnschliffanalysen (optische, CL- und SE-Mikroskopie) durchgeführt .

Im Untersuchungsgebiet tritt nur die Footwall der Scherzone zu Tage, die hauptsächlich aus kalkreichem Grünschiefer mit Lagen aus blau-grauem Marmor besteht. Deformationsmechanismen in Quarz und Kalzit lassen Deformationsbedingungen von ca. 300° - 450 °C erkennen.

Die Footwall ist von zwei konjugierten, steilwinkeligen (60-90°) Störungssystemen geprägt, die NW-SO bzw. NO-SW streichen. Auf Satellitenbildern konnten Lineamente identifiziert werden, die die steilwinkeligen Störungen repräsentieren. Eine Auswertung der Fernerkundungsdaten belegte eine Änderung der Orientierung der Störungssysteme zueinander: im Norden des Gebietes zeigen sie eine rhombische Geometrie (ca. 50°/130°, mit dem spitzen Winkel nach Westen zeigend), während sich diese nach Süden hin zu einer annähernd rechtwinkeligen Beziehung verändert.

Beide steilwinkeligen Störungssysteme lassen eine gleichzeitige Bildung erkennen, sind jedoch auch kinematisch mit der nach SW gerichteten Scherzone verbunden. Sowohl die steilwinkeligen Störungen als auch das flachwinkelige Detachment zeigen duktil-spröd bzw. spröd-duktile Verformungsmechanismen auf, welche auf eine Bildung im Bereich der spröd-duktilen Übergangszone zurückzuführen sind. Das konjugierte Muster der steilwinkeligen Störungen sowie subvertikale Extensionsspalten in der Footwall deuten auf ein generelles vertikales $\sigma 1$ hin und lassen vermuten, dass das Detachment schwach(?) war.

Kleine Versatzbeträge (bis max. 60 cm) an steilwinkeligen Störungen nehmen nur ein geringes Ausmaß (~2-3 %) an SW-gerichteter Extension auf.

Steilwinkelige Störungen zeigen eine polyphase Entwicklung auf, welche an zahlreichen spröden Events und mehrphasiger Fluidaktivität (SiO_2 und CO_3^{2}) zu erkennen ist. Durch Veins, die in ihrer Entwicklung zyklische Schwankungen des Fluiddrucks erkennen lassen, kann rückgeschlossen werden, dass die Bruchaktivität stark von Fluiddrücken beeinflusst und somit die Scherspannung herabgesetzt wurde.

Ar-Ar Altersdaten der Grünschiefer auf Kea belegen ein Alter der SW-gerichteten Extension zwischen ca. 20 und 16 Ma.

1. INTRODUCTION

The Aegean region, located in the south-west of Europe, represents part of the Alpine-Himalaya belt that formed as a result from the convergence between Africa and Eurasia since the Mesozoic. The Hellenic mountain belt, which forms the main part of the Aegean region, started to develop at the end of the Cretaceous with the successive subduction and accretion of Gondwana terranes and the intervening Mesozoic ocean basins to the southern margin of Eurasia (Jolivet et al. 2003; Van Hinsbergen et al. 2005a). The overall compressional regime of the fold-and-thrust belt, which mainly consists of Mesozoic and Cenozoic rocks (Jacobshagen 1986; Ring et al. 2010; Jolivet & Brun 2010), was superseded in the Oligocene by extension, due to the roll back of the African plate/slab (Gautier et al. 2001; Lister et al. 1984). The extension was accommodated on low angled detachment systems, forming the Aegean sea and characteristic of the Cyclades (Faure & Bonneau 1988; Buick 1991a, b; Faure et al. 1991; Gautier et al. 1993; Jolivet et al. 1994a, Iglseder et al. 2011).

The island of Kea, located 60 km southeast of Athens, at the NW end of the W Cyclades, is situated within this extensional environment and exposes a low-angle detachment. It comprises a greenschist facies metasedimentary footwall overlain by a low angle detachment that developed at PT-conditions passing from lower greenschist facies to brittle conditions (Iglseder et al. 2011). Essentially all kinematic indicators point to a top-to-SW to -SSW extension. The fault zone is only preserved in numerous relatively small klippen across Kea, which mainly exposes its footwall.

The island was also affected by two nearly orthogonal prominent high-angled conjugate fault systems. The area around Pisses (southwestern Kea), in particular, shows a high-angle fault symmetry that changes gradually from a rhombohedral to an orthogonal geometry and hence was chosen as the study area.

The goals of the following thesis are to investigate the development of the high-angle fault system exposed in the Pisses region of Kea, to analyse its geometry, explore its relationship to the major Kea low angle detachment and to discuss how the system relates to the tectonics of the Aegean region.

The following questions and theories are considered:

1) What is the geometry of the high-angle fault systems and how do they fit spatially into the regional tectonics – for example, into the arcuate Hellenic trench?
2) Is the high-angle faulting generally related to the SSW-directed low-angle extensional event or does it represent a later overprint by another kinematic event, such as, for example, the Corinth rift ?

3) If a relationship between the high- and low-angle fault systems can be observed, which assumptions can be made in terms of the mechanisms responsible for the development of both fault systems? Two theories are discussed:

   a) The LANFs initiated as high-angle structures that rotated from steep to gentle dips during extension (Buck 1988).

   b) The high-angle faults developed with a primary steep dip and interacted with the LANFs during the late brittle stages of extension (Mehl et al. 2005).

4) Can any fluid interaction be observed and what conclusions can be drawn concerning the development of the high-angle fault system?

2. METHODOLOGY

2.1. ArcGis and WinGeol

The ArcGIS software was used to trace lineaments on QuickBird satellite images. The resolution of these images is 64 cm in grey-scale (panchromatic) and 1.2 m in colour (multiband). Two shape files (one with the coast line of Pisses and one with the lineaments) were loaded into the WinGeol software. An even grid was superimposed on the second layer where lineaments have been evaluated and plotted as rose-diagrams. The size of the rose-diagrams refers to the number of lineaments. More details on www.TerraMath.com.

The lithologies and the deformation conditions were determined from field studies in combination with standard thin-section-microscopy. Microstructures and cements in fault zones were further analysed using microscope-based cathodoluminescence (CL) and a scanning electron microscope (SEM):

2.2. Cathodoluminescence (CL) microscopy

CL is caused by the emission of light from material as a result of it being irradiated with electrons. The technique is used for imaging spatial variations in the trace element composition of minerals such as calcite, quartz and feldspar. Geological (non-conducting) sample materials must be polished and carbon-coated.

For the present study, the different generations of cements were distinguished using a LUMIC HC5-LM hot-cathodoluminescence microscope at the Department of Lithospheric Research, University of Vienna. Images were taken with a 14 kV accelerating voltage and a 0.15 mA beam current, with an exposition time of 951 ms. To improve the image quality, ultra-thin (<20 µm) microscope thin-sections were used.

2.3. SEM

The SEM creates an image of the sample surface by scanning it with a high-energy beam of electrons in a raster-scan pattern. The sample's surface topography can either be studies with SE (secondary electrons) or compositional variations can be observed (BSE – back-scattered electrons). The signals result from the interaction of the electron beam with atoms at or near the surface of the sample.

Secondary electron imaging (SEI) results from inelastic scattering of electrons in orbitals around the atomic nucleii due to interaction with the electron beam. This produces very high-resolution images of the sample surface, revealing details down to about 1 to 5 nm in size. Non-conducting geological specimens must be coated with a conductor, typically carbon.

Back-scattered electrons (BSE) are electrons that have been reflected or back-scattered from the sample by elastic scattering. BSE is often used in analytical SEM together with the spectra made from the characteristic x-rays (EDX – energy dispersive X-ray spectroscopy). As the intensity of the BSE signal is strongly related to the atomic number of the specimen, BSE images provide important detailed information about the distribution of different elements, and thus different minerals, in the sample. BSE imaging requires that the surfaces be polished and coated with carbon.

To investigate the chemical composition of very fine brecciated material (fault gauge) within samples an FEI Inspect^{TM} S50 scanning electron microscope with a BSE detector was used. The high energy electron beam was typically operated at 10-15 KV.

2.4. Argon-argon dating

Argon-argon (or ^{40}Ar/^{39}Ar) dating is a radiometric method that uses the decay of ^{40}K* (* radioactive) to ^{40}Ar to determine the age at which igneous and metamorphic minerals (and thus rocks) cooled through the closure temperature, at which the diffusion of Ar out of the system effectively stops. For white micas, this temperature is ca. 350-400 °C (Harrison et al. 2009; McDougall and Harrison 1999). Samples are irradiated with neutrons in a nuclear reactor, where some of the ^{39}K (present as a known fraction of the total K in the rock) is converted to ^{39}Ar*. The ratio of the radiogenic daughter product, ^{40}Ar to ^{39}Ar* is then measured in a mass spectrometer by heating the sample at distinct, increasing temperature intervals. Plotting the ^{40}Ar/^{39}Ar*-rates against temperature, the sample should show a plateau at a high temperature range where the release of ^{40}Ar/^{39}Ar* is constant and a disruption of the K/Ar system can be excluded. The ^{40}Ar/^{39}Ar* ratios at the plateau are used for the age calculations.

For the present study, two samples were crushed and the white micas were separated by a combination of mechanical methods and magnetic separation, at the University of Vienna. The isotopic analyses were done by Prof. D. Schneider (University of Ottawa). Pure white mica separates (size fractions of 150-200 µm) were irradiated at the 1 MW TRIGA Reactor at the USGS Denver, CO. Isotopic analyses were conducted at New Mexico Institute of Mining and Technology Geochronology Laboratory, Socorro. More details in Schneider et al., 2011.

3. GEOLOGICAL FRAME – AEGEAN REGION

3.1. Geographic setting

Geologically, the Aegean region lies in south-eastern Europe, comprising the Aegean Sea and the surrounding Rhodopes (southern Bulgaria and Greece) in the north, the Hellenides (Greece) in the northwest, west and south, and the Menderes Massif (Turkey) in the east. Kea, an island of the Western Cyclades (Greece), is a part of the Hellenides.

Fig. 1: Geographic overview of the Aegean region and the location of Kea.

3.2. The evolution of the Aegean region

The Aegean region represents part of the Alpine-Himalaya orogenic belt, stretching from the Pyrenees to parts of the Indonesian archipelago, that started to form at the end of the Cretaceous as the Tethyan ocean began to close.

The Hellenides, which make up the largest part of the Aegean region, are a fold and thrust belt that formed over several tectonic cycles since the Jurassic, with the main orogenic events in Paleogene and Neogene times. The orogen consists of sedimentary and magmatic rocks with mainly Mesozoic and Cenozoic ages. The polyphase metamorphic overprints, due to subduction and subduction related magmatism, characterise the mineralogical-petrological composition of the Hellenides (Jacobshagen 1996; Jolivet & Brun 2010; Ring et al. 2010). On the mainland of Greece, the Hellenide nappe pile is well preserved whereas in the Aegean sea it has been subjected to extensional tectonics since the Oligocene and is only sporadically exposed on relatively small islands (Gautier et al. 2001; Lister et al., 1984).

Paleogeographic reconstructions of the Mesozoic reveal continental fragments that rifted off from the northern margin of Gondwana in the late Paleozoic. Ocean basins (Pindos, Meliata and Vardar, fig. 2) started to form in the late Permian and Triassic, from which some ophiolites, now found throughout the Hellenides, were derived (Jacobshagen 1986).

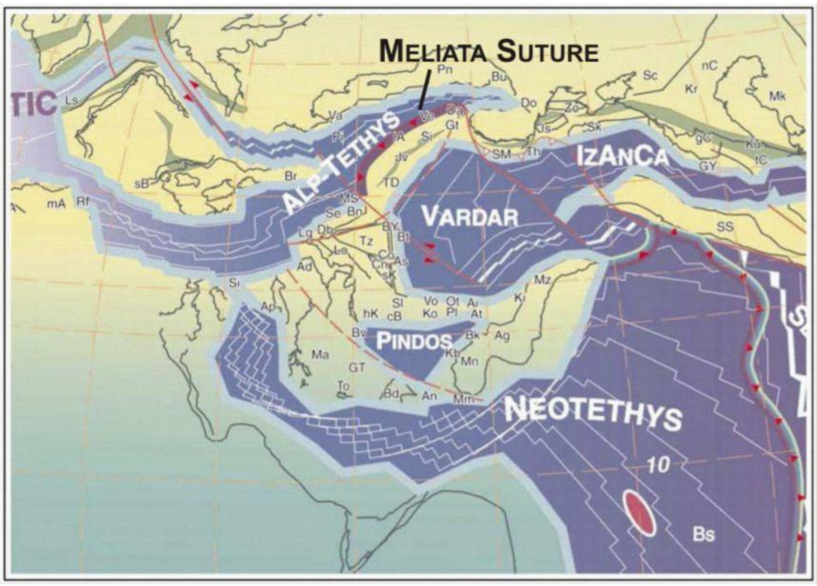

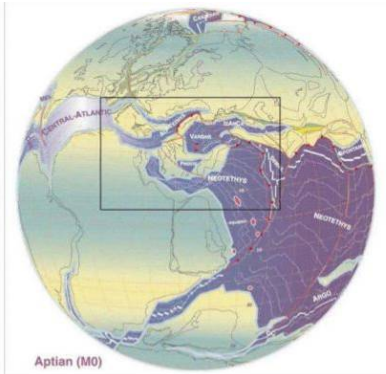

Fig. 2: Paleogeography from lower Cretaceous (Aptian); modified after Stampfli (2002)

Short description of the Tethyan ocean basins:

In the Pindos zone, sea-floor spreading was initiated in the Early Triassic whilst in the Meliata zone it culminated in Middle Triassic (Ladinian) and was subducted by the end of the Jurassic. The Vardar zone started to form in the early Jurassic and began its subduction history in latest Jurassic times. In the final step, the Pindos ocean was subducted in the late Jurassic and early Paleogene (Channell and Kozur, 1997).

The paleographic domains that now form the Hellenides were subducted successively and partly accreted to the southern margin of Eurasia due to the convergence between Africa and

Eurasia. However, the main evolution that formed the Hellenides and shaped the Aegean region started at the end of the Cretaceous with the closure along the Vardar suture zone (Jolivet & Brun 2010).

Geodynamic processes such as oceanic and continental subduction, mountain building, high-pressure metamorphism, arc magmatism, backarc extension and the development of metamorphic core complexes are only a few examples for this complicated evolution. Before explaining the geological evolution of the Aegean, a short introduction of subduction zones and their related geological processes in general, and the parameters determining whether contraction and/or extension occurs within a subduction zone, is given below.

Insertion: Subduction zones in relation to geodynamic processes

a) General overview

Subduction occurs at convergent plate boundaries, with one tectonic plate (lithosphere) moving under another tectonic plate. Both oceanic and continental subduction lead to crustal deformation, with folding, thrusting (forming nappes) and, due to isostatic compensation of the crustal thickening, the formation of an elevated topography – mountain building.

Convergence is driven by large-scale convection due to heat-differences in the asthenosphere and lithosphere. Denser lithosphere sinks into the lighter lithosphere at an angle of approximately 25° to 45° to the surface of the Earth. At a depth of ca. 80-120 km, high-pressure conditions convert the subducting basalts and sediments into (ultra-)high pressure metamorphic rocks, such as eclogites and blueschists. During this transition, hydrous materials break down, producing large quantities of water, which at such great pressure and temperature exists as a supercritical fluid. These fluids rise into the overlying mantle where they lower the pressure in the mantle to the point of partial melting, generating magma. Due to the lower density of the magmas (which are basaltic in composition) compared to the surrounding mantle, they rise, ultimately reaching the Earth's surface, resulting in a volcanic eruption, forming long chains of volcanoes – volcanic arcs. Arc magmatism occurs 100-200 km away from the subduction trench and around 100 km above the subduction slab (Stern 2002).

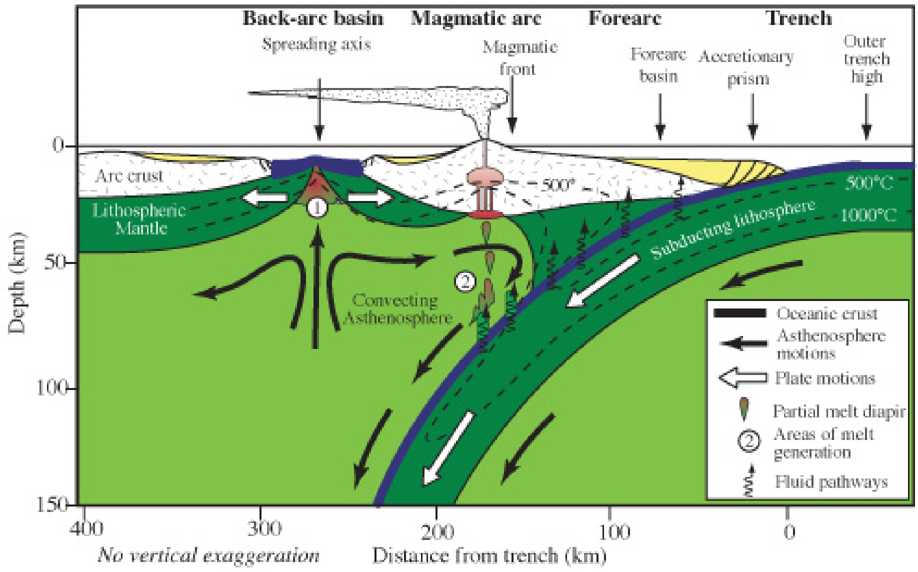

Fig. 3: Cross-section through a subduction zone (Stern 2002).

b) Subduction zones related extension

During ongoing convergence, subduction zones change their position with respect to the overriding plate. They either advance toward the overriding plate or retreat seaward (Chase 1979, 1980; Uyeda 1982; Royden & Husson 2006). A retreat or "roll-back" of a subducting slab commonly arises when the rate of the overriding plate's convergence with the trench is smaller than the subduction rate of the underriding plate (Dewey & Bird 1970; Royden 1993). In that case, this causes large-scale horizontal extension – back arc extension - in the overriding plate (Garfunkel et al. 1986; Lonergan & White 1997).
Further regional extension can also occur in a general shortening regime above so called extrusion wedges (fig. 4). During plate convergence in a subduction zone, an extruding slice can develop bounded by a basal thrust and a normal-sense shear zone or fault at its top (Vannay et al. 2004).

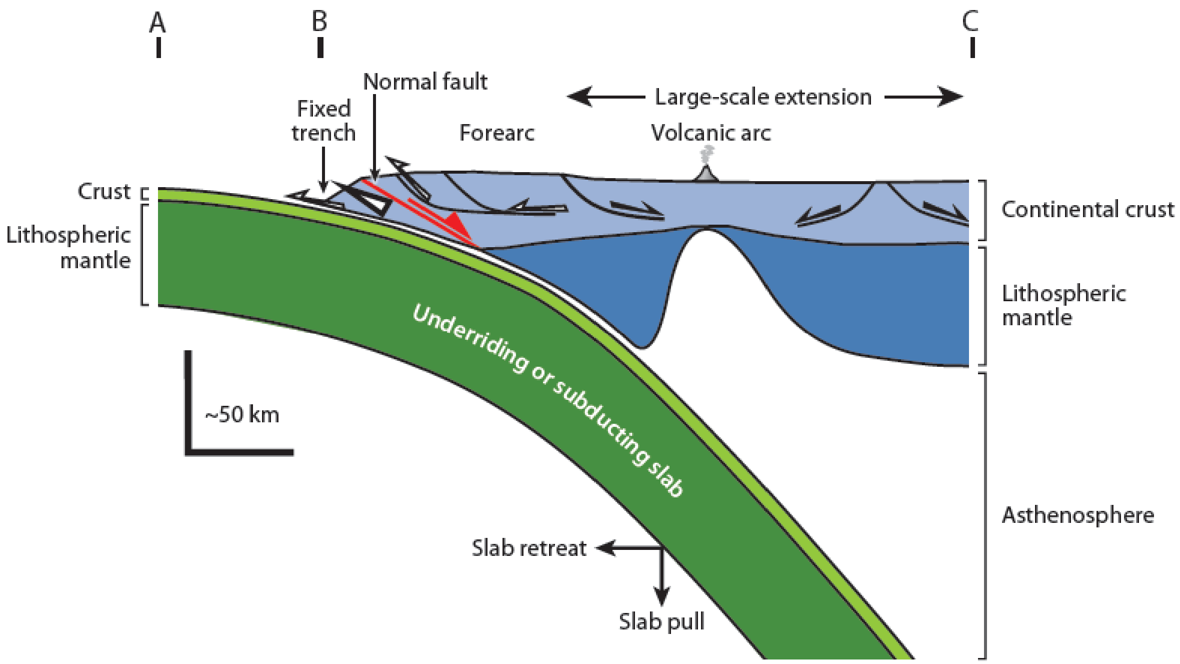

Fig. 4: Illustration of a subduction zone (Ring et al 2010). The white triangle marks an extrusions wedge below a normal fault.

Commonly accepted parameters that may induce rollback are (1) a slow-down of the convergence velocity of the subducting plate (Jolivet & Faccenna 2000), (2) the negative buoyancy of the subducting slab (Royden 1993), and (c) an increase in slab length to ~150 km. In particular, when heavy slabs have been subducted to depths exceeding ~80 km and their lengths are >~150 km, rollback may become important (Schellart 2005).

Another feature that plays a decisive role in the velocity of a roll back is the 660-km discontinuity in the asthenosphere. This boundary separates the upper and lower asthenosphere and is defined by a phase change from spinel to perovskite and therefore reflects an increase in density that slows down the penetration of the subducting slab.

Thus the slab-pull force reaches its maximum when the slab-tip approaches the 660-km discontinuity. When the slab starts to penetrate the discontinuity (fig. 5), the higher density of the lower mantle forces the slab to fold (a). The highest impact on the extension of the overriding plate provides the draping of the slab (b and c), (Isacks & Molnar 1969).

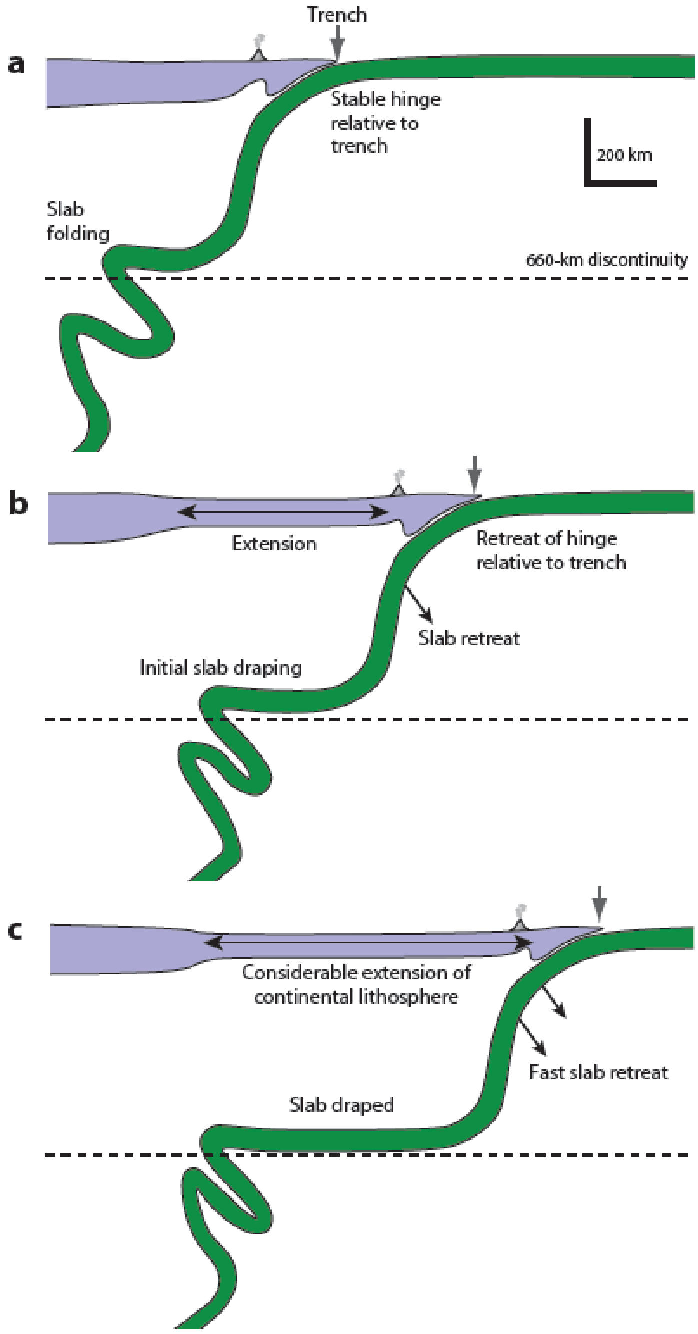

Fig. 5: Illustration of the interaction of a subducting slab with the upper/lower mantle discontinuity (Ring et al. 2010)

c) Low-angle normal faults (LANFs) and metamorphic core complexes

Low-angle normal faults (LANFs or detachment faults) dip at less than 30° and separate a hanging wall block from a footwall block, often with tens of km of displacement, with deformation conditions changing from ductile to brittle conditions. LANFs occur on most continents, not only in extensional but also in overall contractional settings (e.g. Selverstone 1988; Burchfiel at al. 1992) and at slow-spreading mid-ocean ridges (e.g. Tucholke & Lin 1998).

In continental extensional settings, the thinning of the upper crust caused by detachments enables the middle and lower crust to be exhumed relatively fast to the Earth's surface, forming so-called metamorphic core complexes (MCCs). The characteristic of such MCCs is the juxtaposition of higher-grade metamorphic rocks (eclogite-, granulite- to amphibolite-facies) below low grade to non-metamorphic rocks along LANFs (Lister et al. 1989, Wernicke 1981). Another feature of MCCs is an antiformal shape, a consequence of the isostatic uplift due to removal of hanging wall material along the detachment. The exposure of rocks from great depths to the surface causes a high heat flow and can lead to partial melting in the footwall and the emplacement of granitoid intrusions that may cut the hanging wall.

Below, three different crustal extension models can be distinguished resulting into two main end member types of MCCs:

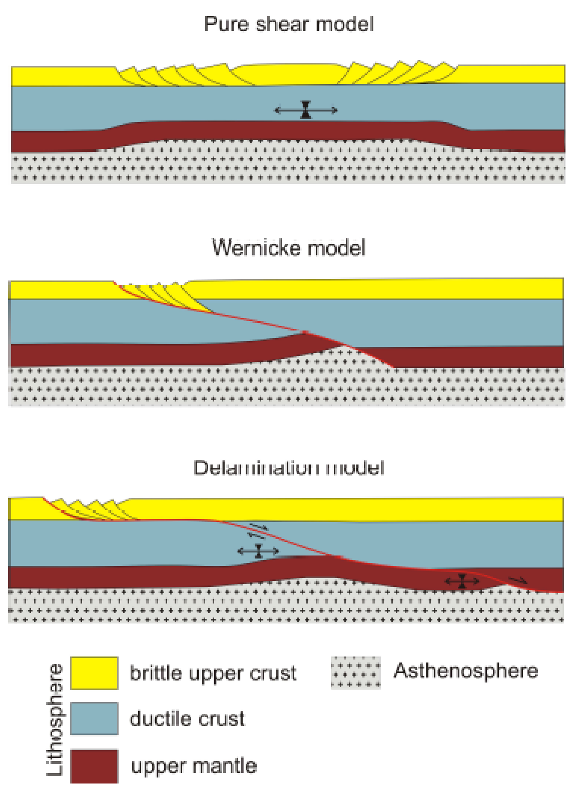

Fig. 6: Synthetic (Wernicke and Delamination model) and antithetic (Pure shear model) MCCs (Voit 2008, modified after Lister et al. 1986)

Symmetrical and asymmetrical MCCs. Asymmetric MCCs, which have been often described (Wernicke 1981) have extension in only one direction. In contrast, symmetrical MCCs have the same amount of extension in two directions. Both have uplift of high grade metamorphic rocks in the footwall with ductile deformation overprinted by brittle deformation.

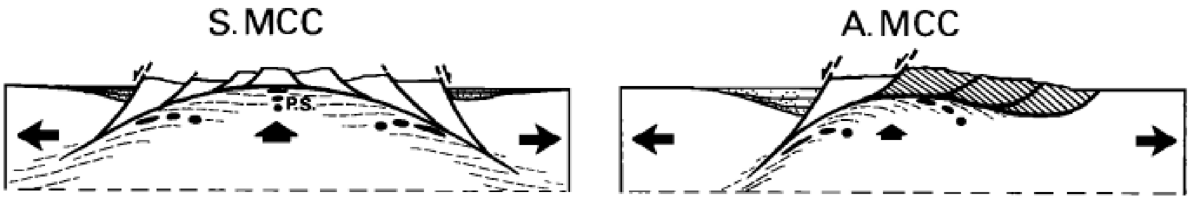

Fig. 7: Illustration of symmetric and asymmetric, antiformal MCC (Malavieille 1993)

The evolution of the Aegean region since the late Cretaceous:

The main evolution of the Aegean region started with the ocean closure along the Vardar suture zone in the late Cretaceous (Jolivet & Brun 2010). The paleogeographic domains at that time were, from North to South: The Rhodope-Sakarya Block, the Vardar-Izmir Suture, the Pelagonian microcontinent, the Pindos ocean, the Apulian continent and the eastern Mediterranean oceanic domain (fig. 8, Ring et al. 2010).

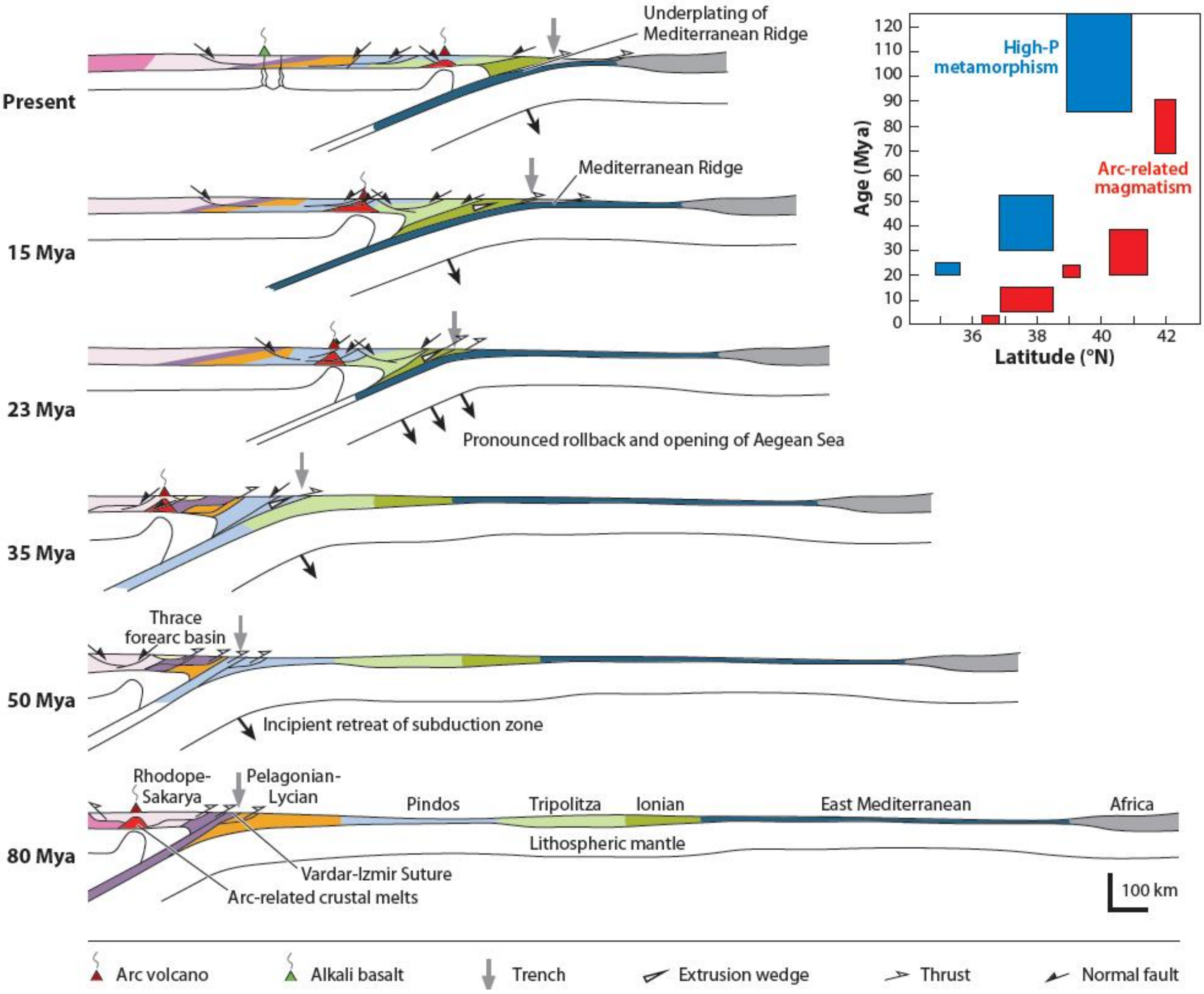

Fig. 8: Cross-section interpreting the position of paleogeographic domains and their formation since 80 Mya (Ring et al. 2010). The age versus latitude diagram on the upper right documents the southward shift of the subduction zone by means of the origin of subduction-related high-P metamorphism and arc-related magmatism (adapted from Facenna et al. 2003).

At ~80 Mya the Pelagonian-Lycian block was amalgamated to the Rhodope-Sakarya block along the Vardar-Izmir Suture, which led to crustal thickening north and south of the suture. High-P metamorphism occurred in the Vardar-Izmir Oceanic Unit and the Pelagonian-Lycian Block (Ring et al. 2010). A subduction zone related magmatic arc developed in the present-day Balkans (Jolivet & Brun 2010). Subsequently, the relatively fast convergence between the African and Eurasian plates came almost to a halt at ~65-67 Ma (Pe-Piper and Piper 2007). The anchored slab then started to retreat, causing extensional deformation in the Rhodope-Sykarya block (Jolivet & Brun 2010).

Around 50 Mya, the convergence velocity between the African and Eurasian plates increased again, the Pindos ocean started to subduct and an overall compressional regime affected the Aegean domain. The subduction of the Pindos Ocean Unit caused reactivation of the Pelagonian-Lycian Block, active compression in the frontal zones of the Balkans and extensional deformation, with the formation of metamorphic core complexes in the Rhodope-Sakarya Block. This leaves unanswered the problem of the mechanics of these simultaneous but oppositional types of deformations (Jolivet & Brun 2010). Extension in the Rhodope also led to volcanism and granite plutonism in the northern parts.

Ongoing subduction of the Pindos ocean induced southward propagated thrusting of the sedimentary Pindos and the Tripolitza domain. At depth, blueschists and eclogites were generated, seen today within the Olympos, Ossa and Almyropotamos windows, as well as in the Cyclades, at 55-45 Ma. The Cycladic Blueschists were partly exhumed in extrusion wedges (Ring et al. 2007b) while thrusting was still active further to the south (syn-orogenic extension), preserving HP-LT parageneses (Jolivet et Brun 2010).

At 30-35 Ma, the absolute northward motion of Africa decreased and a fast slab retreat commenced. This initiated an enormous amount of extension, leading to the opening of the Aegean sea basin (Jolivet & Faccenna 2000). The southward propagation of thrusting continued up to the early Miocene with understacking of the Ionian and parts of the Tripolitza units, which then start to quickly exhume below the Cretan detachment, allowing the preservation of HP-LT rocks.
A magmatic arc originated in northern Greece. In the Rhodope, sedimentary basins started to develop.

In Oligocene and Miocene times the Cycladic Blueschists exhumed in a second stage (post-orogenic extension) along low-angle detachments, below which HT core complexes were formed (Lister et al. 1984). During the Aquitanian marine sediments were deposited on top of the Cyclades core complexes. At about 15 Ma the magmatic arc was active in the Cyclades. Exhumation of HP-LT metamorphic units below the Cretan detachment continued until ca. 10 Ma, with a synchronous deposition of sediments during the Miocene (Jolivet & Brun 2010).

From ca. 10 Ma to ca. 5 Ma, extension was localized in the Cretan Sea. Then, at ca. 2-3 Ma the North Anatolian Fault enters the Aegean region, localizing extension in Evia and the Gulf of Corinth (Le Pichon et al. 1995; Dinter 1998, Jolivet & Brun 2010). The active volcanic arc was at that time situated in the southern Cyclades (Ring et al. 2010).

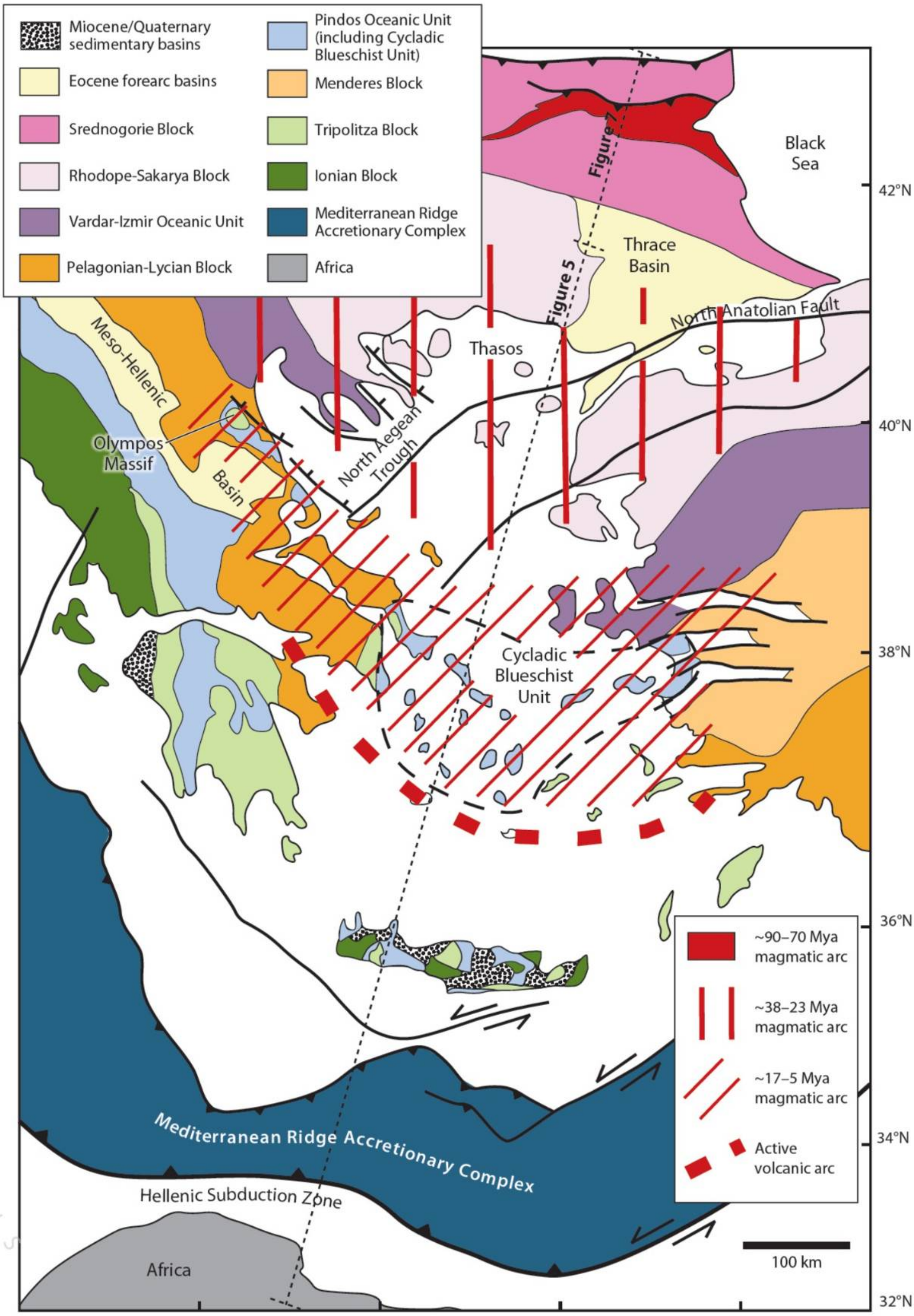

Fig. 9: Tectonic domains of the Aegean region (Ring et al. 2010, modified after Jolivet & Brun 2010). Ages of subduction related magmatic activity documents the southward migration of the subduction zone. The dashed black lines illustrate the position of the cross section shown in fig x.

3.3. Cycladic Blueschist Unit

The Cycladic Blueschist Unit is exposed on the islands of the Cyclades, South Evia, South Attica (the area south of Athens) and western Turkey (South Izmir). It consists of three tectonic units: Cycladic Basement, Cycladic Blueschists and the Upper Unit.

The Cycladic Basement is built up of Paleozoic schists, orthogneiss, marbles, metapelites and volcanics (Dürr et al. 1978; Ring & Layer 2003) intruded by Triassic granitoids (Engel & Reischmann 1997; Reischmann 1997).

This is overlain by the Cycladic Blueschists, a late to post-Carboniferous series of metabasic and metasedimentary rocks (Dürr et al. 1978).

The Upper Unit traces the suture between the Pindos Oceanic Unit and the overlying Pelagonian Lycian Block. This is mainly represented by rocks of the ophiolitic Selçuk Mélange. These are overlain by a partial ophiolite sequence consisting of serpentinites, and non-metamorphic Cretaceous and molasse sediments of Oligo- to Miocene age (Okrusch & Bröcker 1990).

The 5 main metamorphic events that characterise the Cyclades are generally described by M0 – M4 and are outlined below:

A Variscan metamorphic event **(M0)** can be observed in the Cycladic Basement which crops out mainly on Serifos, Paros, Naxos, Ikaria and Ios.

The Cycladic high-pressure (blueschist) event **(M1)** formed during synorogenic subduction in Eocene times, followed by rapid exhumation (Trotet et al. 2001a, b).

Oligocene-Miocene back-arc extension (Lister et al. 1984) (**M2**; LANF) caused reworking and retrogression of the high-pressure metamorphic rocks at medium pressure/temperature conditions (greenschist facies). Blueschist-facies rocks showing varying degrees of greenschist facies overprinting crop out on Andros, Tinos, Syros (eclogites), Serifos, Sifnos, Kythnos, Milos, Ios, Amorgos and Naxos. On Kea, Kythnos, Andros, Tinos, Paros, Ios and Serifos, greenschist-facies rocks are predominant; relicts of blueschist assemblages occur in greenschist facies minerals, such as epidote.

During the Miocene, a magmatic arc developed in the Cyclades, forming granodioritic intrusions and inducing local low-pressure contact metamorphism **(M3)** (Altherr & Siebel 2007). Such granitoids occur on Serifos, Naxos, Tinos, Mykonos and Ikaria.

In the southern Cyclades, a volcanic arc has developed since 5 Mya (**M4**) which is still active and is seen on Milos, Kimolos, Thira, Nisyros and Astypalaya (Fytikas et al. 1984).

The post-orogenic extensional regime in the Cyclades since Oligocene and Miocene times caused the development of large-scale detachment systems. Bi-directional extension kinematics have been documented in the north-western Cyclades, with top-to-NNE/NW movement on Tinos, Andros, Mykonos, Delos, Paros and Naxos (Jolivet et al. 2010) and top-to-SW/SSW movement on Serifos (Grasemann and Petrakakis 2007), Kea (Iglseder et al. 2011) and Kithnos (Lenauer 2009, Laner 2009). In the south-eastern Cyclades, detachment systems reveal a top-to-N/NNE movement.

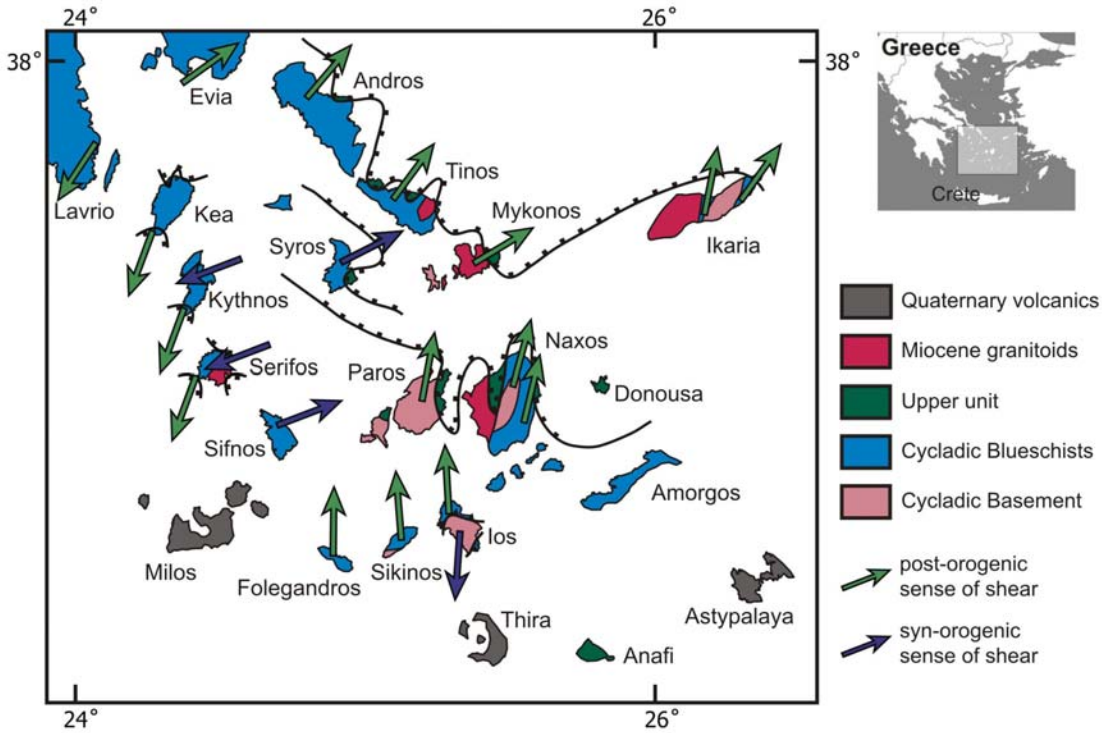

Fig. 10: Major lithological units of the Cyclades and orientation of detachment systems (modified after Huet et al. 2009, Grasemann et al. (in review)).

3.4. Block rotations in the Aegean region

Block rotations in the Aegean domain since the Miocene have been the subject of numerous studies (e.g. Walcott & White 1998; Kondopoulou 2000; Van Hinsbergen et al. 2005). It is generally accepted that the Aegean region features two blocks showing opposite senses of rotation. The western Aegean region, reaching from northern Albania to at least the northern part of Peloponnese and Evia in the east, shows clockwise (cw) rotation. The eastern Aegean region, south- and eastward of the West Aegean Block, shows counterclockwise (ccw) rotation. A discrete lineament, the Mid-Cycladic lineament, is considered to form the boundary between these blocks.

Van Hinsbergen et al. (2005), who focused their research in the western block, suggest cw rotation in two episodes (fig. 11). The first episode took place between ~15-13 and 8 Ma, with a rotation of 40°, the second occurred after 4 Ma, with an additional rotation of 10°. The boundaries of that block, this being the structures that accommodated the rotation, are the Scutari-Pec fault zone in the north (Kissel et al. 1995), the Ionian thrust in the west and the Hellenic subduction zone. Van Hinsbergen et al. (2005) suggest that in the Cyclades and the Rhodope at least the early rotation phase occurred contemporaneously with the formation of extensional detachments.

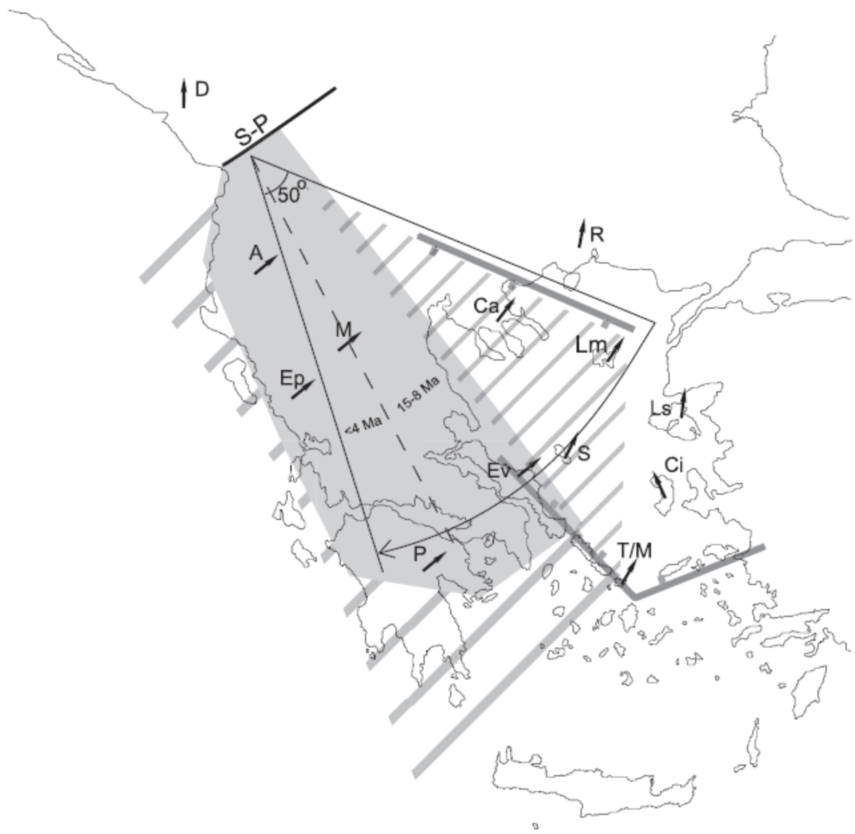

Fig. 11: Illustration of the clockwise rotation of the western Aegean region since the middle Miocene. The shaded area refers to a rotation of 50°cw, the finely hatched area shows a rotation of 30-40°cw. The widely hatched area also shows rotation of 50°cw but the data are based on structural observations. A=Albanides; Ca=Chalkidiki peninsula; Ci=Chios; D=Dinarides; Ep=Epirus; Ev=Evia; Lm=Limnos; Ls=Lesbos; M=Mesohellenic basin; P=Peloponnesos; R=Rhodope; S=Skyros; S-P=Scutari-Pec transform; T/M=Tinos and Mykonos. (van Hinsbergen et al. 2005)

3.5. Recent and active extension

Active kinematics in the Aegean region are driven by the retreat of the subducting African plate and the contemporary westward motion of the Anatolian plate, along the North Anatolian Fault (NAF; Le Pichon & Angelier 1981b; Jackson 1994, Jolivet 2001; Armijo et al. 2003; Flerit et al. 2004). Initiated by the northward motion of the Arabian plate towards Eurasia in the Miocene, Anatolia started to escape westward along the NAF and EAF (East Anatolian Fault) in the Pliocene and pushed into the Aegean domain no earlier than 2-3 Myr ago (Le Pichon et al. 1995; Dinter 1998).

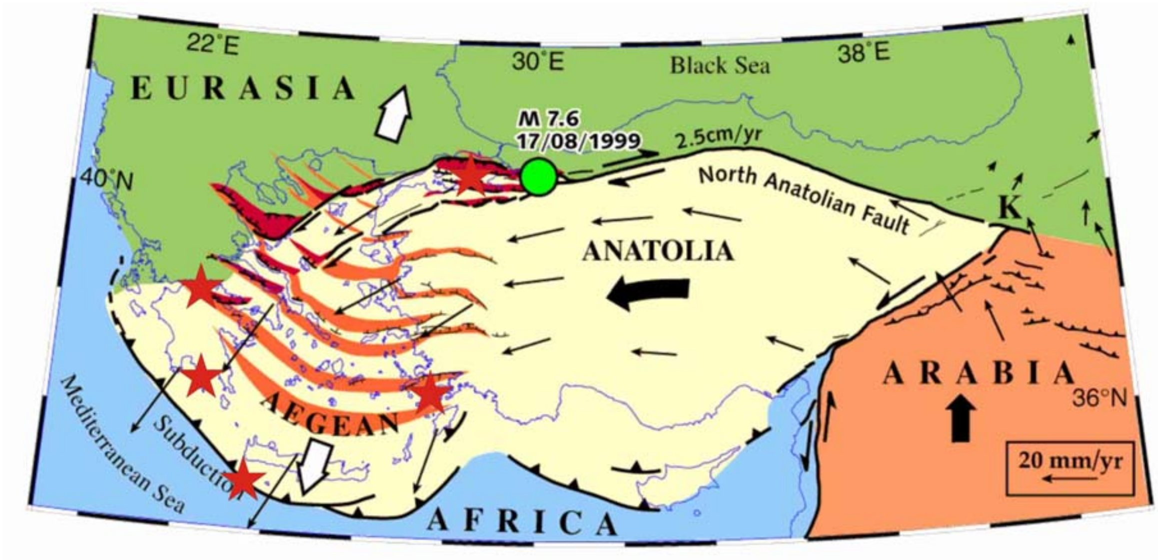

Fig. 12: Illustration of extensional kinematics in the Aegean caused by the retreat of the Hellenic subduction zone and the westward escape of the Anatolian plate. Red stars mark areas of main active extension (Armijo et al. 1999).

Most of the extension is now localized at the NAF, the Corinth-Patras rift, in Western Turkey and also in Crete and Peloponnese where it is parallel to the arc (Armijo et al. 1992, Lyon-Caen et al. 1988).

3.6. Comparison between Oligocene-Miocene and Recent extension

The general strain pattern from the Oligocene to the present has not significantly changed (Jolivet 2001). Oligocene-Miocene extension proceeded from north to south due to slab retreat (Jolivet et al. 1998). The recent westward motion of the Anatolian plate, combined with the still ongoing southward retreat of the subduction zone, cause east-west-shortening and enhanced north-south-directed extension in the Aegean.

Extension velocities of about 1.5 cm/yr in both the Corinth-Patras Rift and in the east part of Western Turkey have been measured (McClusky et al. 2000; Briole, 2000).

As the active strain pattern of the Aegean and the Oligo-Miocene finite strain field show some striking similarities in terms of direction and rates of extension, one can extrapolate such rates for the intervening 20-30 Ma. This translates into 300-450 km of total ca. N-S directed extension (Walcott & White 1998), which is compatible with reconstructions of the paleoposition of the Hellenic subduction zone. The velocity of 1.5 cm/yr, which was previously distributed over the entire Aegean region, is presently localized along a single structure, the Corinth-Patras rift (Jolivet 2001).

Extension led to variations in crustal thickness and caused the Aegean Sea to break up into three different provinces: North Aegean (< 24 km crustal thickness), Cyclades (rather flat

Moho at 25 km) and Cretan Sea (crustal thickness of 22-23 km; Tirel et al. 2004). Tirel et al. (2004) suggested a two-stage model of the Aegean extension responsible for the observed thickness variation. The major extension (approximately 100 %) in the whole Aegean occurred from Oligocene to middle Miocene and caused the reduction of crustal thickness from ~50 km to 25 km (Walcott & White 1998). From upper Miocene to the present, extension is very localized in North Aegean, due do the extrusion of Anatolia and in the Cretan Sea as a consequence of African slab retreat (Tirel et al. 2004). The Cyclades behaved as a rigid block translated toward the SW, without significant internal deformation (Walcott & White 1998).

3.7. The Hellenic subduction zone

The Hellenic subduction zone forms an arcuate trench with a rather limited trench-parallel length (ca. 600-800 km). Such laterally narrow subduction zones have rapid retreat rates and form concave profiles (Schellart 2005). Fig. 13 illustrates the development of the subduction zone since 80 Ma.

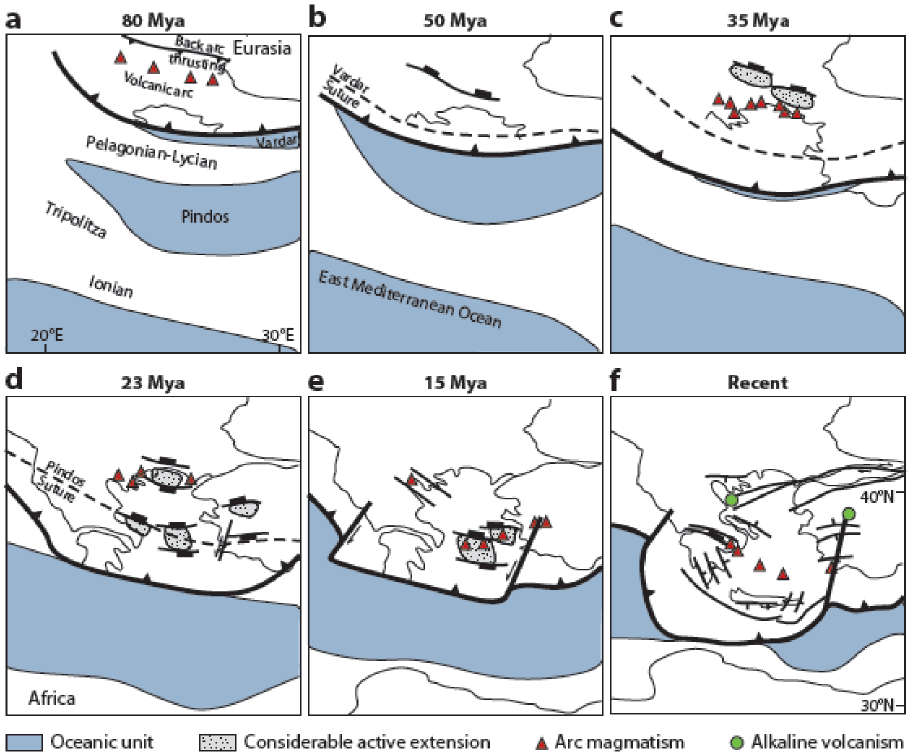

Fig. 13: Evolution of the subduction zone in the eastern Mediterranean (Ring et al. 2010, modified from Brun & Faccenna 2008). Images a-c: successive subduction of the Vardar ocean, Pelagonian-Lycian block, Pindos ocean and Tripolitza and Ionian units, d: initiation of fast rollback in the south of the Aegean domain, generating a concave profile, e: outboard movement of the subduction system of the Aegean sea along slab tears on both sides of the retreating slab, f: the spatially restricted slab rollback caused the curvature of the subduction zone.

It is commonly accepted that a single subduction slab was active since ~200 Ma (Faccenna et al. 2003, van Hinsbergen et al. 2005). During the Jurassic and Cretaceous periods, the subducting slab penetrated through the 660-km discontinuity without any significant degree of roll-back. After a time gap of ca. 20 Ma at 60 Ma, the slab started to drape over the 660-km discontinuity (van Hinsbergen et al. 2005) supporting fast rollback since the Oligocene. The eastern Mediterranean subduction system, seen south of mainland Greece and the Cyclades, shows a major difference to the western one since there the slab has not yet sunk across the upper-lower mantle boundary (Facenna et al. 2003, Edwards & Grasemann 2009).

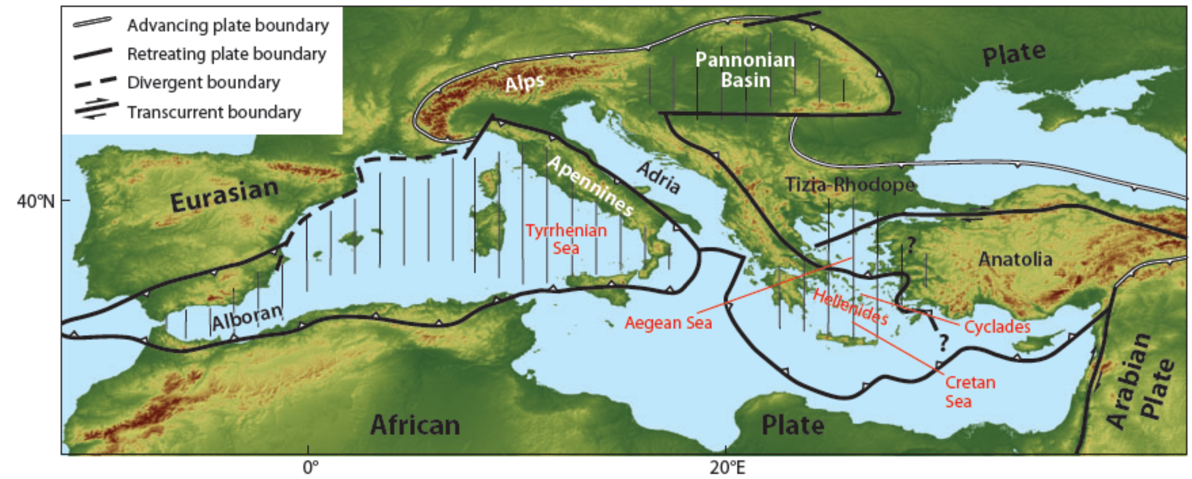

Fig. 14: Plate boundaries and movements in the Mediterranean. Vertical lines indicate extended regions above retreating plate boundaries (Ring et al. 2010)

3.8. Kea

3.8.1. Previous geological researches

Davis (1972) carried out the first detailed geological mapping on Kea (fig. 15) and reported that the island contained metamorphic rocks, with three different petrological units:

1) Marbles with a thickness of more than 700 m and which are intense folded.
2) The lower part consists of gneiss and schists occupying most part of the island.
3) Ferromanganesian ore deposits (limonite and hematite), mostly occurring in the marble horizons

Two fold-systems were observed - a younger system with NE-SW axial orientation and an older system with WNW-ESE oriented fold axes.

Above the dominant metamorphic rocks, Davis described an intensely weathered surface which upon non-metamorphic dolostone klippen rest, showing a slight schistosity only in the north of the island.

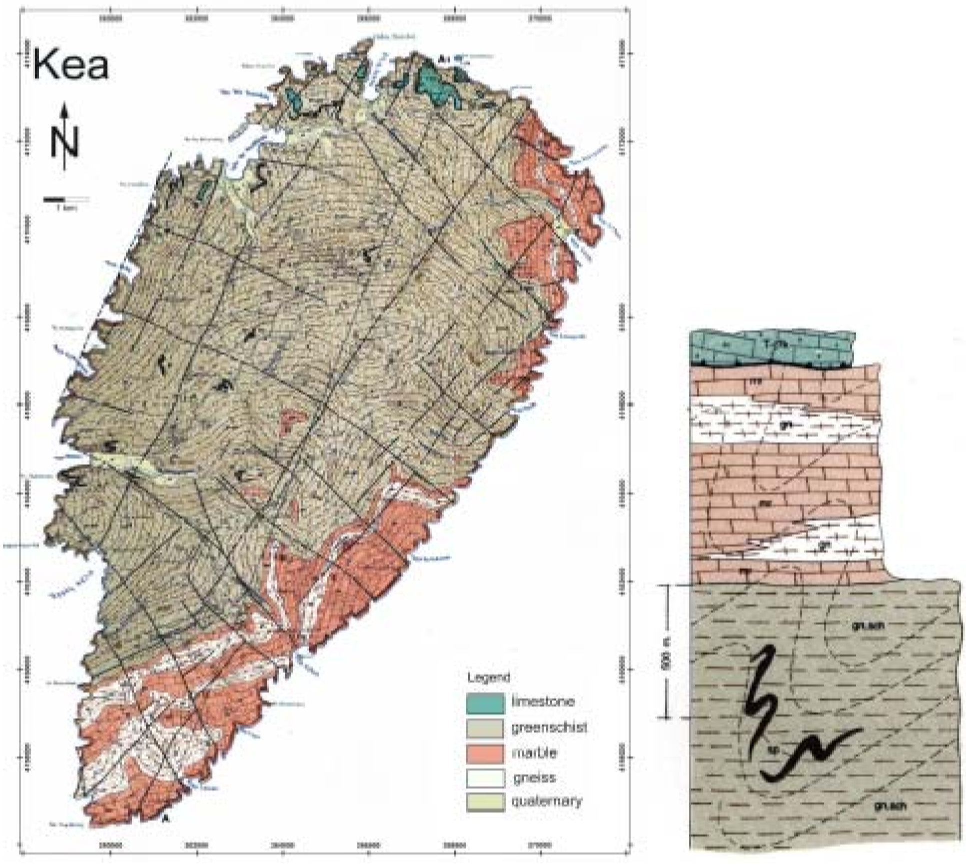

Fig. 15: Geological map and a litho-stratigraphic profile of Kea by Davis (1972); black lines present normal faults.

3.8.2. Lithological and structural overview

The island of Kea is located ca. 60 km southeast of Athens, in the Aegean Sea, and forms part of the Western Cyclades. The island lies within the active extensional regime of the Aegean region and is one of the many islands exposing the Cycladic Blueschist Unit.
Recent geological research on the island by members of the Accel-team during the last five years includes re-mapping of the whole island combined with detailed structural investigations. This showed that the island represents a crustal-scale shear-zone with top-to-SW kinematics. A three-fold tectonostratigraphy has been identified: footwall, fault-zone and hanging wall.

1) The **footwall** has an exposed structural thickness of >450 m and outcrops over the entire island. It predominantly consists of chloritic schists (chlorite, carbonate, epidote, actinolite, muscovite and talc) with local variations in the mineral assemblage. Predominantly along the east and southern coast, as well as in the west around and south of Pisses, the chloritic schists are interlayered with up to ca. 30 m thick blue-grey calcitic marble mylonites with thin quartzofelspathic layers; these are probably repeated by folding. Talc schists and serpentinites occur in the footwall near the detachment.

2) The **fault zone** is preserved in klippen of up to ca. one square kilometer in size that are scattered over the whole island, but occur predominantly in the northern- and southernmost parts. The fault zone is characterised by up to ca. 30 m thick calcite ultramylonites that are underlain by m-thick cataclastically deformed footwall schists and overlain by dolomitic breccias and cataclasites that are partly ankeritised (Rice et al. 2010).

3) The **hanging wall** consists of breccias of dolostones and limestones overlying the fault zone at some, but not all klippen (Iglseder 2011).

Kea forms an elongate dome structure over the whole island: The mean foliation poles plunges at 74-230°, whilst the foliation planes in the north dip slightly more steeply to the NW. In the extreme south, they dip shallowly to the SW. Stretching lineations in all lithologies plunge either NE or SW, although the shear criteria consistently reveal a top-to-SW movement. The greenschists and interlayered marbles were affected by intense folding. The main fold axes are parallel to the stretching lineation and dip shallowly northwards. Their fold axial surfaces plunge sub-parallel to the foliation. The maximum temperature conditions of the footwall lay between ca. 350 to 450° C.
Voit (2008), who studied the north of Kea in detail, subdivided brittle structures into 3 groups: (1) foliation parallel distinct brittle fault zones, in which the cataclasites show a top-to-SW movement, (2) a later population of brittle NE dipping normal faults and (3) a NNE-SSW and SE-NW striking conjugate fault system. Iron-rich fluid infiltration in a very late stage of deformation caused ankeritisation of primarily marble and dolomite and deposition of mainly hematite and magnetite (Voit 2008).

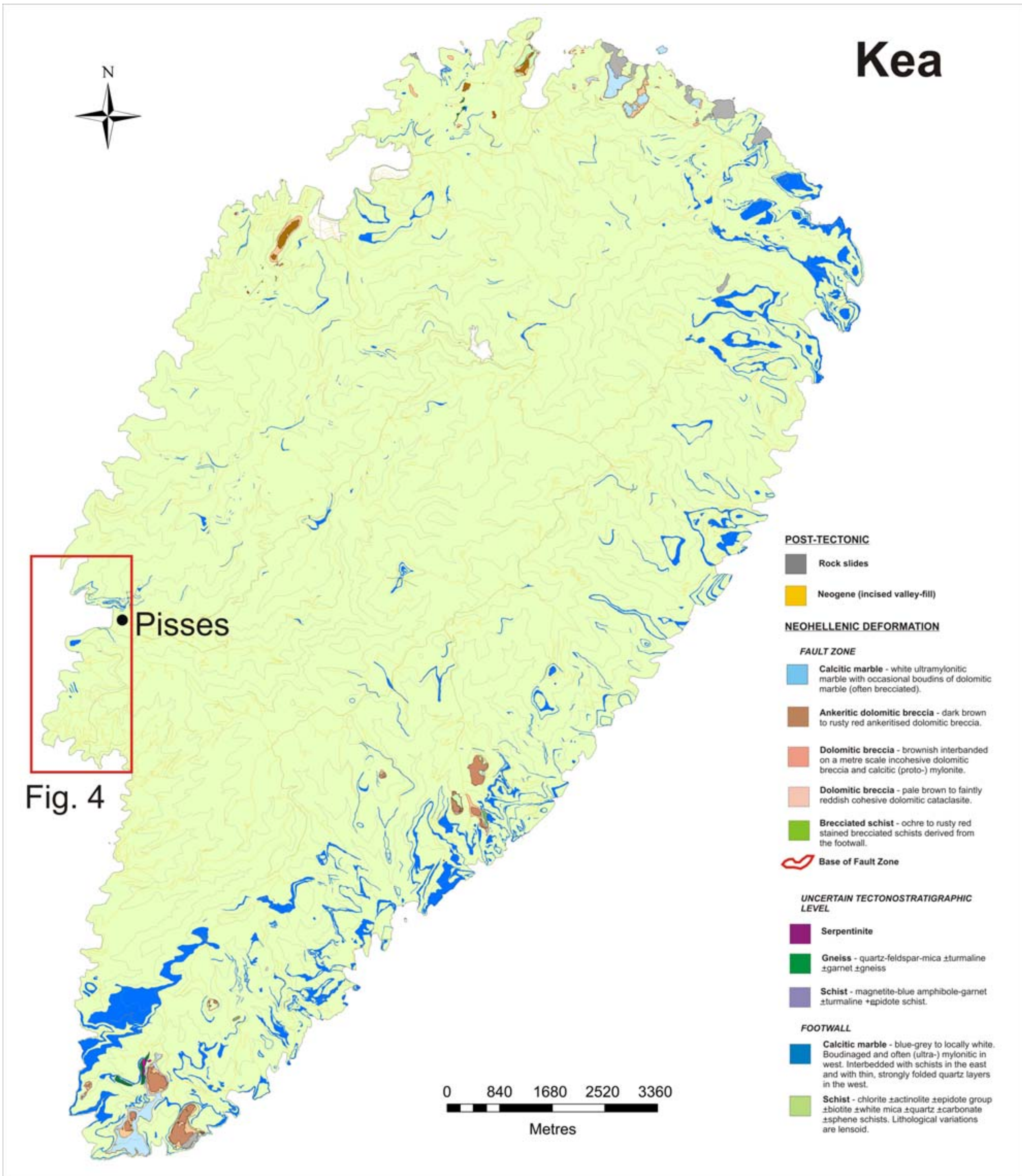

Fig. 16: Map of Kea (Rice et al. 2010). The red rectangle displays the research area.

3.8.3. Research area:

The mapping area, which is about 2.5 km² in size, is situated on the west coast of the island, north and south of Pisses (fig. 16). The rocks were best exposed along the coastline and this is where most data were collected. In the upcountry, where the outcrop-frequency was lower, the possible effects of anthropogenic changes of the landscape had to be taken into account when making the lineament analysis. The construction of terraces for farming over nearly all the island have been evident since the first settlement and gained importance in the post-1950 history (Cherry et al. 1991). Most were abandoned in the last twenty years or so.

Fig. 17: a general view of the mapping area (looking to the SW from north of Pisses). Note the excellent coastal exposures.

4. RESULTS

4. 1. Satellite lineament analysis

The island of Kea, especially the area around Pisses, shows a very conspicuous pattern of lineaments on satellite images. The lineaments were traced in an area ca. 1 km to the north and ca. 2 km to the south of Pisses (the area is shown in the red box in fig. 16 above) and evaluated afterwards using rose-plots.

Remote sensing analysis of the lineaments showed that two dominant strike directions are present, trending ca. NE-SW and NW-SE (Fig. 18). From the north of Pisses southwards, the angle between these two directions changes gradually from a rhombohedral geometry (ca. 50°/130° angles between fractures, with the acute angle facing westwards) into an orthogonal geometry (ca. 90°/90°: Fig. 19). While the dominant NE-SW strike direction stays essentially constant across the whole area, the other direction shows a gradual rotation, such that both from north to south and from west to east, the strike of the fractures changes from an approximately NW-SE to a more NNW-SSE direction.

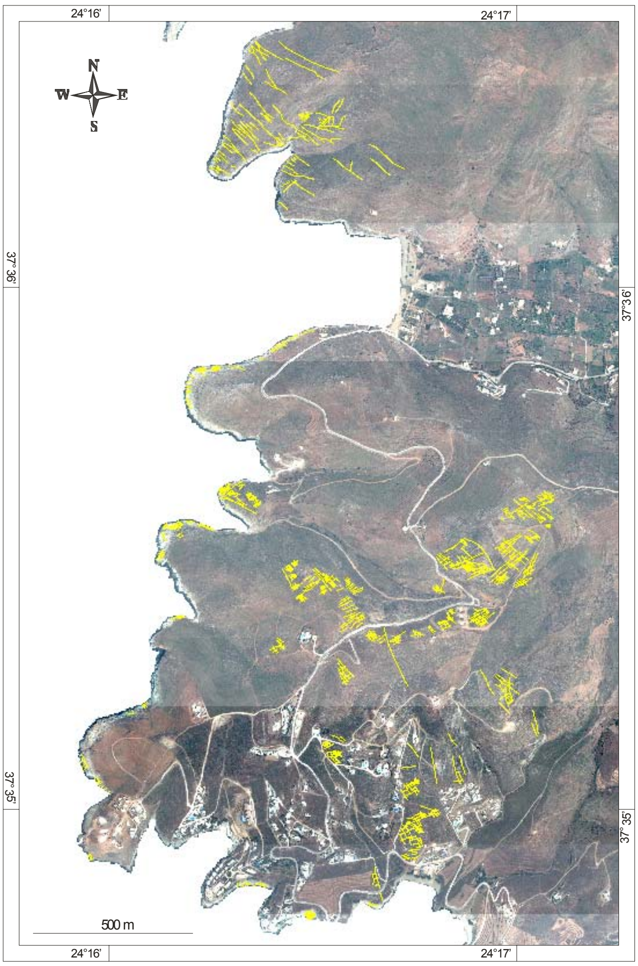

Fig. 18: Distribution of lineaments mapped from satellite images

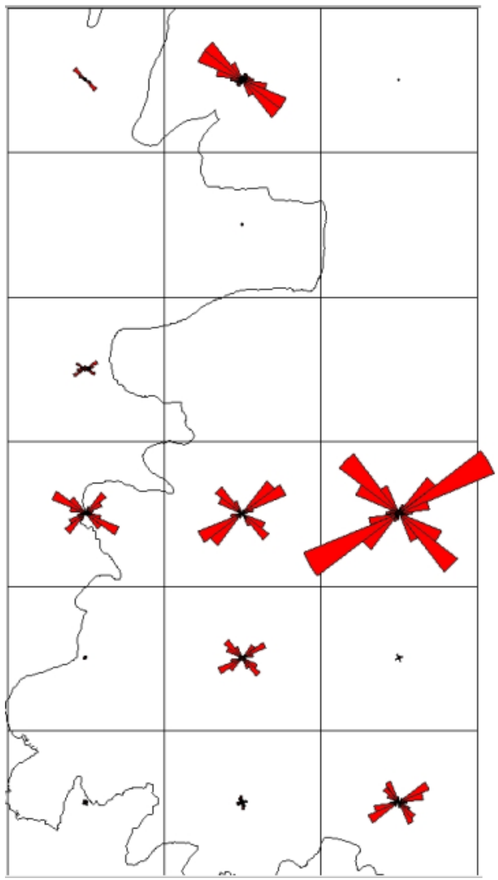

Fig. 19: Rose-plots of lineament orientations in Fig. x.

4.2. Field data evaluation

4.2.1. Lithology and general structural inventory

Kea represents a low-angle crustal-scale detachment zone (Iglseder et al. 2011). Most of the island comprises a footwall, overlain by a relatively limited number of outcrops of the detachment zone and even fewer consisting of the hangingwall. The present study area only exhibits the lower part of the tectonostratigraphy, which still is affected by deformation.

The main lithologies in the study area consist of chlorite-carbonate schists, locally overprinted to form cataclasites, with mylonitic blue-grey calcitic marbles as either occasional thin (up to 10 cm) interlayers or as thicker bands (m- to 10-m-scale), probably repeated by folding (Fig. 20, 21). Outcrops with significant occurrence of marbles were seen only twice in the study area, at Kea 1 and Ch 1 (outcrop numbers are shown in appendix I).

More detailed information about the mineral assemblages and deformation conditions are given in chapter 4.3.1.

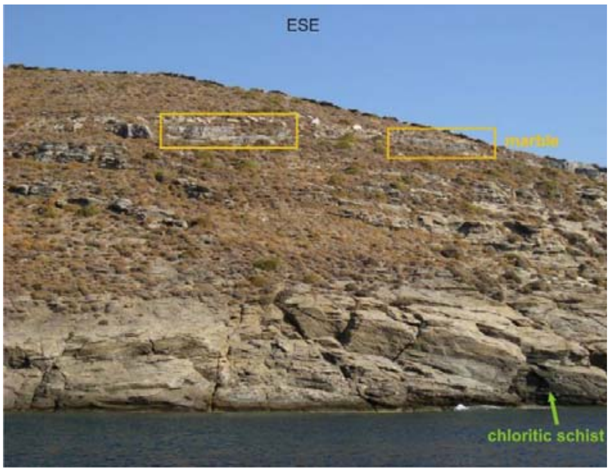

Fig. 20: The main lithologies in the mapping area

Fig. 21: Marble-outcrop at Pisses. Outcrop number 1, view to the east.

Across the area, foliation planes are essentially flat lying, with only minor variations in orientation. Subareas passing from the NE to the SW show only slight changes of the mean foliation dip-direction. In the NE of Pisses foliation planes plunge shallowly to the NE, in the area south of Pisses they are distributed in all directions whereas farther in the SW the foliation planes dip gently to the SW. Therefore the whole study area forms a slight, elongate dome structure.

Colours in fig. 22 refer to the foliation planes of different sub-areas. Yellow marks the north-eastern parts of the mapping area, the colour changes from yellow to green and dark green gradually towards the south-western. Stretching lineations are well developed in all lithologies and have a consistent NE-SW to NNE-SSW azimuth direction.

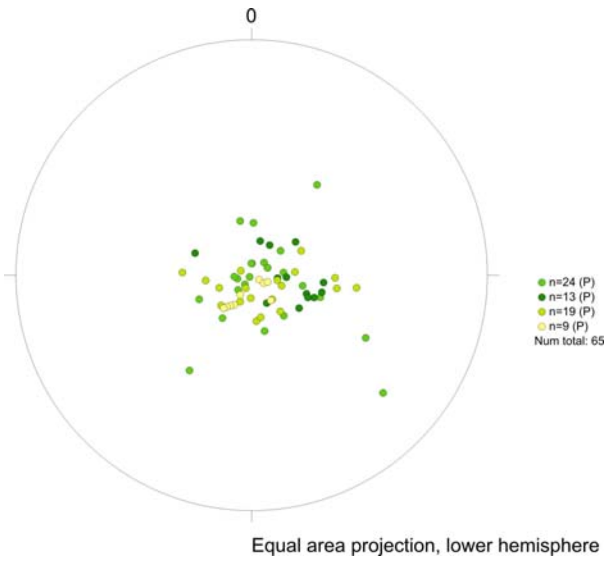

Fig. 22: Poles and great–circles of foliation planes. Colours refer to different sub-areas from the NE (yellow) to the SW (dark green).

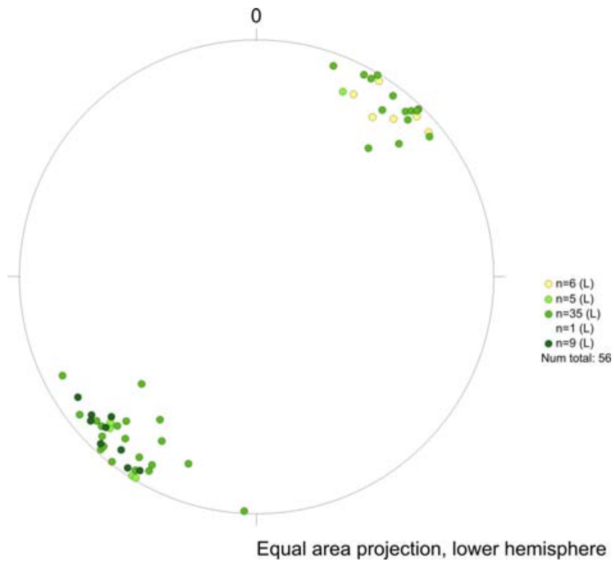

Fig. 23: Lineations show a very clear NE-SW trend.

Kinematic indicators, such as SCC'-fabrics or rotated clasts consistently reveal a top-to-SW movement (Fig. 24 & 25).

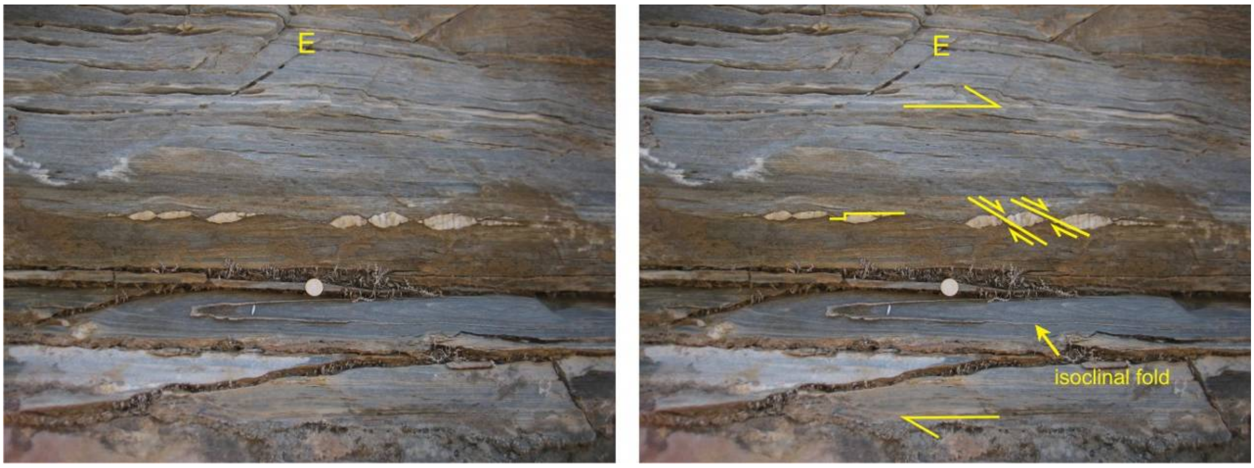

Fig. 24: Sigmoidal quartz-boudins in mylonitic marble with antithetic displacement. Their wings, show a stair-stepping geometry, indicating a top-to-SW kinematic. The fold-axis of the isoclinal fold plunges gently to the NW. Outcrop number 18.

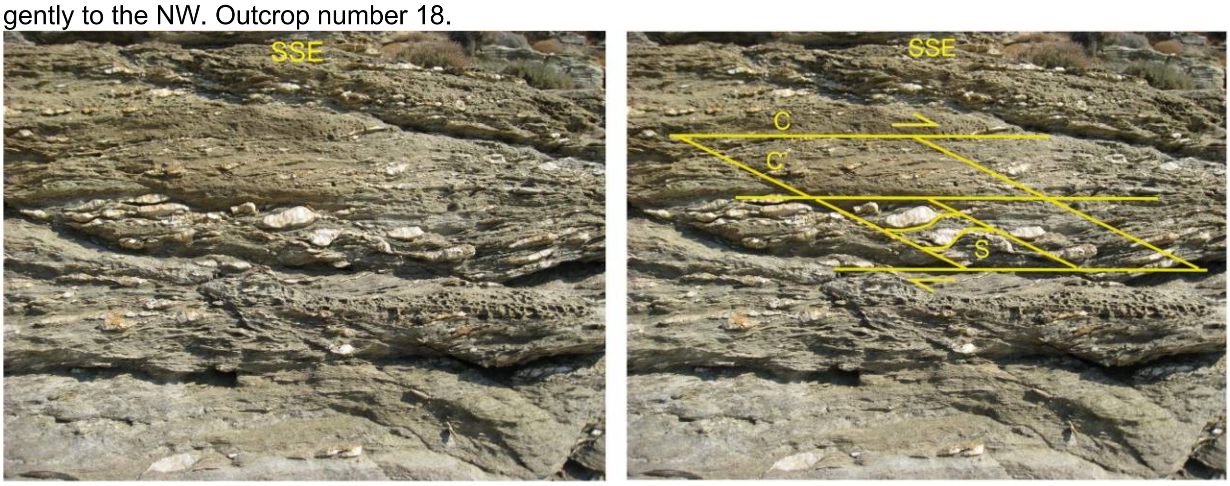

Fig. 25: SCC'-fabric in calcitic schist show a SSW kinematic. Outcrop number 19.

Schists and marbles are commonly isoclinally folded with axes showing a wide variation in azimuth, although all have low plunge angles (fig. 26), within the orientation of foliation planes. Only one outcrop showed evidence of a strongly folded foliation, with fold axes sub-parallel to the main lineation (Fig. 28, 29). Sheath folds developed in blue-grey mylonitic marble also have axes sub-parallel to the regional stretching direction and are indicators of high-strain ductile deformation (Fig. 27).

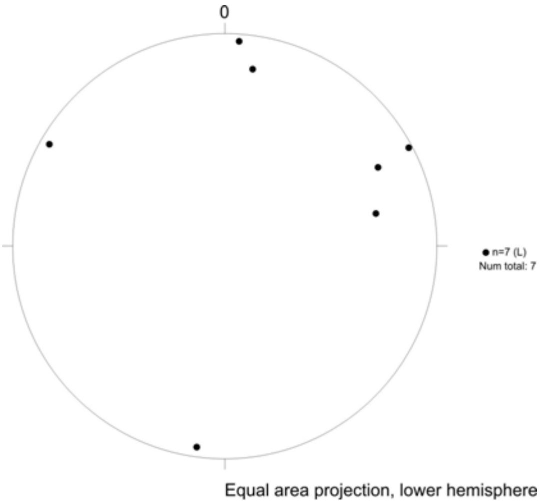

Fig. 26: Fold-axes of isoclinal folds are flat-lying with a wide range of axial directions

Fig. 27: Sheath fold in blue-grey mylonitic marble reveals top-to-SSW extension. Outcrop number 17.

Fig. 28: Second order folds in greenschist, with s- and m-patterns. Outcrop number 7.

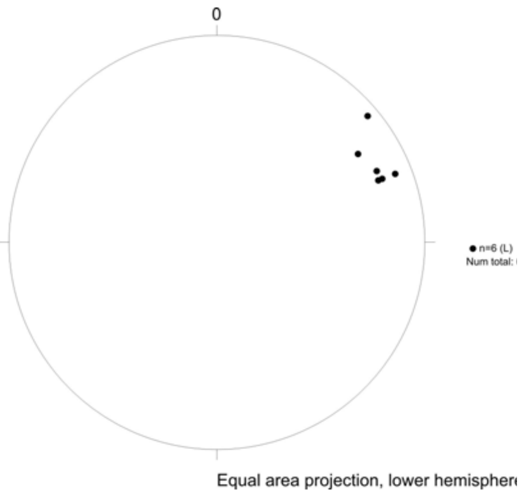

Fig. 29: Fold axes are sub-parallel to the stretching direction.

4.2.2. Development of high- and low-angle fault systems

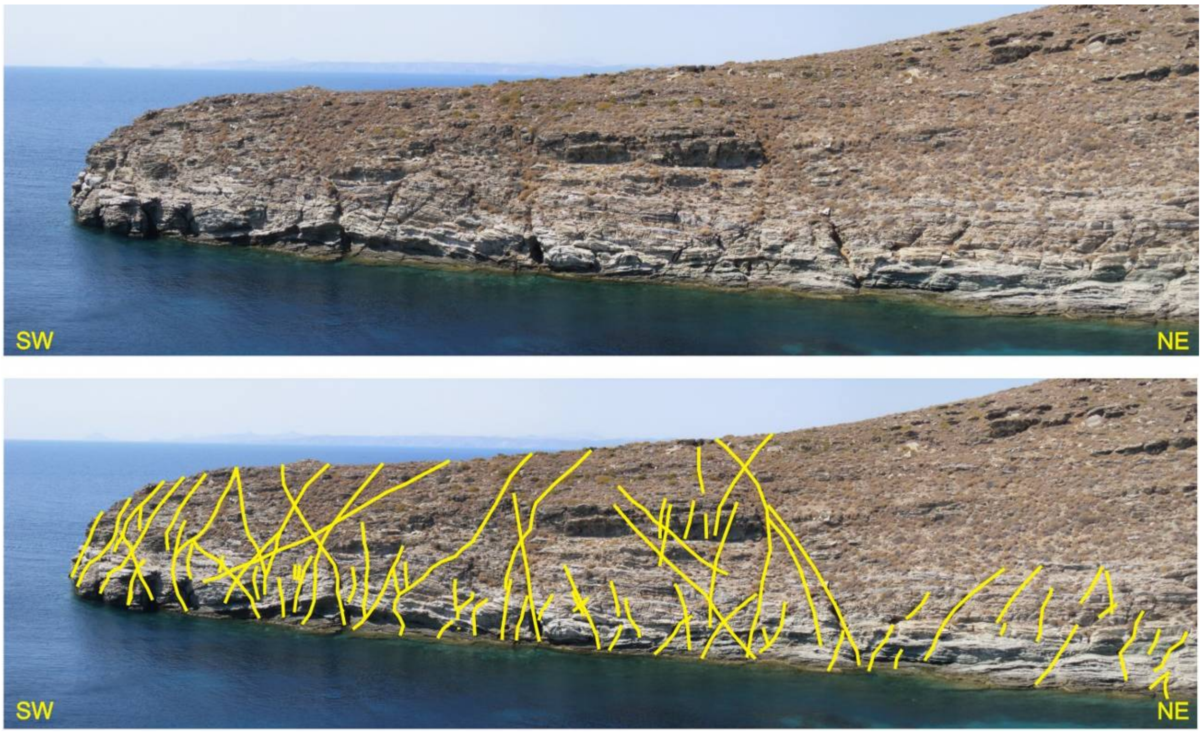

Fig. 30: High-angle extensional fault-system developing from mainly conjugate fractures; vegetation usually marks the location of fractures along the sea-cliffs.

The main fault systems on the island of Kea, which the lineaments seen in the satellite images reflect, strike NW-SE and NE-SW and are dominantly brittle in character. Both fault systems dip relatively steeply, at angles between 60° and 90° in the pelitic schists, and are mainly conjugate. In the marbles, dip angles are generally steeper (80°-90°) and are localized to form discrete planes, suggesting the fractures were refracted to steeper angles with increasing rock competence. The spacing between the fractures in schists averages ca. 2 to 4 m, whereas fractures in marbles are closer spaced, at about 0.5 to 1.5 m. In marbles, the two conjugate fracture sets cross-cut each other at nearly 90° (orthorhombic geometry) whilst in schists they have a rhombohedral relationship.

The map below (fig. 31) shows all measured faults of the study-area. Outcrops from which the data are combined in the plots are explained in Appendix II.
The distinctly different fracture behaviour of schists and marbles is highlighted in Fig. 32 and 33. Both data sets come from the area south of Pisses where one large outcrop of marble (Appendix I, Ch 1) exists.

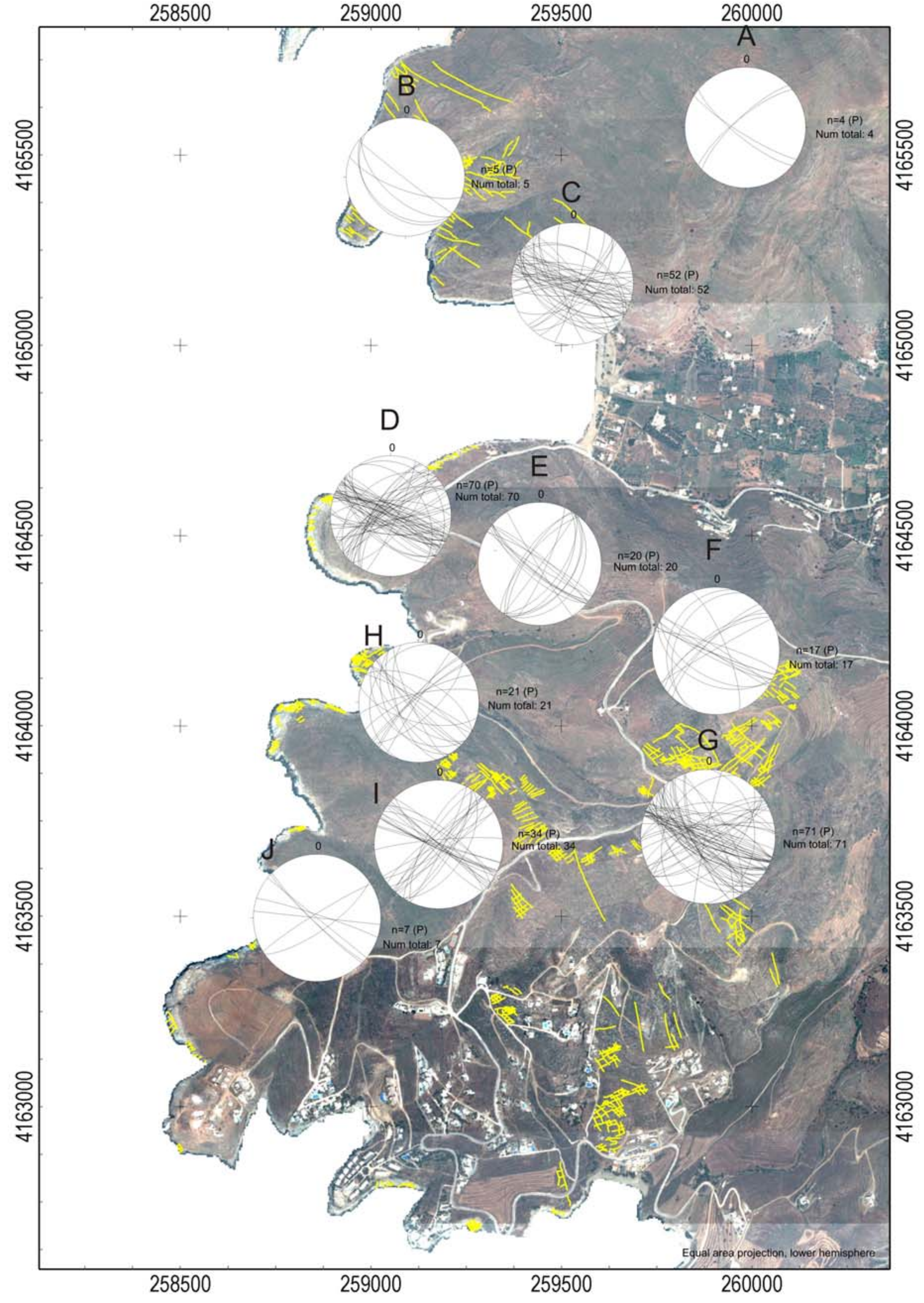

Fig. 31: Measured fault planes of the study area. Capital letters refer to summarised data of different outcrops which are explained in appendix II.

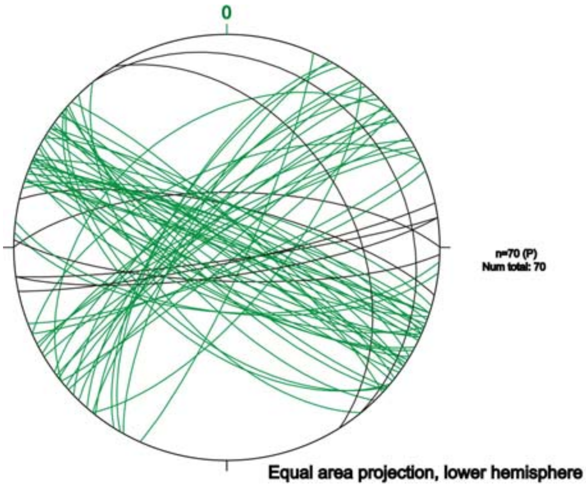

Fig. 32: Fault-planes in greenschists (fig. x, D); the green colour refers to the main fault systems.

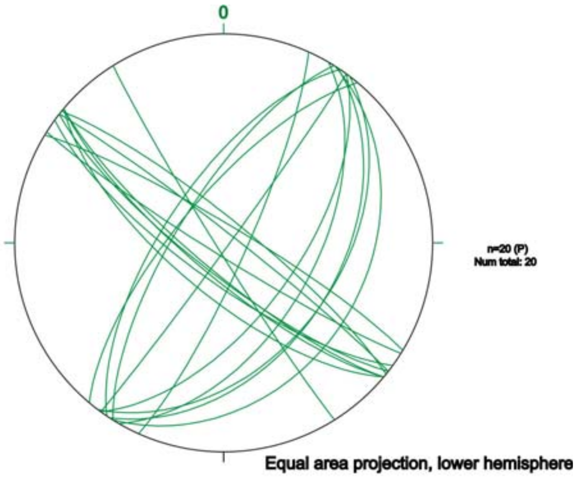

Fig. 33: Fault-planes in marbles (fig. x, E)

Riedel-fractures on the fault planes indicate normal fault displacement (fig. 35); reverse offsets were never observed. Strike-slip movements on NE-SW striking faults were seen only twice, with displacements of about 15 cm. In one instance, the offset was dextral and in the other sinistral.

Due to the lack of marker horizons in pelitic schists, offsets could only rarely be estimated; the maximum recorded in normal faults was ca. 60 cm (fig. 34).

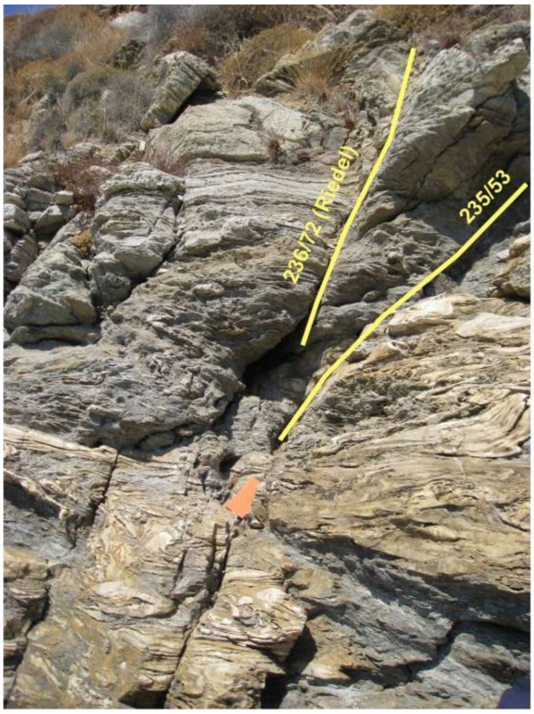

Fig. 34 (top): Normal drag along brittle/ductile high-angle faults. Outcrop number 22.

Fig. 35 (left): Isoclinal folds in greenschists cut by brittle faults with a Riedel-geometry. Outcrop number 17.

Cross-cutting relationships reveal a synchronous development of both of the high-angle fault systems. They transect each other, generally without any visible displacement. Fig. 36 demonstrates an example of a WNW-ESE-striking fault that cuts through a NE-SW striking fault with a slight sinistral displacement of about 5 cm.

Fig. 36: A WNW-ESE striking fault that cuts through a NE-SW striking fault. Outcrop number 28.

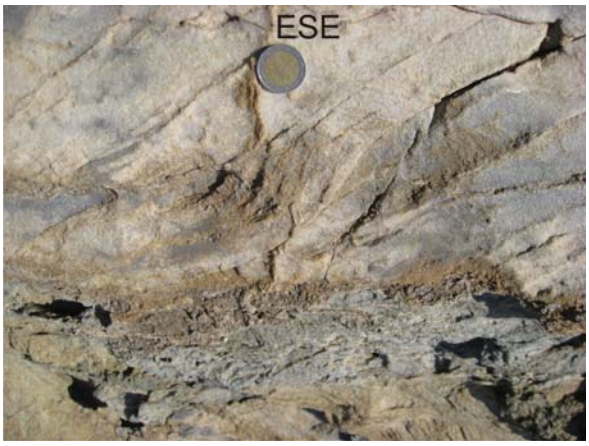

Fig. 37: Joint set bent into fault drag. Outcrop number 27.

The fractures are dominantly brittle in character but in some cases also indicate ductile deformation. Both transitions – from ductile to brittle and from brittle to ductile – were observed. Fig. 34 shows a NE-SW striking fault in greenschists that initiated by ductile deformation, with the development of fault drag in the schists, and subsequently evolved into a brittle structure forming cataclasites. Fig. 37 shows a high-angle joint sets that were bent by fault drag into a steep NE-SW striking fault and therefore reveals a transition from brittle to ductile deformation.

Extension veins were seen occasionally and were filled with quartz. They are very steeply dipping (almost 90°) and strike NW-SE, defining a NE-SW minimum principal stress direction (fig. 39).

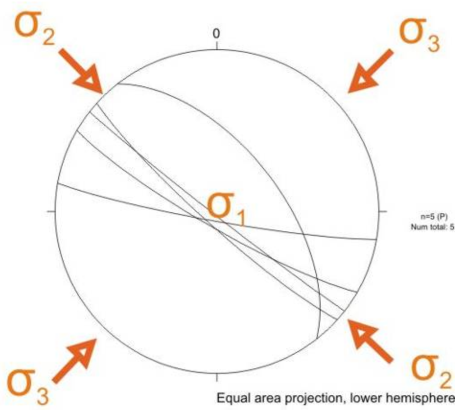

Fig. 38 (up): Extension veins reveal a vertical maximum principal stress direction and NE-SW trending minimum principal stress direction.

Fig. 39 (left): Extension veins reveal ductile deformation as well. Oucrop number 17.

Both the conjugated high-angle fault systems and extension veins (Fig. 38), suggest an essentially vertical maximum principal stress direction.
Commonly, the high-angle faults penetrate the whole footwall. However, it was also observed that the high-angle fault set was transected by a low-angle fault gouge zone with a top-to-SW movement (fig. 40). Consequently, both the high- and low-angle normal faults developed coevally.

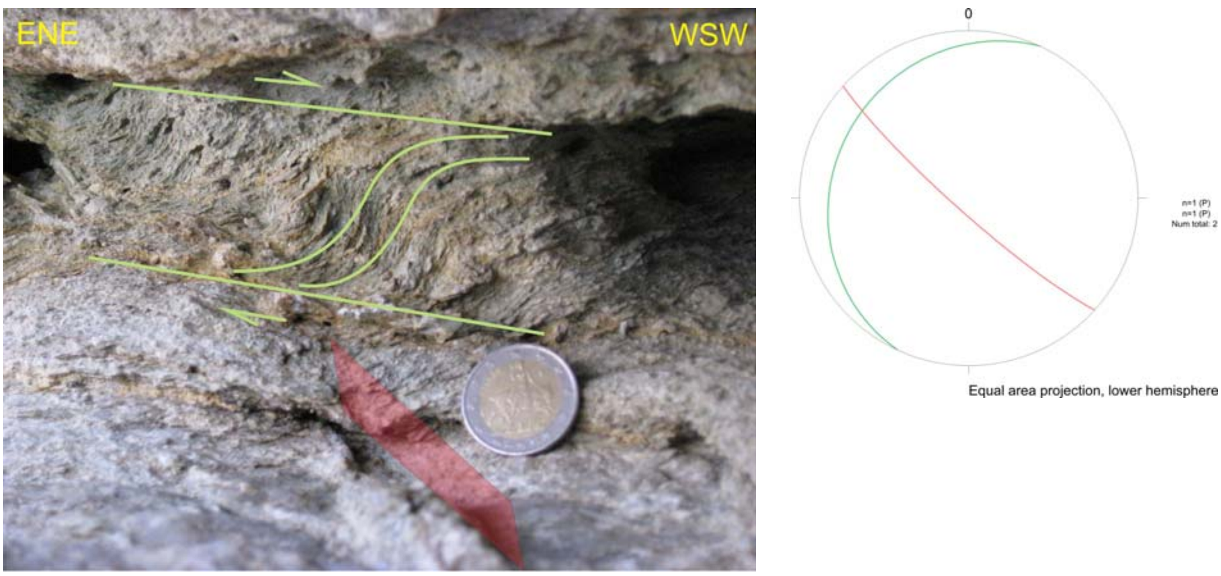

Fig. 40: Low-angle fault gouge (green) cuts through the high-angle fault-system (in red). Outcrop number 28.

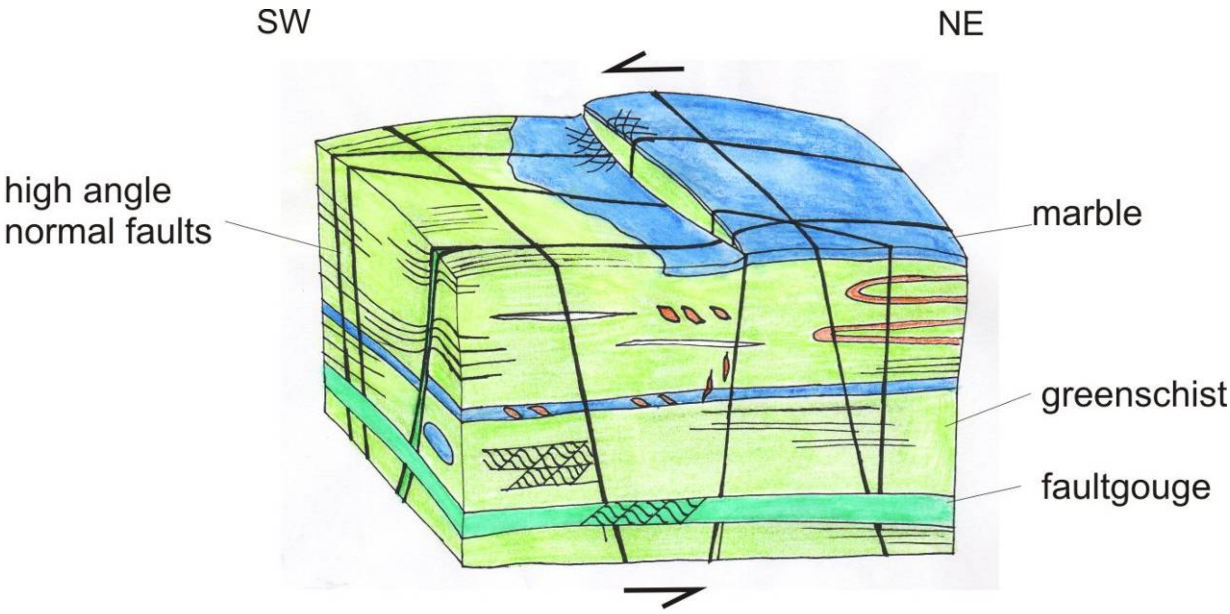

Fig. 41: Synoptic diagram of the structural inventory of the mapping area around Pisses.

4.2.3. Displacement gradient and extension

4.2.3.1. Introduction:

It is generally accepted that faults develop with an elliptical tip line, with increasing displacement towards the centre of the fault (e.g., Barnett et al, 1987, Kim & Sanderson 2005). The intersection of elliptical faults with the Earth's surfaces exposes a part of the primary ellipse. The displacement gradient indicates the relationship between the maximum displacement and the length of the fault and is of the form: d_{max}/L.

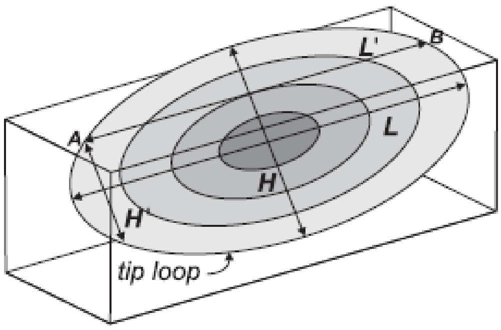

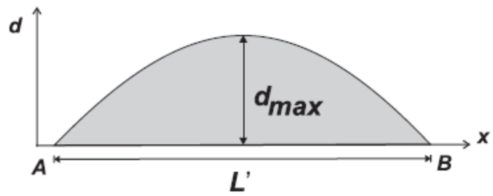

Fig. 42: Fault ellipse with different displacement distribution; density of shading increases with increasing displacement towards the centre of the fault (Kim & Sanderson 2005).

Fig. 43: Displacement-distance versus fault length diagram (Kim & Sanderson 2005)

Displacement gradients for geological faults are in the range of 10^{-1} – 10^{-2} compared to 10^{-4} – 10^{-5} for seismic ruptures. This suggests that faults develop from many slip events (Kim & Sanderson 2005). Wells and Coppersmith (1994) explain that slip sense, tectonic setting or geographic region may cause slightly different results in the relationship between the maximum slip on a rupture and the surface rupture length of the fault but does not significantly modify the correlations.
As a fault develops, slip occurs on individual segments or groups of segments. Thus a displacement-distance profile and the ratio of d_{max}/L depend on the distribution of these events and the rate of fault propagation (Peacock and Sanderson, 1996).

Two models for fault initiation and growth have widely been accepted:

1) *A fault is a single smooth continuous surface of displacement discontinuity, which becomes larger as the slip increases* (Kim & Sanderson 2005, after e.g. Watterson 1986; Walsh & Watterson 1987, 1988; Marrett & Allmendinger 1991, Cowie & Scholz 1992a, b).
2) A fault grows primarily by the linkage of individual segments (e.g. Segall and Pollard, 1980; Ellis and Dunlap 1988; Martel et al. 1988, Peacock and Sanderson 1991, Cartwright et al. 1995, Kim et al. 2000).

Figure 44 illustrates several fault growth models:

(a) Constant d_{max}/L-ratios are usual for small, isolated faults.
(b) Filbrandt et al (1994) suggested that d_{max}/L-ratios change significantly during the early stages of fault growth.
(c) Walsh et al. (2002) gave an alternative fault growth model, in which the fault length stays constant for much of the duration of faulting. They suggest that a progressive increase in displacement-length ratio may reflect a fault system maturity.
(d) A “fault linkage model” demonstrates fault development due to the linking of earlier isolated faults which then produce additional fault length (Peacock & Sanderson 1991; Cartwright et al. 1995; Kim et al. 2000)

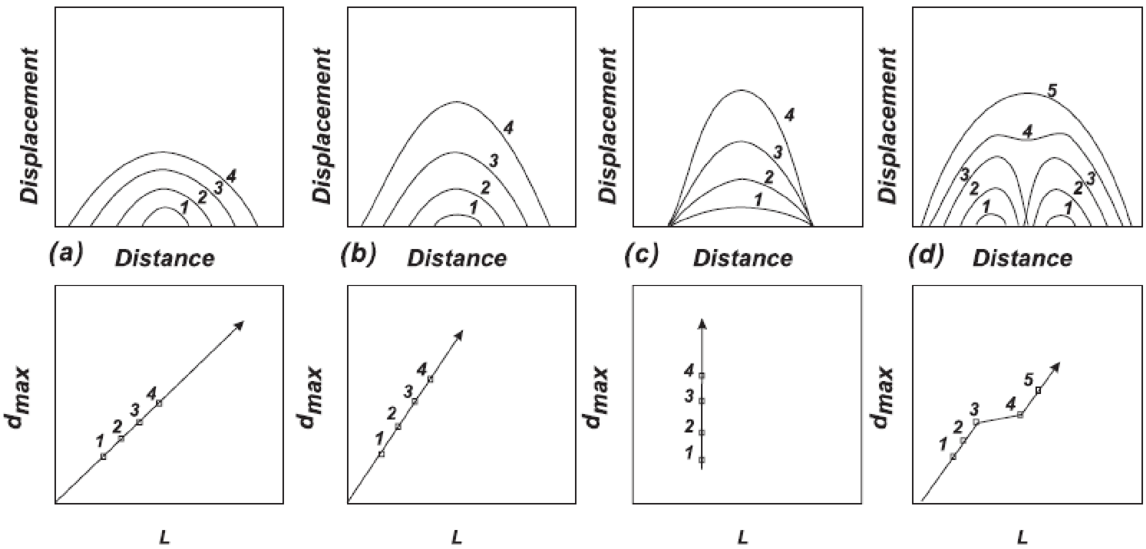

Fig. 44: Fault growth models (Kim & Sanderson 2005 after Filbrandt et al. 1994 (b), Walsh et al. 2002 (b), Peacock & Sanderson 1991; Cartwright et al. 1995 and Kim et al. 2000 (d))

Peacock and Sanderson (1991) identified three stages in the growth of linked fault segments:

1) The tips of isolated faults propagate towards each other (stage 1)
2) Faults overlap and affect each other without forming any obvious connection (soft linkage-stage).
3) Faults link by breaching across the rocks in the relay zone (hard linkage-stage).

Both the hard and soft linkage-stages attain high d_{max}/L-ratios.

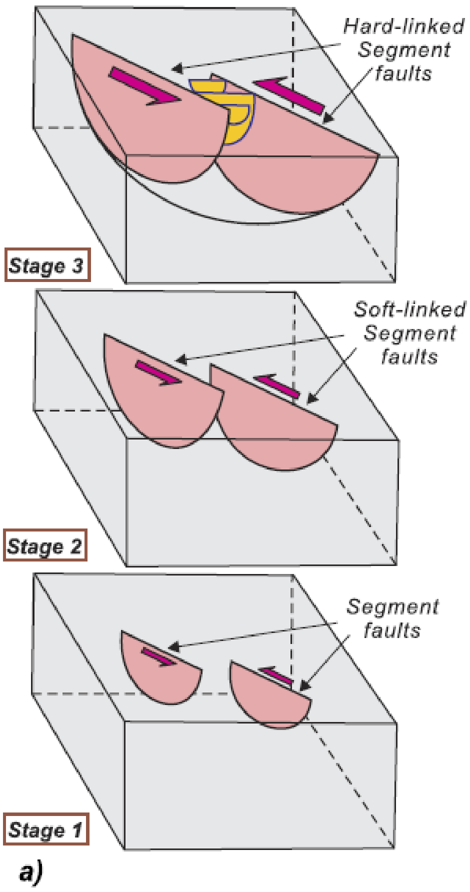

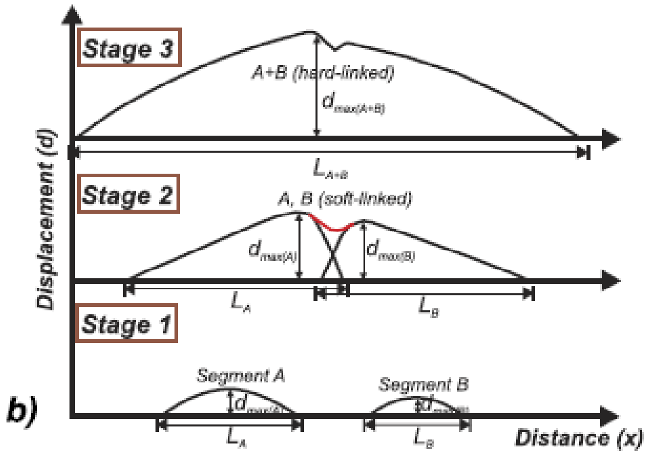

Fig. 45 (top): d_{max}/L-ratios for different stages of fault-linkage (Kim & Sanderson 2005).

Fig. 46 (left): Development of fault-linkages (Kim & Sanderson 2005).

4.2.3.2. Displacement gradient

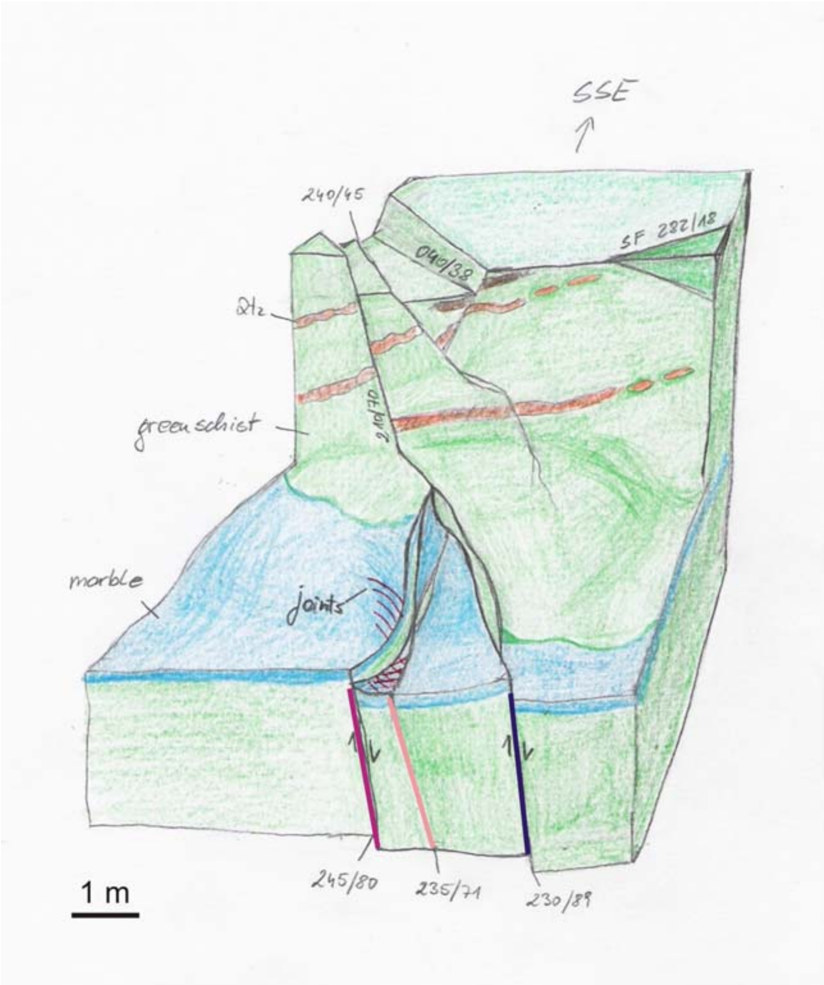

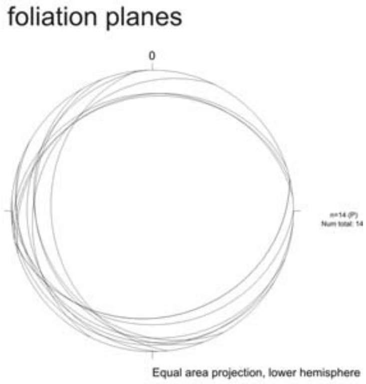

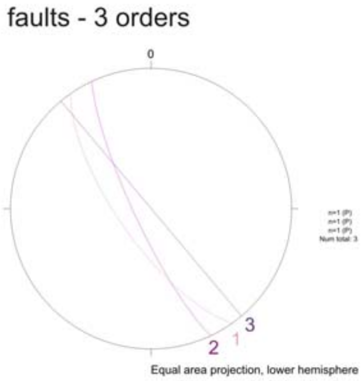

Fig. 47 (left): Field-sketch of outcrop number 27 at Kastellakia Bay (south of Pisses). Faults show cross-cutting relationships, offsets of quartz and marble layers show different displacements.
Fig. 48 (upper right): Foliation planes reveal a gentle dome and basin structure.
Fig. 49 (lower right): Fault planes intersect each other. Colours and numbers refer to successively developed faults.

In general, due to the lack of marker horizons in greenschists, offsets could only rarely be observed. However, one outcrop (number 27) at Kastelakia bay in the south of Pisses shows a clear displacement of quartzofeldspathic and marble layers lying within greenschists in bands of a few cm in thickness. Foliation planes form a gentle dome-and-basin shape (fig. 48). Fig. 47 and 49 demonstrate a development of NW-SE striking faults that transect each other and show a continuous development in terms of dip-angle. The successively developed fault planes change from a 71° to an almost perpendicular dip-angle.

On fault 2 (seen above) the fault length and several displacements could be measured. Fig. 50 shows one part of the fault, fig. 51 shows the displacement distribution over the whole length of the fault with a calculated displacement gradient of 0,082 ≈ 10^{-1}.

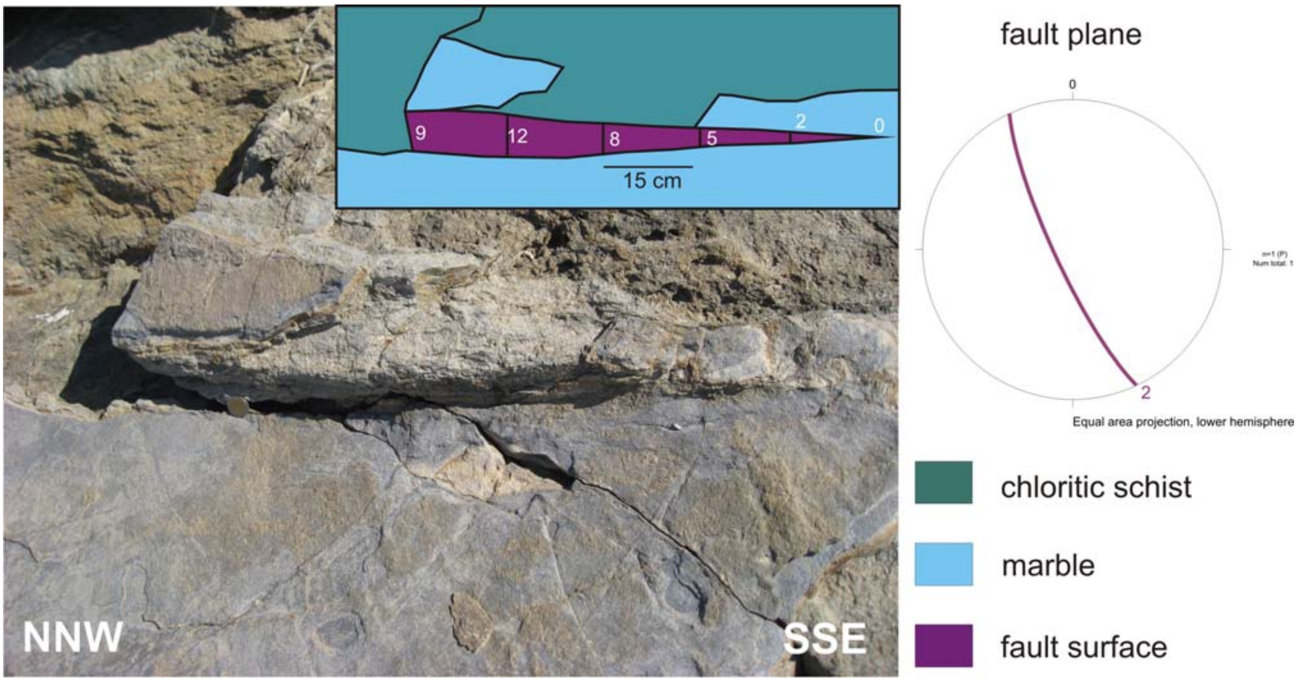

Fig. 50: Displacement distribution along a NNW-SSE striking fault. Outcrop number 27.

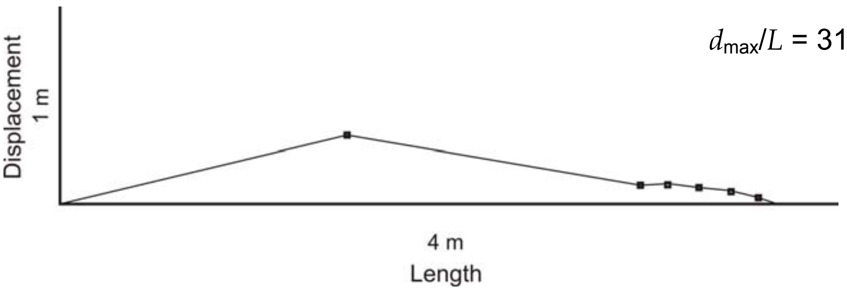

d_{max}/L = 31/375 = 0,082 ≈ 10^{-1}

Fig. 51: Displacement/vertical length profile of the fault shown in fig. x:

It is generally recognised that d_{max}/L-ratios are scale-invariant (Cowie & Scholz 1992b; Dawers et al. 1993; Anders & Schlische 1994; Dawers & Anders 1995) shown in fig. 52.

The measured displacement gradient (shown as the red square in fig. 52) is typical of a geological fault. However, since the fault systems originated at the brittle-ductile transition zone it can be assumed that the faults developed with a constant length in the early stages with increasing displacement and thus should plot vertically between the earthquake rupture data line (ca. 10^{-4}) and natural fault data line.

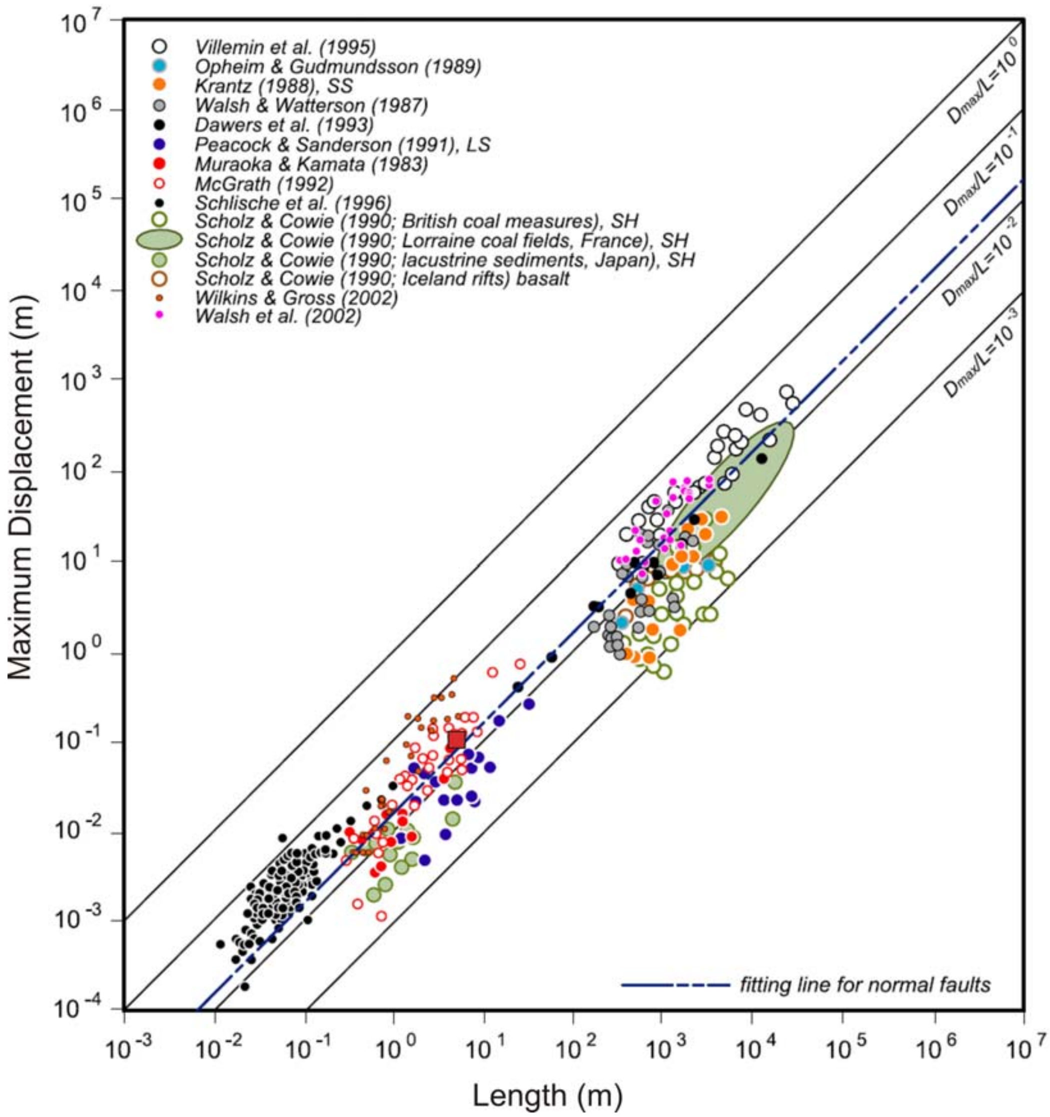

Fig. 52: Plots of maximum displacement (d_{max}) against fault length (L) in normal faults (modified after Kim & Sanderson 2005). The red square shows the position of the calculated displacement length scaling.

Fig. 53: Fault linkage in greenschist with cemented fault gaps. Outcrop number 29.

Fig. 54: Fault linkage in marble. Outcrop number 20.

4.2.3.3. Extension

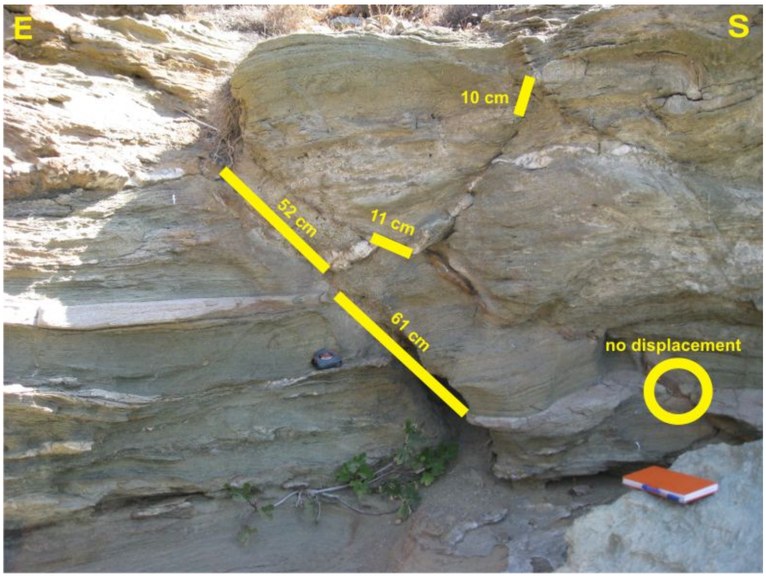

Fig. 55: Various offsets of quartz layers within greenschist. Outcrop number 27.

Small offsets (max. 60 cm), coupled with rather steeply dipping faults at a spacing of about 4 m indicates the extension is not higher than 2 – 3 %.

4.3. Micro-analyses

4.3.1. Mineral assemblage and deformation conditions

The mineral assemblage of the pelitic schists, which showed only slight differences over the whole area, mainly consists of white mica, quartz, feldspar (albite), chlorite, calcite, and occasionally apatite. SEM analyses (chapter 4.3.2) further show inclusions of rutile in muscovite and chlorite and of pyrite and chlorite within quartz. These mineral assemblages are characteristic for greenschist facies metamorphic conditions. The high amounts of calcite and quartz probably reflect a partially carbonate-rich (marl) sedimentary protolith. In general, the rocks are fine-grained but show also feldspar porphyroclasts wrapped around by the foliation that suggest a retrograde overprinting of higher-grade metamorphic rocks. These two metamorphic events directly reflect two of the major metamorphic events characteristic of the Cyclades Blueschist Unit:

1) Synorogenic subduction of the Pindos ocean unit, causing high-pressure – low-temperature conditions during the Eocene (M1).

2) Postorogenic large-scale extension along low-angle normal faults causing a greenschist-facies overprints of M1 high-pressure rocks in Oligocene and Miocene times (M2).

Distinct shear-sense indicators such as rotated clasts and SCC'-fabrics consistently point to a top-to-SW movement (fig. 56, 57).

In the following text, three abbreviations have been used to describe the figures:

ppl: plain polarised light,

xpl: crossed polarised light,

stp: shows the usage of a gypsum sensitive tint plate

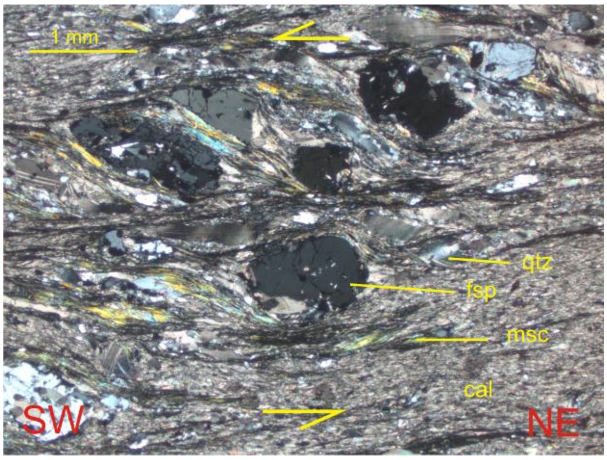

Fig. 56: Calcite mylonite with very fine grained calcite and feldspar porhpyroclasts; SCC'-fabrics and sigma-clasts clearly reveal dextral shear sense; a quartz crystal in the middle left shows subgrains (xpl). Outcrop number 4.

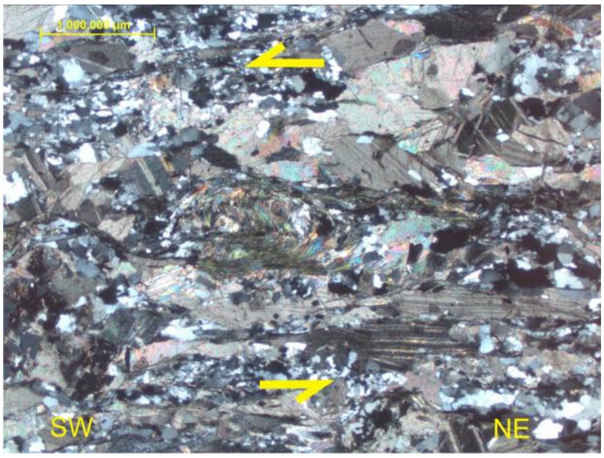

Fig. 57: Mylonitic carbonate schist with different kinds of deformation twins. Mica shows an overprinting of an earlier foliation (top-to-SW). Outcrop number 5.

Temperature estimations for deformation conditions were made with the following parameters:

Insertion: Microstructures

Intracrystalline deformation:

Crystals normally accommodate/possess 'errors' in their crystal lattices. These lattice defects can be divided into point defects and line defects/dislocations. In such defects, positions in the lattice can be either vacant or filled with extra lattice points (atoms or molecules). During ongoing deformation, the lattice defects move within a crystal by mechanisms such as dislocation glide and dislocation creep, without causing brittle fracturing. These processes result in **undulose extinction** and the formation of a **lattice preferred orientation (LPO)**.

Undulose extinction denotes that crystals extinguish inhomogeneously.

LPO occurs when dislocations move in a specific direction through the crystal and thus create a uniform crystallographic orientation for a particular mineral.

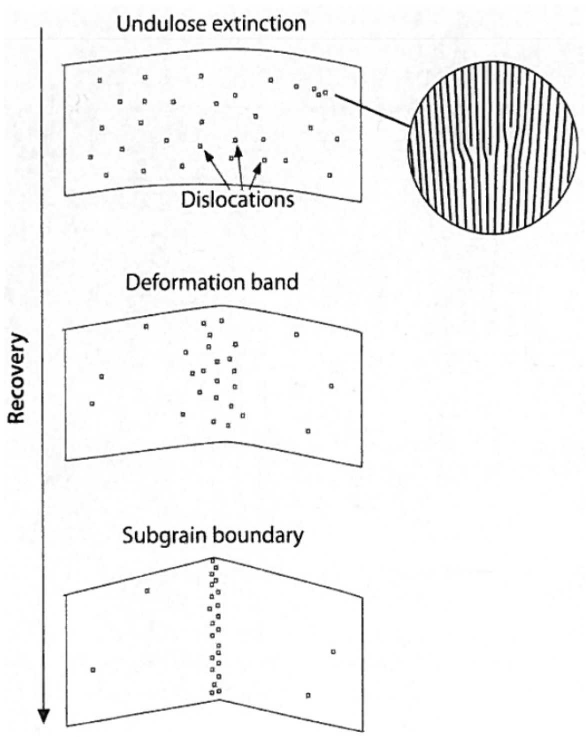

Fig. 58: Dislocation densities in minerals (Passchier & Trouw, 2005)

When a stress acts on a mineral, the dislocation density increases. But there are also processes that reduce the dislocation density (**recovery**). During this recovery process, dislocations can be grouped into regular planar networks (subgrain boundaries). These subgrain boundaries can form within a host grain or between adjacent grains and separate two crystal fragments that have rotated slightly with respect to each other. In thin-sections, subgrains can be recognised as parts of a crystal that are separated from adjacent parts by discrete, sharp, low relief boundaries with slightly different but homogenous extinction orientations (Passchier & Trouw, 2005).

Twinning

Some minerals tend to form deformation twins in addition to undergoing dislocation creep and glide. Primarily calcite and plagioclase generate deformation twins, mostly under lower temperature deformation conditions, forming wedge-shaped or tabular twins in contrast to the straight and stepped habit of growth twins. The geometry of deformation twins, which operate in specific crystallographic directions, has been proposed as indicators of the temperature of deformation (Fig. 59).

Calcite twinning, in particular, provides one of the most promising temperature gauges since the crystal-plastic deformation in calcite is mostly by mechanical e-twinning at temperatures below 400 °C (Groshong 1988).

Narrow straight twins suggest temperatures below 200 °C (Type I). Wider twins dominate above 200 °C, up to 300 °C (Type II). Increasing strain at temperatures below 170 °C rather leads to growth of new twins and then widening of older ones. Above 200 °C, pre-existing twins generally tend to widen. At temperatures above 200 °C twins may also show intersection or bending (Type III). Above 250 °C, twin boundaries form a serrate shape (Type IV).

It has to be noted that twinning can accommodate only a limited amount of strain so that additional strain can provoke pressure solution, dislocation creep or recrystallisation (Passchier & Trouw 2005; Burkhard 1993).

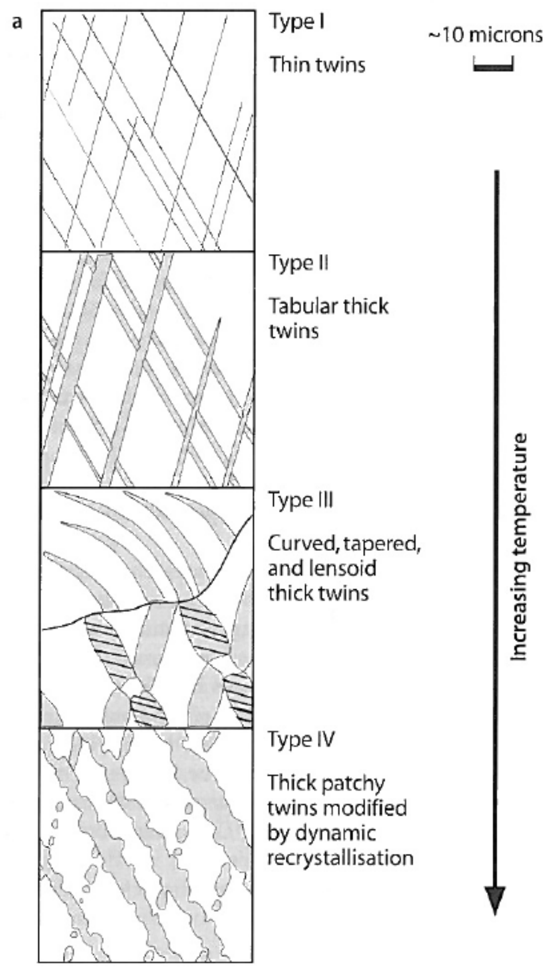

Fig. 59: Different types of deformation twins in calcite and relative temperature estimation (Passchier & Trouw, 2005)

Dynamic recrystallisation:

Besides recovery, another process causes a reduction in dislocation density in deformed minerals: **grain boundary mobility**. If two neighbouring minerals possess different dislocation densities, a local displacement of the grain boundary may occur. In that case, the mineral with the lower dislocation density (the less deformed mineral) grows at the expense of the mineral with the higher density (the more deformed mineral). This process results in a **recrystallisation** and therefore mainly affects changes in grain size, shape and orientation within the same mineral.

There are three kinds of mechanisms of recrystallisation. Which of these occurs depends on the temperature and strain rate:

Bulging (BLG) recrystallisation: At low temperatures, grain boundary mobility causes the formation of new, small grains mostly along the boundaries of old grains. This process is also known as **low-temperature grain boundary migration**.

Subgrain rotation (SGR) recrystallisation: When dislocations in a crystal are relatively free to climb from one lattice plane to another, they may move continuously to subgrain boundaries. This causes an increase in the angle between the crystal lattice on both sides of the subgrain boundary. Progressive subgrain rotation then generates a new grain.

High-temperature grain boundary migration (GBM) recrystallisation: At relatively high temperatures, grain boundary mobility removes dislocations and possibly subgrain boundaries by sweeping through entire crystals. Grain boundaries then develop a lobate shape.

Fig. 60: The three main types of dynamic recrystallisation and their relation depending on temperature and strain rate (Passchier & Trouw, 2005).

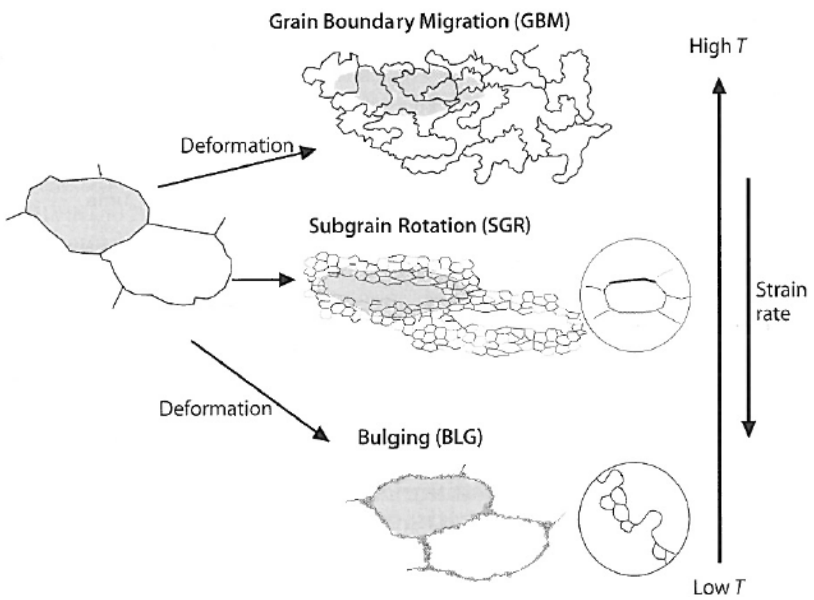

Different minerals deform under different strain rate and temperature conditions. The figure below shows some minerals and their deformation conditions.

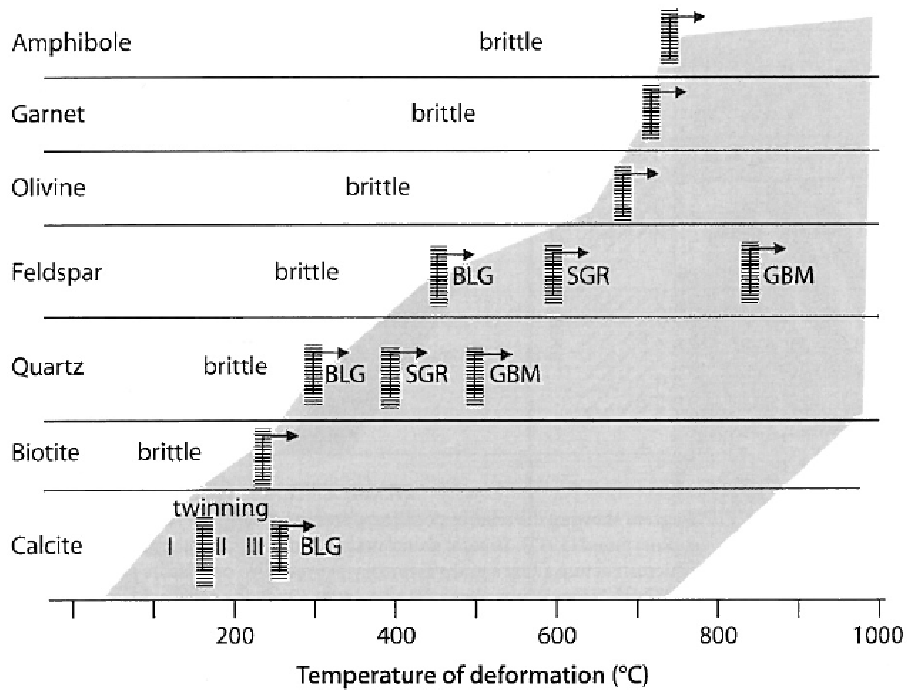

Fig. 61: Temperature dependence of the main types of dynamic recrystallisation for different minerals. Bars show transition zones, arrows indicate the effect of strain rate. The greyish domain reveals the domain of plastic deformation. (Passchier & Trouw, 2005)

In the samples studies, quartz grains generally show undulose extinction and usually also subgrain formation (fig. 66). Sutured grain boundaries show evidence for grain boundary migration (GBM) which suggests a deformation temperature at >450 °C. Quartz is also sometimes cracked, indicating later deformation at temperatures below ca. 300° C.

Calcite generally shows deformation twins. Calcitic mylonites (fig. 62) contain almost all kinds of deformation twins. They show partly very thick twins, which are often tabular shaped (fig. 64) and tapered as well (fig. 65). The deformation conditions for calcite therefore are estimated at around 200 – 300 °C.

Feldspars are generally cracked, demonstrating that M2 deformation temperatures definitely lay below 450 °C (fig. 63).

All the parameters together suggest a deformation temperature at around 300 to < 450 °C.

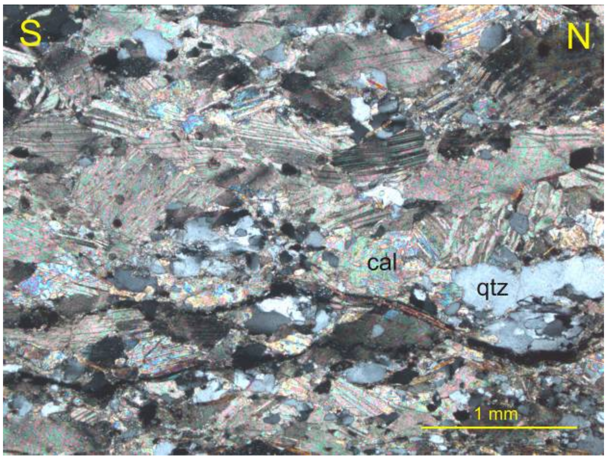

Fig. 62: Calcite mylonite with several types of deformation twins; quartz shows undulose extinction and low temperature bulging (xpl). Outcrop number 15.

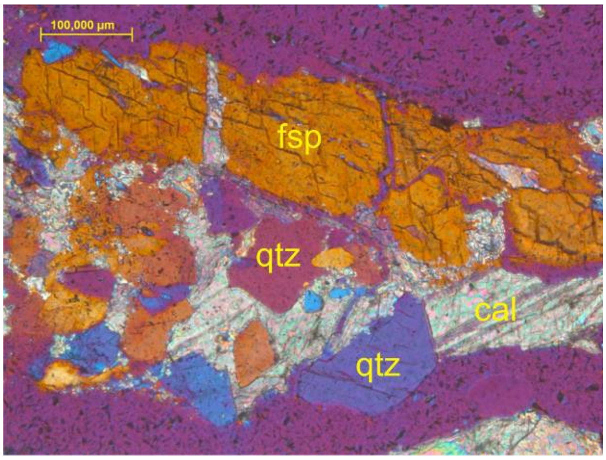

Fig. 63: Part of a calcite mylonite with cracked feldspar; the three orange coloured feldspar grains reveal that they once formed a single grain that has been broken and separated by brittle deformation (detail from fig 62), xpl & stp.

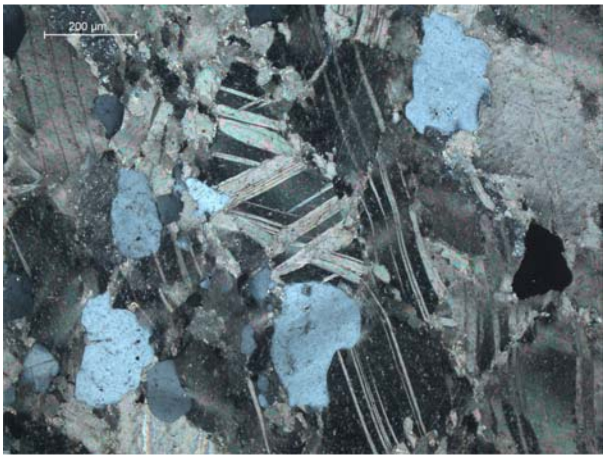

Fig. 64: Tabular thick twins in calcite (Type II), as well as tapered and gently bent twins (Type III); detail from fig. 62 (xpl).

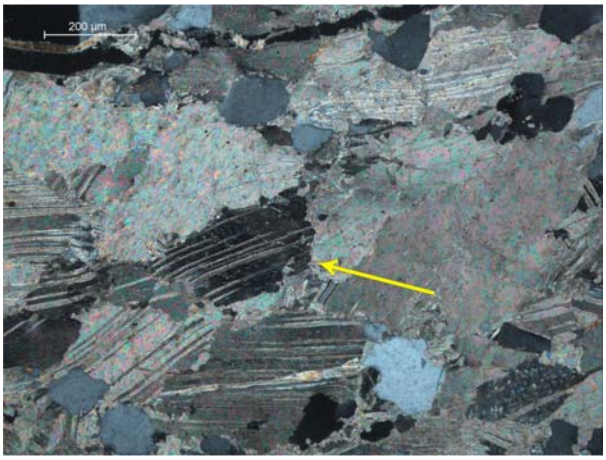

Fig. 65: Tapered, slightly curved twins in calcite (detail from fig. 62), xpl.

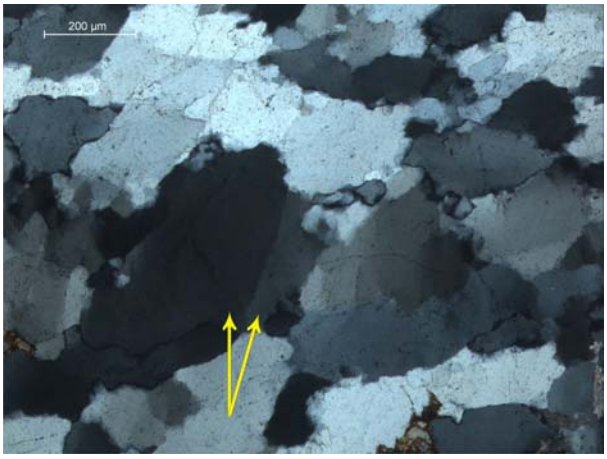

Fig. 66: Quartzite layer (within a carbonate schist); quartz shows undulose extinction, subgrain formation and grain boundary migration, yellow arrows point to two subgrains separated by a sharp subgrain boundary (xpl). Outcrop number 13.

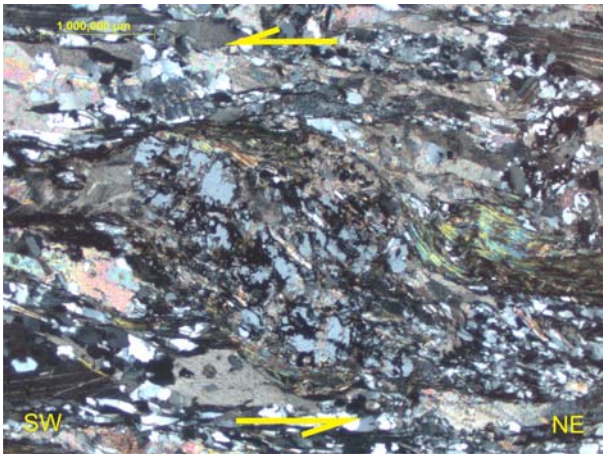

Fig. 67: Delta clast with a top-to-SW shear sense; the clast is a highly altered feldspar grain (xpl). Outcrop number 12.

4.3.2. Faults and fluids

In the following chapter, high-angled fractures, faults and veins are analysed in terms of their microstructural development and interaction with through-going fluids.
Depending on the origin of the fractures and faults, three types of crack-propagation can be distinguished (fig. 68).

Mode I: opening mode, where a tensile stress acts normal to the plane of the crack, with no shear stress
Mode II: sliding mode, where a shear stress acts parallel to the plane of the crack and perpendicular to the crack front
Mode III: tearing mode, where a shear stress acts parallel to the plane of the crack and parallel to the crack front

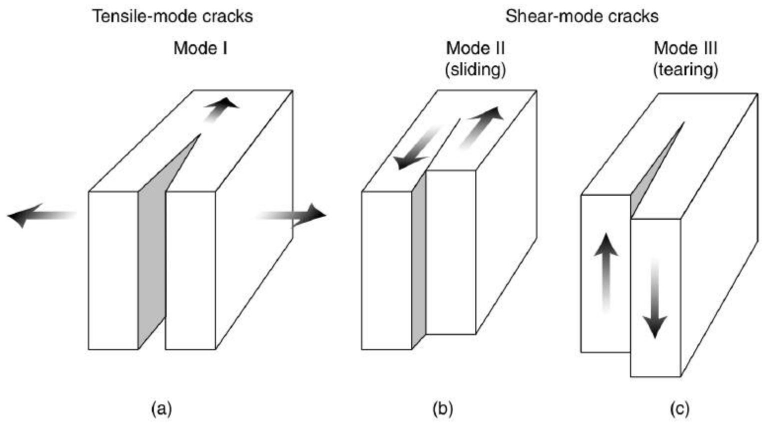

Fig. 68: Three types of crack propagation

In the field, most of the high-angled fractures were filled with carbonate cements and characterised as potentially mode I cracks due to the scarce evidence for an offset and the lack of a cataclasite. However, thin-section analysis (see below) showed clear evidence of fault development by shearing, since cataclasites do occur within most of the fractures. The width of the faults was very narrow, with openings of 0 to a few cm. At only one outcrop, in marble to the north of Pisses, was the gap wider, up to 60 to 70 cm (fig. 34). The fillings of the gaps mainly consist of calcite, ankerite, quartz and dolomite. Microstructural fault developments are described on some samples below.

Fig. 69 (left): Polyphase fluid-filled fractures in marble. Outcrop number 1.

Fig. 70 (top): Polyphase fluid/cement-filled, brittle faults in greenschists. Cross-cutting relationships reveal alternating activity on both faults. W-E striking fracture cuts through a NW-SE striking fault which was then by the E-W fault ductiley deformed. Outcrop number 4.

<u>Sample KM3a (outcrop number 12)</u>

Fig. 71 shows a typical example of a polyphase mode II crack with different generations of syntaxial cement growth. The figure shows only one half of the crack-fill vein, with the host rock on the right side. In thin-section and the SEM, this shows a complex growth history (1-5):

1) In the first stage, brittle deformation produced a fine-grained ultracataclasite that consists of host-rock material. A small part of this was analysed by chemical mapping with the SEM; this reveals deformed quartz and muscovite. Since muscovite cannot easily deform due to the crystal texture, the muscovite must have grown together with quartz and both are derived from the host-rock (fig. 72). A noticeable feature of the quartz-rich ultracataclasite is an optically preferred orientation of the quartz grains, seen with a sensitive tint plate.

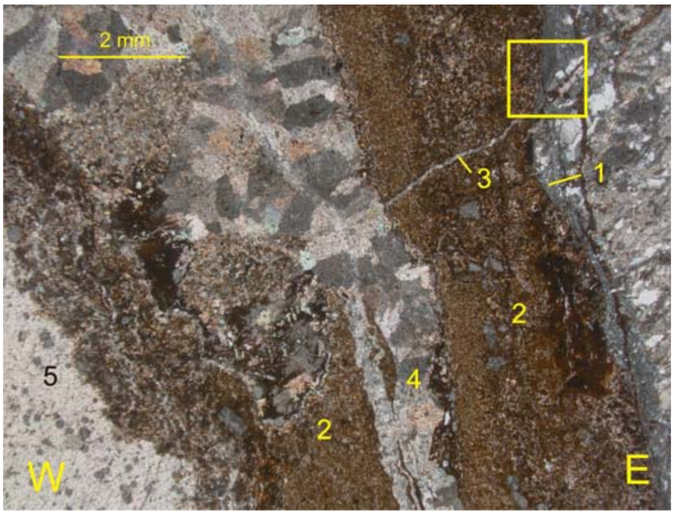

Fig. 71: Polyphase mode 2 crack (xpl)

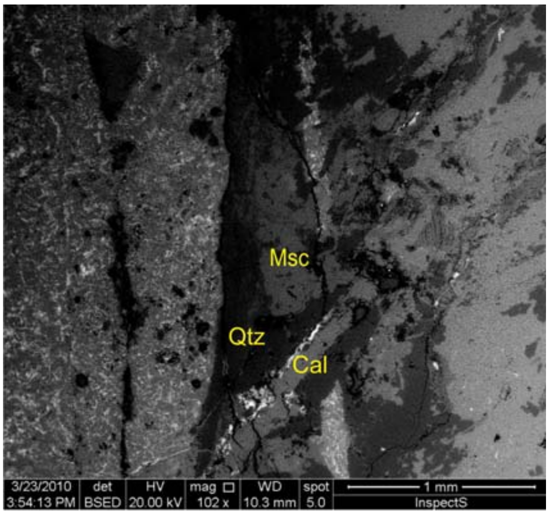

Fig. 72: BSE-image of an ultracataclasite (detail from fig. x)

2) In the next stage, fracturing partly transected the ultracataclasite and was filled with an ankeritic fluid.
3) Subsequently, a low-angle, brittle fracture cut through the earlier two phases.
4) Carbonate-rich fluids within holes in the rock led to calcite crystallisation within the ankeritic cement and also partly reworked it. Where there was enough space, calcite formed palisade shaped crystals (fig. 74). The inner part of the calcite vein shows a periodic fracturing and subsequent sealing known as crack-seal growth (Ramsay, 1980), demonstrated by offset calcite minerals of the same crystallographic orientation (fig. 76).
5) The final fluid generation consists of calcite. Idiomorphic crystals were formed and show very narrow deformation twins (fig. 75).

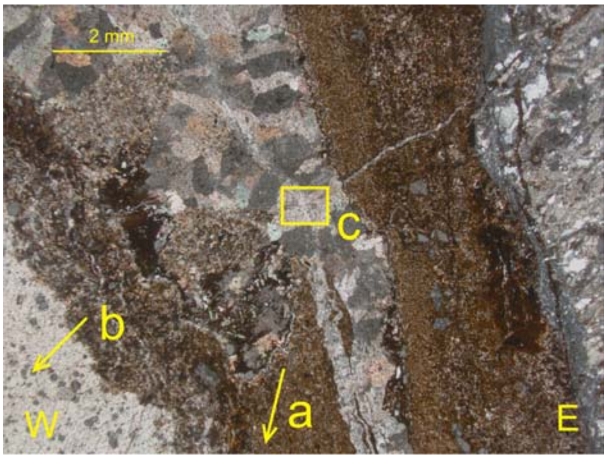

Fig. 73: KM 3a; areas marked with small letters are shown in detail in figures 74, 75 and 76 (xpl).

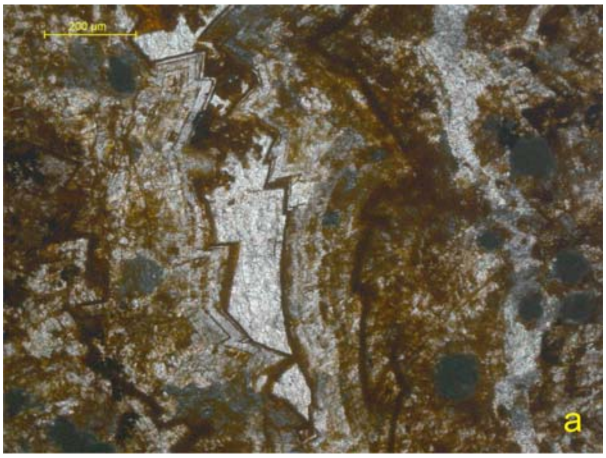

Fig. 74: Ankeritic and calcitic fluids forming palisade shaped crystals (xpl)

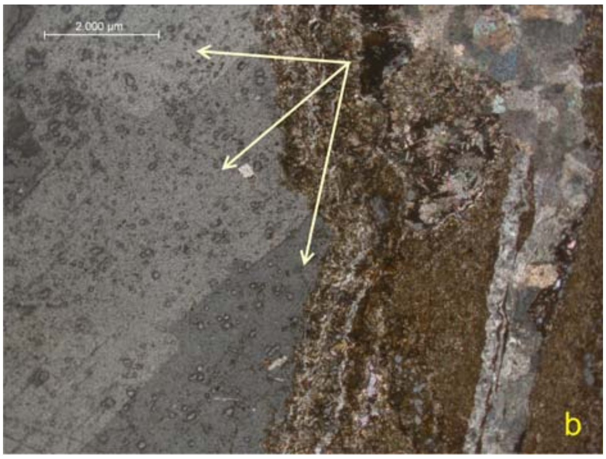

Fig. 75: Idiomorphic calcite crystals (xpl).

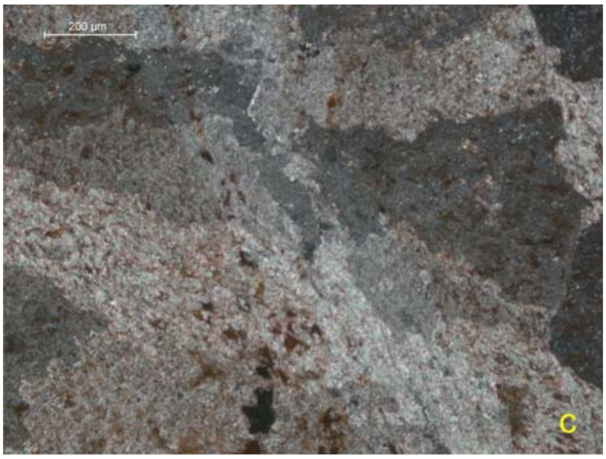

Fig. 76: Crack-seal mechanism within calcite vein (xpl).

<u>Sample KM16 (outcrop number 29)</u>

Sample KM 16 shows a mode I crack that is filled with crystals deposited by successive carbonate-rich fluids during a polyphase evolution. Four generations of crystallisation can be distinguished:

1) At first a calcitic fluid crystallised out, forming large grains. Subgrains and narrow straight deformation twins reveal ductile deformation at low temperatures. Cracks show a brittle overprint (fig. 79).
2) A dolomitic fluid led to the formation of palisade-shaped dolomite crystals. Zoned crystals were observed using SEM-analysis. Different grey shades refer to different amounts of Mg and Ca as well as Fe (fig. 81).
3) Another dolomitic fluid led to the crystallisation of very fine dolomite grains.
4) In the last stage, an Fe-rich fluid deposited ankeritic as zoned idioblastic crystals.

In general, a high amount of Fe was inferred for all generations of fluid crystallisation since CL-images showed almost no luminescence due to the high amount of Fe (Götze 2002).

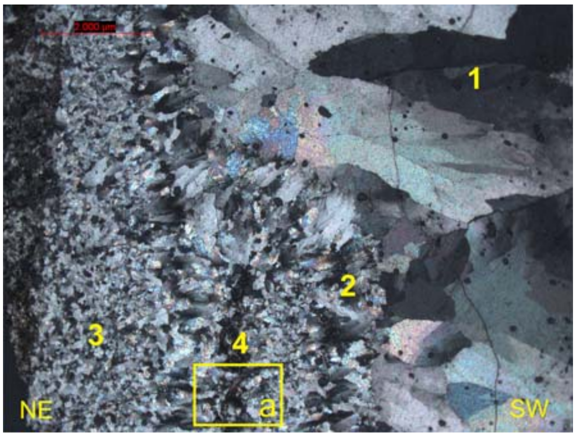

Fig. 77: Polyphase crystallisation of carbonate fluids (xpl).

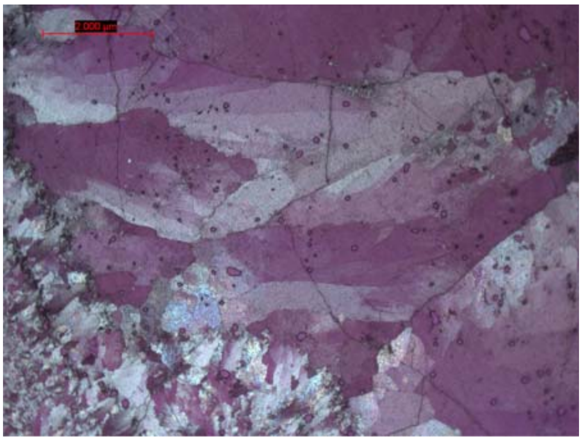

Fig. 78: Subgrains in calcite (stp).

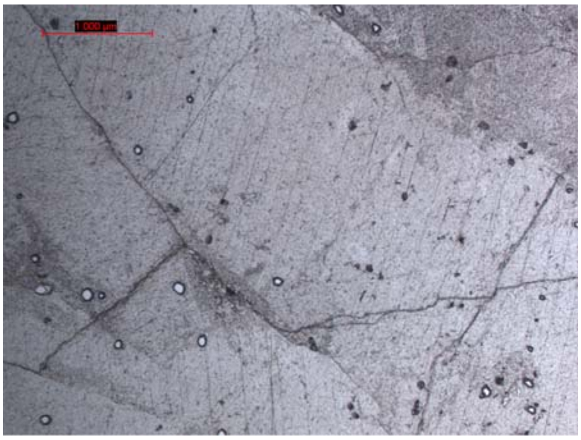

Fig. 79: Low-temperature deformation twins in calcite. Cracks reveal a later brittle overprint (xpl).

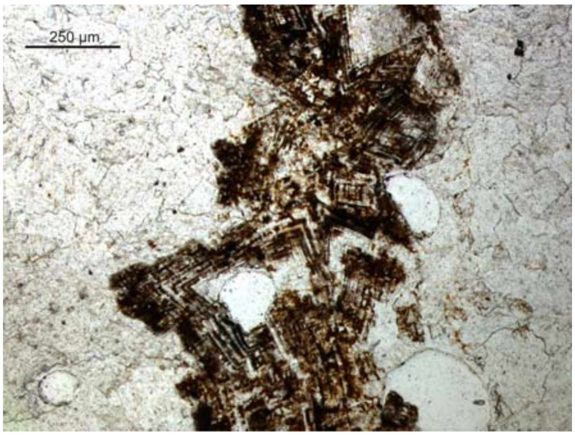

Fig. 80: Zoned ankeritc crystals in a calcite vein (ppl).

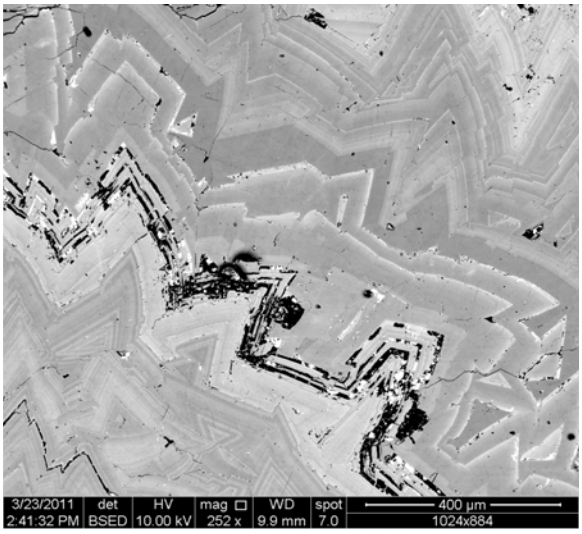

Fig. 81 (left): (BSE-image) Zoning of dolomite crystals. Dark grey refers to dolomite without Fe, mid grey to dolomite with little amount of Fe, light grey to dolomite with higher amount of Fe (chemical maps are shown below in Figs 82-84). The white colour shows calcite, black shows areas where calcite is dissolved.

Chemical composition of dolomites showing very minor differences in the amounts of Fe:

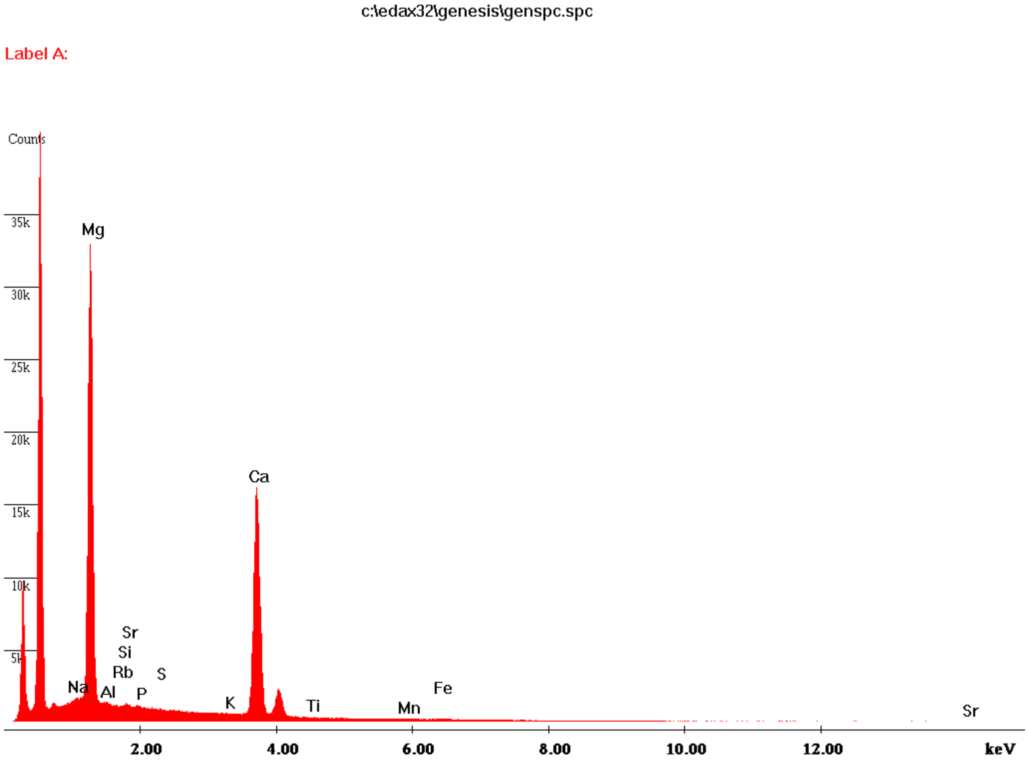

Fig. 82: Dark grey part of the zoning in dolomite in Fig 81.

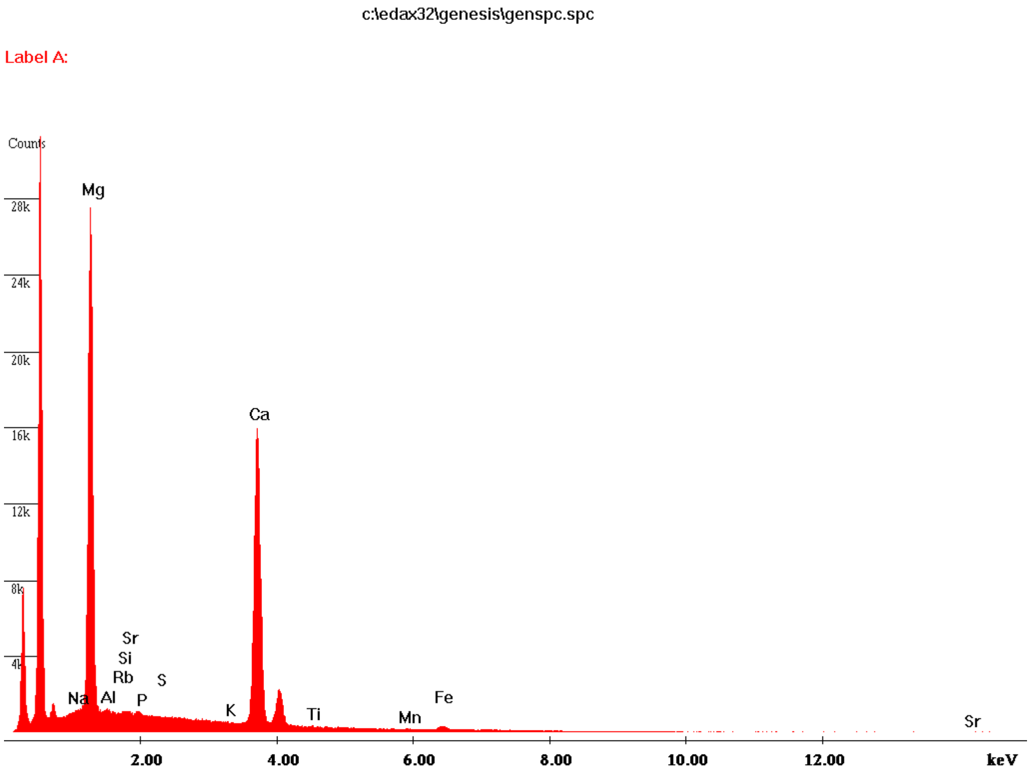

Fig. 83: Mid grey part of the zoned dolomite in Fig 81.

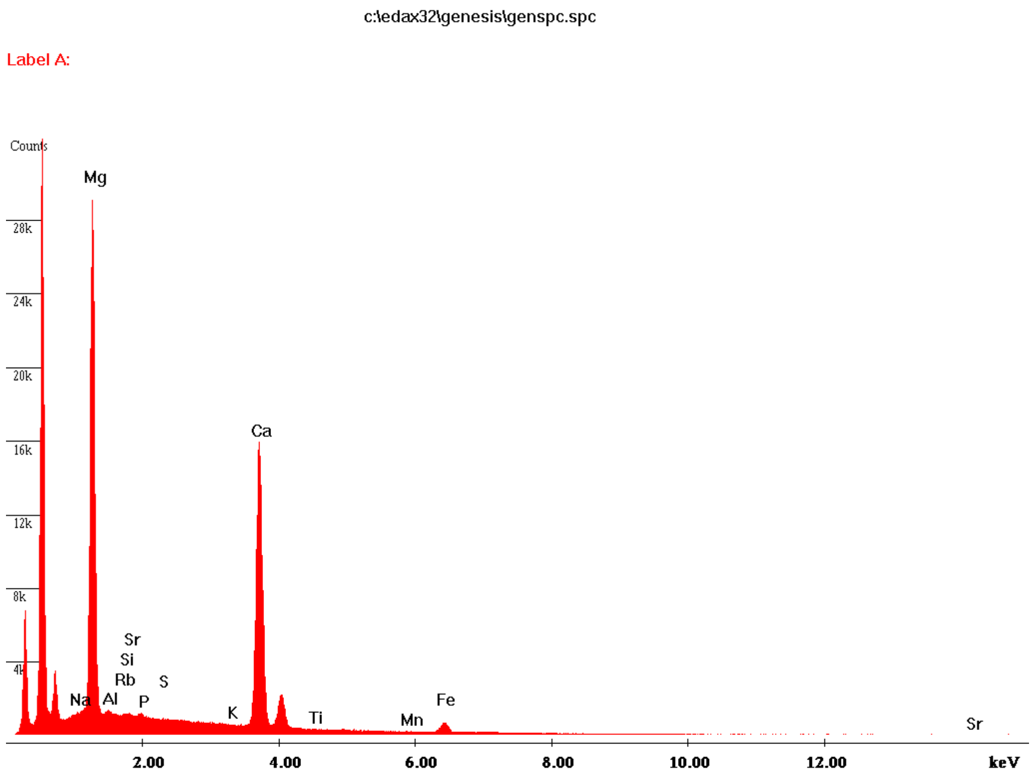

Fig. 84: Light grey part of the zoned dolomite in Fig 81.

Sample KM2b (outcrop number 4)

Sample KM2b is a deformed impure marble with two polyphase mode 2 cracks (fig. 85, 89 and detail pictures). SEM-analyses of thin-section KM2b were made to gain further insights into the general mineral assemblage of the host-rocks (already mentioned in chapter 4.3.1.) and also to characterise the extremely fine-grained cataclastic material within the fault zones. Chemical maps of different minerals are shown in the appendix.

The host-rock mainly consists of fine-grained calcite forming a pressure-solution cleavage. Two different phases of calcite (appendix III) were recognised; these show minor differences in the amount of Fe and Mg concentrations. Light grey calcite contains a higher amount of Fe and Mg compared to darker grey calcite.
Embedded and rotated “left over grains” of quartz and feldspar (fig. 87, 88) within the foliation show brittle deformation, with fragments separated by foliated calcite/mica. The host-rock can therefore be described as a foliated cataclasite.

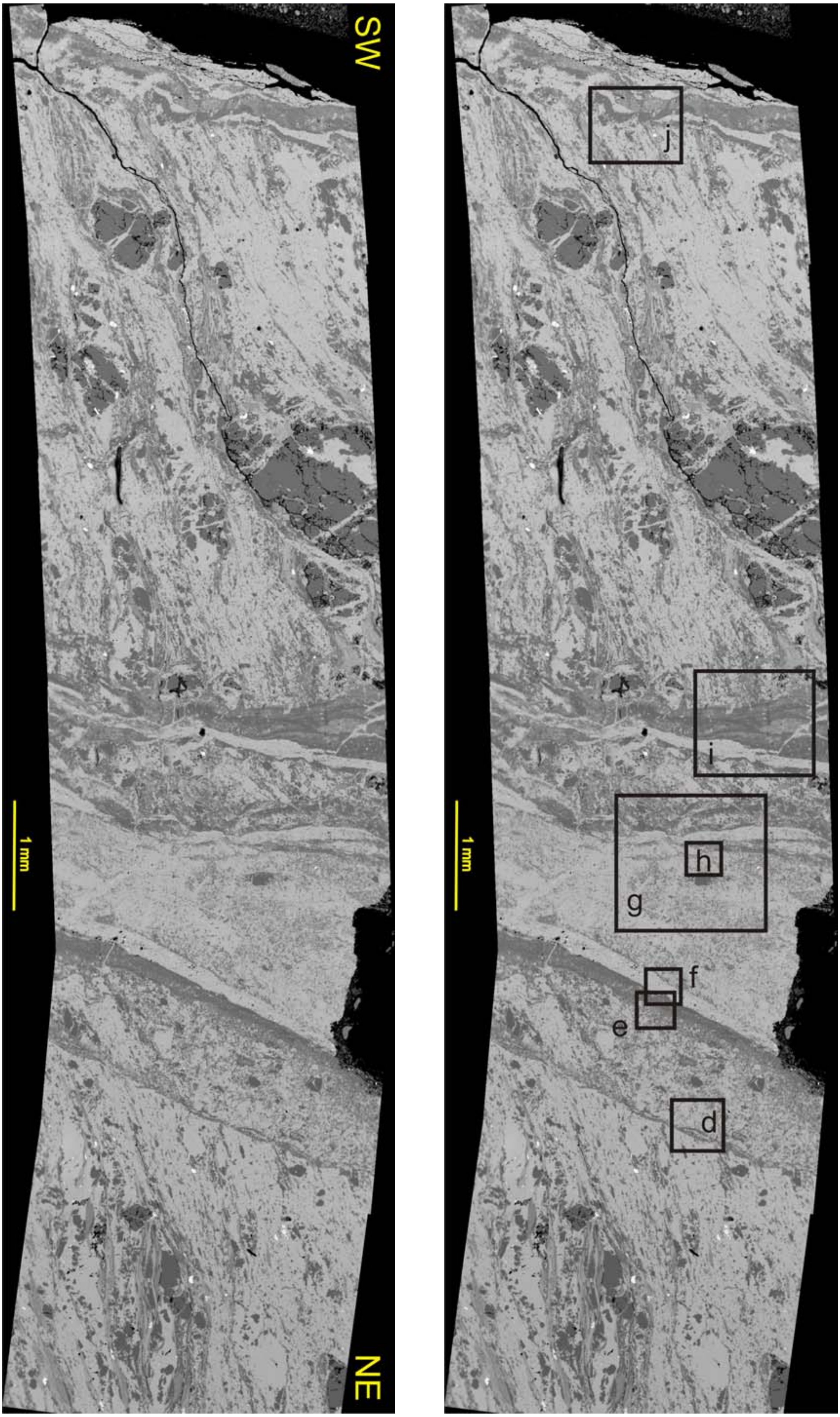
SW
NE
1 mm
1 mm
j
i
h
g
f
e
d

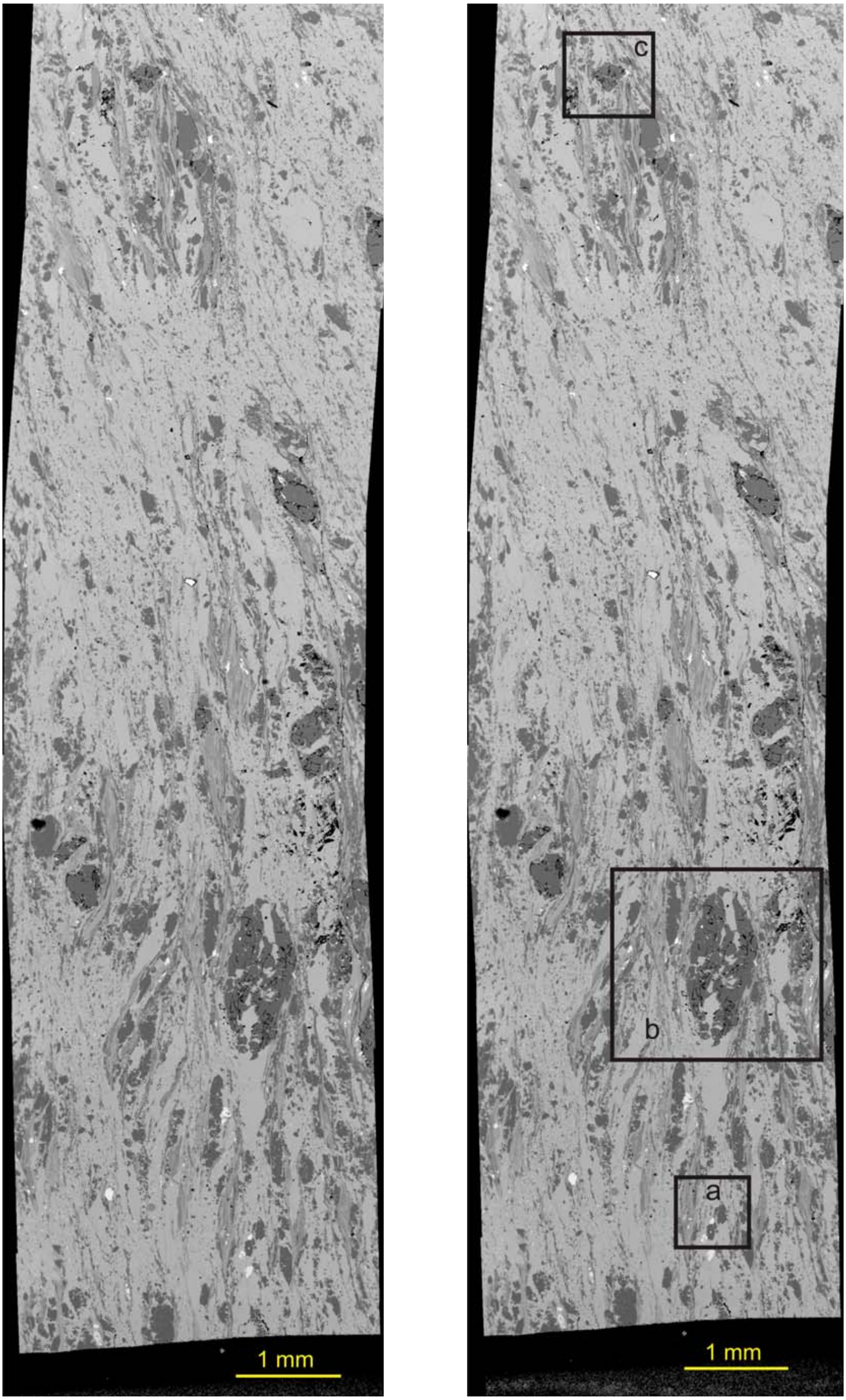

Fig. 85: Profile through sample KM2b (BSE-image); details are shown below.

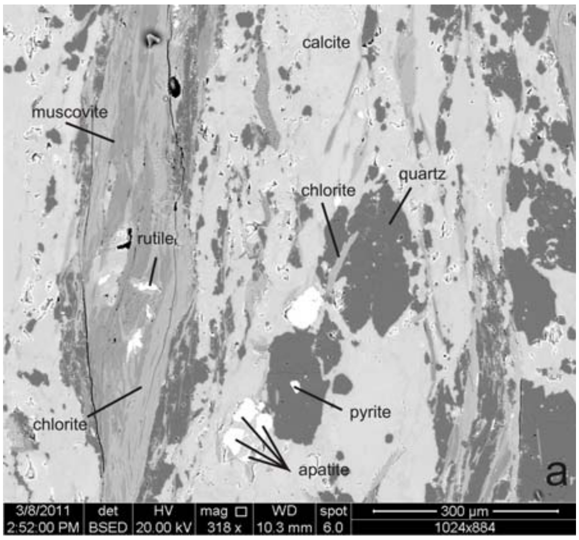

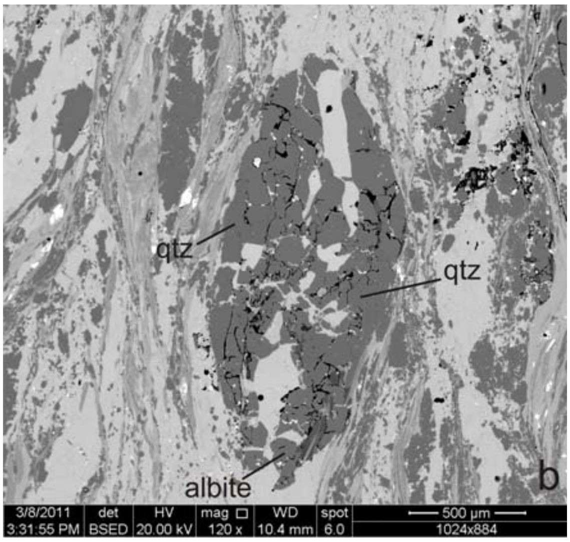

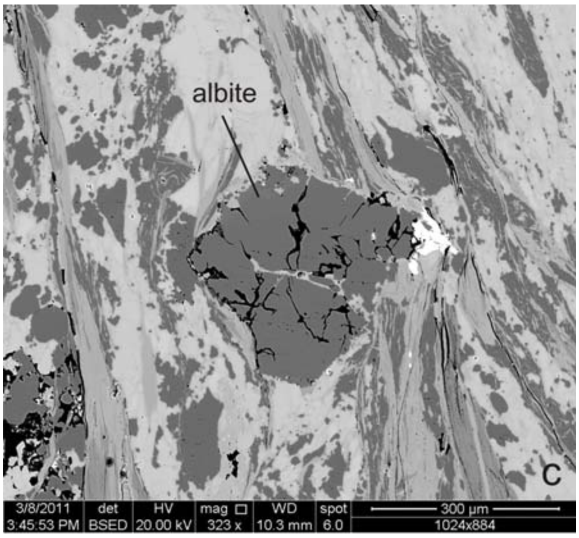

Fig. 86 (top left): Overview of the general mineral assemblage of the greenschists.

Fig. 87 (top right): Broken quartz grains with calcite filling the spaces; the mineral aggregate consists of albite and chlorite.

Fig. 88 (left): Example of cracked and rotated albite porphyroclast overgrowing the foliation and also weakly wrapped around by the main foliation.

Fault zones:

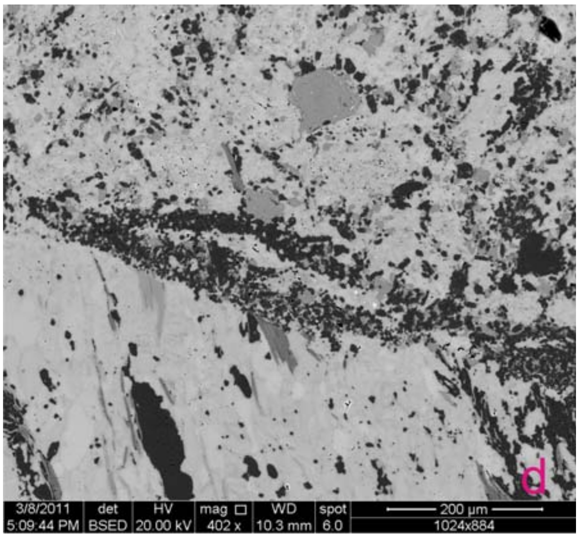

Sharp boundary between host-rock and cataclastic zone. The black grains are quartz.

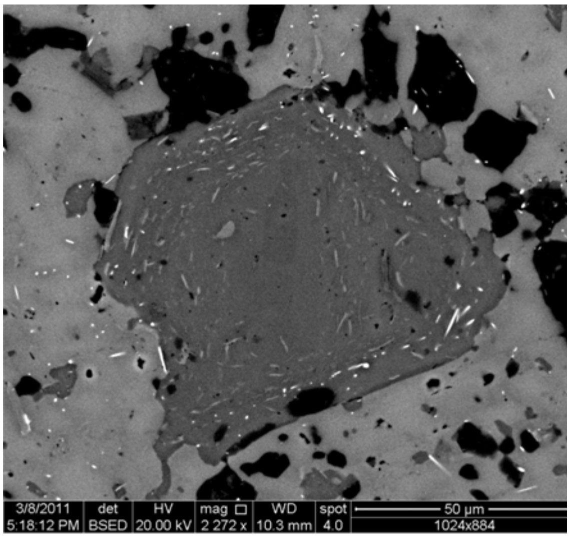

Orthoclase porphyroclast with inclusions. White inclusions comprise rutile, pale grey inclusions are calcite. (detail from the fig. on the left)

Smooth transitions between two ultracataclasites and a quartz vein.

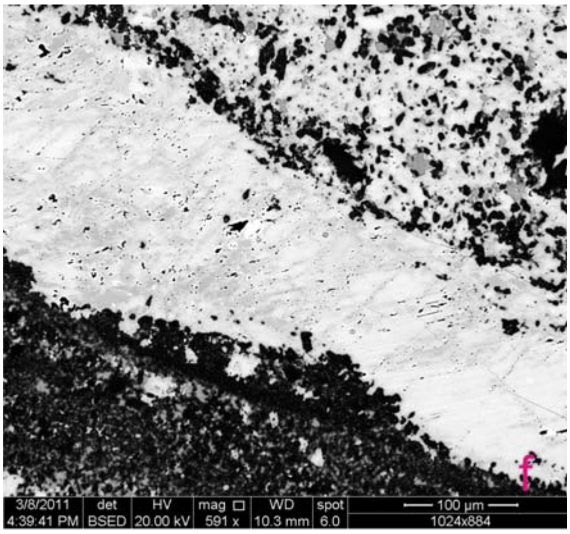

Calcite vein with inclusion trails of quartz showing a “crack seal mechanism”.

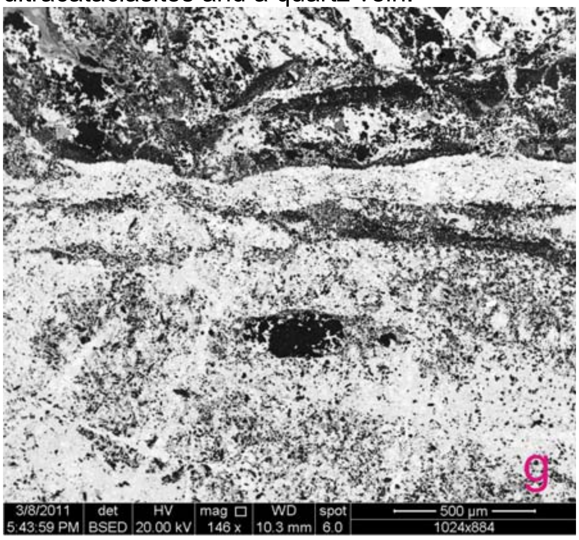

Diffuse transition between a calcite-cemented vein and an ultracataclasite.

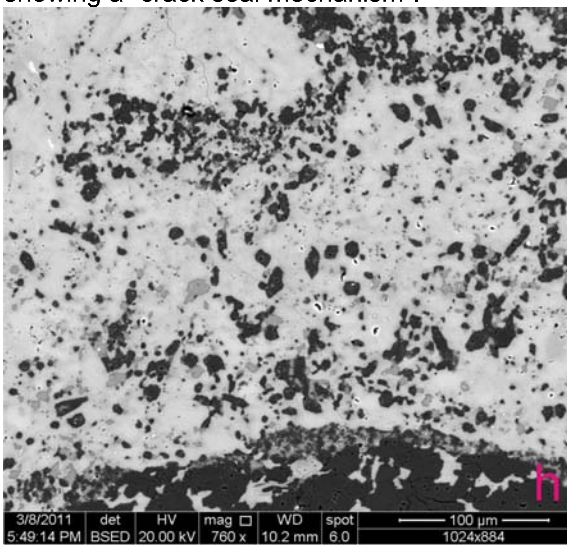

Reworked host-rock material developed by a fault-valve mechanism.

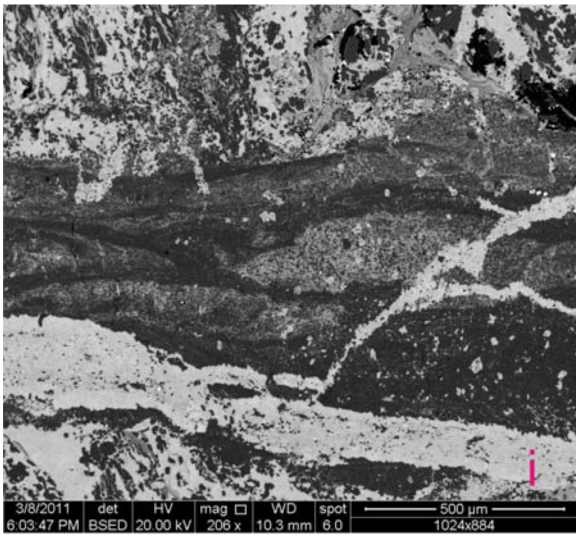

A fine ultracataclasite showing later overprinting by brittle fracturing.

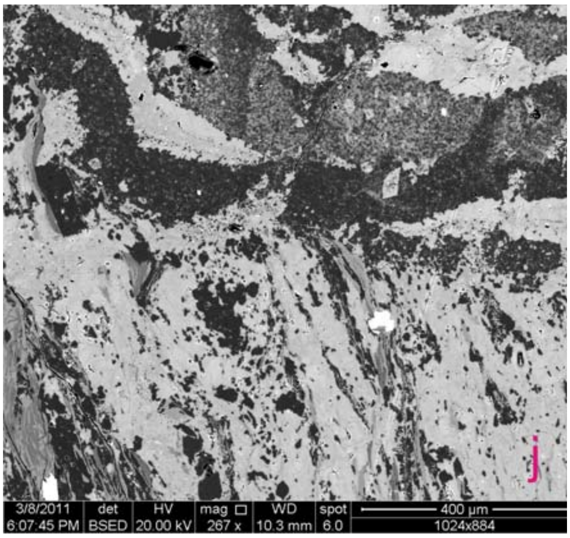

Gradual boundary between the host-rock and the protocataclasite.

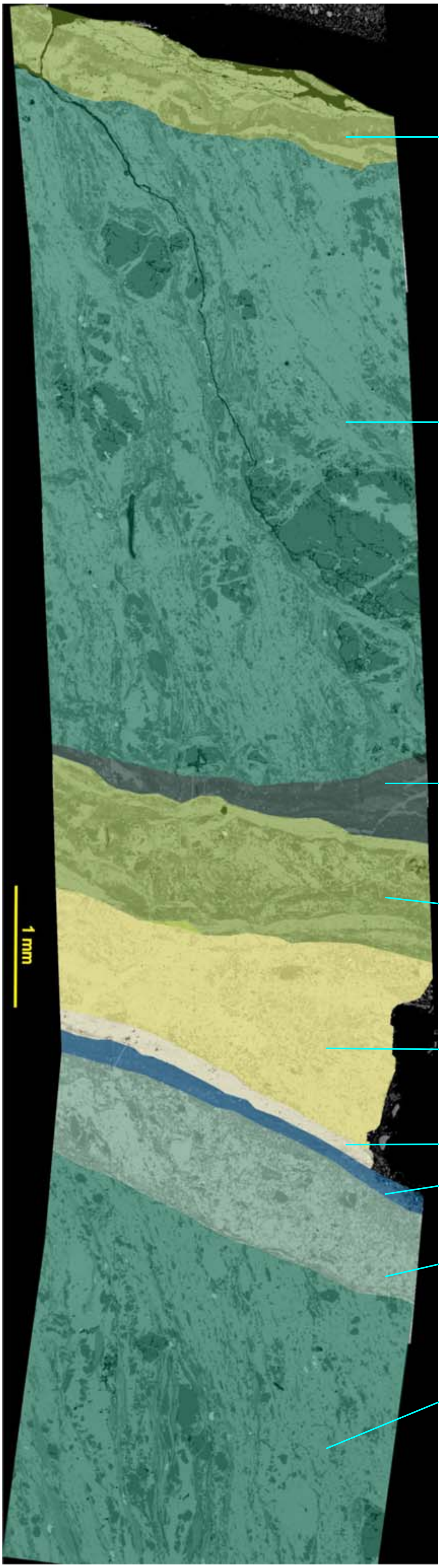

Fig. 89: Profile through sample KM2b, colours highlight different fault generations.

fault 2:

5) protocataclasite

host rock (foliated cataclasite)

fault 1:

6) fine grained ultracataclasite

5) protocataclasite

4) vein developed by fault valve mechanism

3) calcite vein

2) very fine grained, ultracataclastic quartz

1) ultracataclasite

host rock (foliated cataclasite)

Fault 1 shows six different phases of fault development and fluid activity (detailed below, not in chronological order, fig. 85-89):

1) Brittle deformation of the host-rock formed cataclasites that transects the host -rock with sharp boundaries.
2) This is an ultracataclasite that fragmented a large quartz grain and dispersing it along the fault surface. The micro-crystals partly show an optically preferred orientation, recognised with a sensitive tint plate.
3) A calcite vein developed in multiple stages, with inclusion trails of quartz nearly perpendicular to the fault plane, during crack-seal growth (Ramsay, 1980). The calcite vein shows tabular shaped deformation twins seen in both the PPL- and SEM-images, indicating low temperature deformation. The CL-image of the same part reflects at least two different phases of calcite. The higher luminescence is caused by a higher amount of Mn in small calcite grains. A later generation of a calcite-rich fluid led to the growth of bigger grains with lower luminescence.

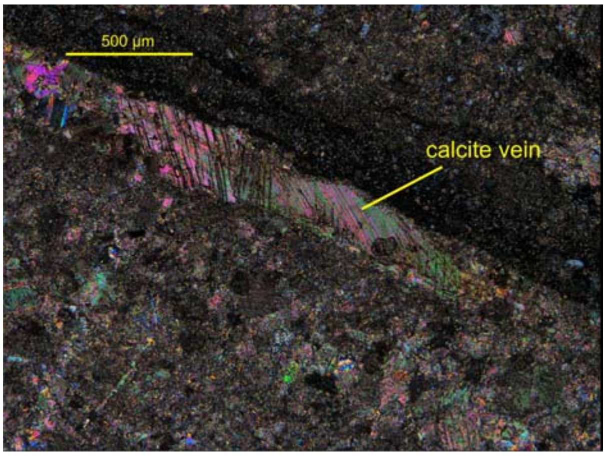

Fig. 90: Calcite vein with deformation twins (xpl).

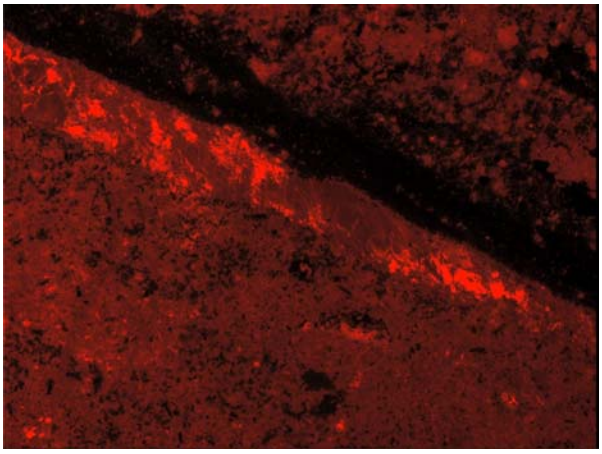
Fig. 91: Different phases of calcite in CL-image

4) Another generation developed during “fault-valve behaviour”. Faults that act as impermeable seal can become highly permeable channel-ways for fluid discharge when the fluid-pressure rises high enough to form a supra-hydrostatic fluid-pressure gradient. The fault-valve opens when an earthquake breaks the seal allowing the fluid to escape, reducing the fluid pressure (Sibson 1990). The SEM-image shows host-rock material reworked due to several cycles of carbonate-rich fluid injections. Different generations of calcite in the CL-image above also indicate a polyphase evolution.
5) This protocataclasite developed due to simultaneous alteration of part of the fault-valve and a fine-grained ultracataclasite.
6) Brittle deformation of the host-rock formed a fine-grained ultracataclastic zone.

Fault 2 shows the same development as part 5, only.

Sample KM6 (outcrop number 13)

Sample KM6 shows the interaction of high-and low-angled faults within a quartz-mylonite:

The cleavage of the **host rock** is represented by alternating layers of coarse and fine grained quartz with parallel grains of white mica. Coarse grained quartz reveals a slight shape preferred orientation (SPO) and sutured grain boundaries show evidence for grain boundary migration (GBM). Both SC-fabrics and the lattice preferred orientation of quartz indicate a dextral shear-sense (top-to-SW).
Brittle deformation can be observed on fine grained ultracataclastic layer-parallel and high-angled faults.
Brittle high-angled faults are partly cemented by ankeritic and calcitic fluids (fig. 92/1 &2) in multiple stages. The first vein shows a displacement by ductile drag along low-angled SW-directed shear whereas the second vein shows no evidence for low-angle faulting. Brittle-ductile transitions consequently indicate a high- and low-angle fault development at the brittle-ductile transition zone.

Fig. 92: Quartz-mylonite showing interaction of high- and low- angled fault development (xpl).

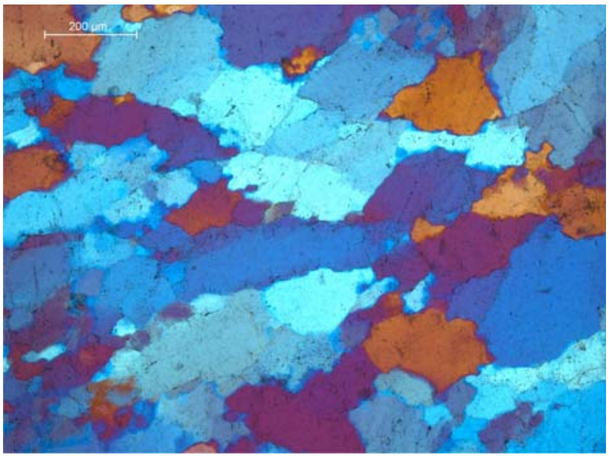

Fig. 93: LPO of quartz grains reveal top-to-SW (top right) ductile kinematics (stp).

Sample KM7 (outcrop number 13)

An extension vein (mode I crack) cuts the foliation at a high-angle and was filled by a quartz-rich fluid. Low temperature bulging (seen on the grain boundaries) and subgrain rotation recrystallisation (SGR) indicates ductile deformation. The vein was overprinted by brittle deformation that can be seen in undulose extinction and micro-cracks.

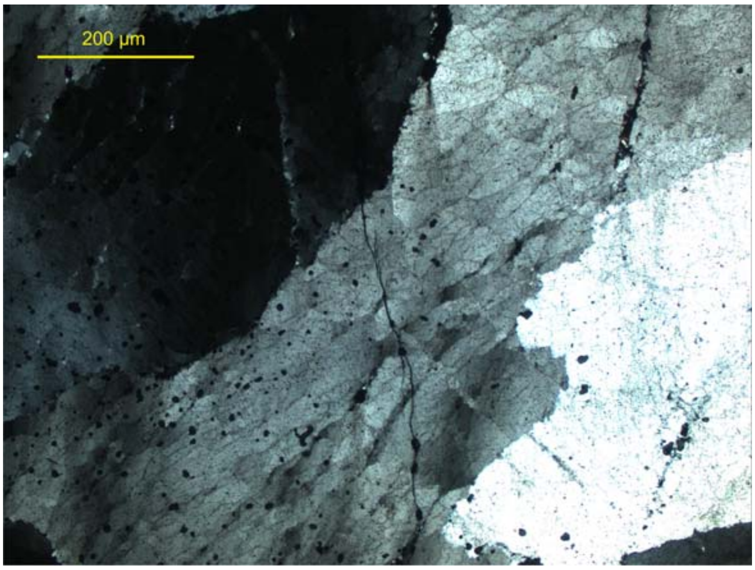

Fig. 94: Extension vein filled with quartz showing ductile bulging to brittle (microcracks) deformation (xpl).

4.4. Age constraints

Since the high- and low-angle fault systems are genetically linked, with both showing transitions from ductile to brittle deformation and vice-versa, and white-mica has an accepted Ar/Ar isotopic closure temperature of ca. 350 °C to 400 °C (Harrison et al. 2009; McDougall & Harrison 1999), which corresponds to the deformation conditions at the brittle-ductile transition zone, the Ar/Ar data from the Kea greenschists (Dave Schneider, University of Ottawa) were considered to constrain a deformation age. Overall, the data show cooling ages ranging from <16 to > 20 Ma (Fig. 96), with the sample from the mapping area itself (Kea 06-19) giving an age of ca. 20 Ma years. Therefore, the SW-directed extension must have occurred in the early Miocene.

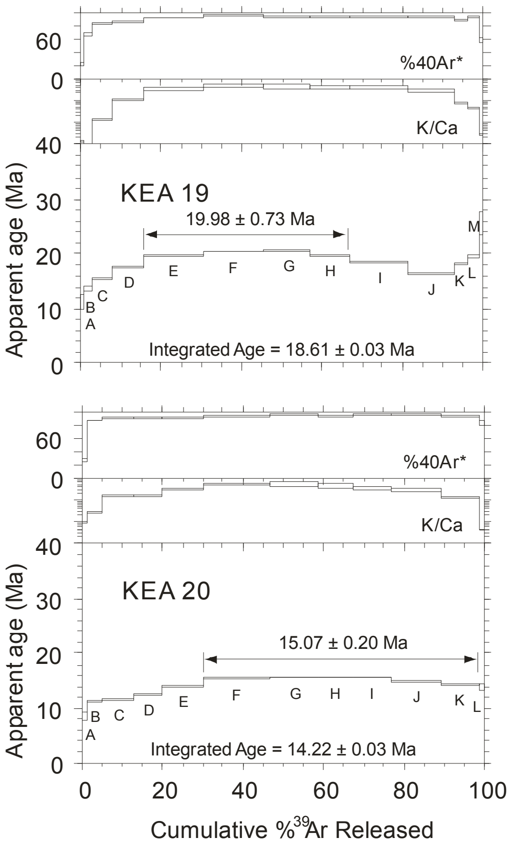

Fig. 95: Ar-release diagram of samples Kea 19 and 20. The plateau ages reveal ages of ca. 15 and 20 Ma, respectively (D. Schneider).

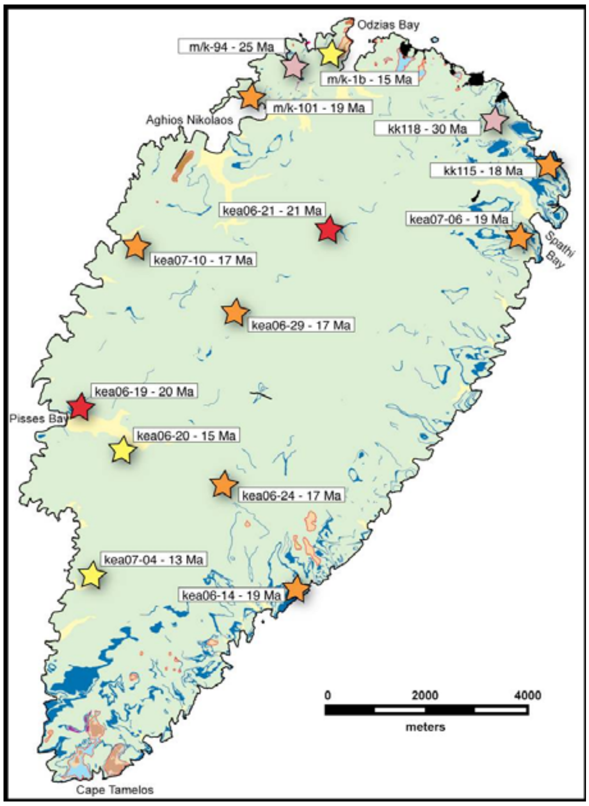

Fig. 96: Ar/Ar-data from Kea. Samples marked pink provided poor spectra and have been ignored. Red samples point to an age >20 Ma, orange markers to 17–19 Ma and yellow markers <16 Ma (D. Schneider).

5. DISCUSSION

The following discussion refers directly to the questions outlined in the introduction:

1) The NW-SE and NE-SW trending high-angle fault systems change their orientation relative to each other, from a rhombohedral geometry in the north of Pisses to an orthogonal geometry southwards. Since both high-angle fault systems show a symmetrical conjugate development, the maximum principal stress direction must have been vertical for both. Cross-cutting relationships show that the two systems were active at the same time and this implies “chocolate tablet boudinage” deformation.

Extension perpendicular to the main stretching might reflect arc-parallel extension related to the concave shape of the Hellenic trench, causing roll-back extension in several directions, namely, towards the SW, S and SE.

Tirel et al. (2004) published a map of the Aegean crustal thickness, inferred from gravity inversion, to constrain the variations in space and time of crustal thinning since Oligo-Miocene times.

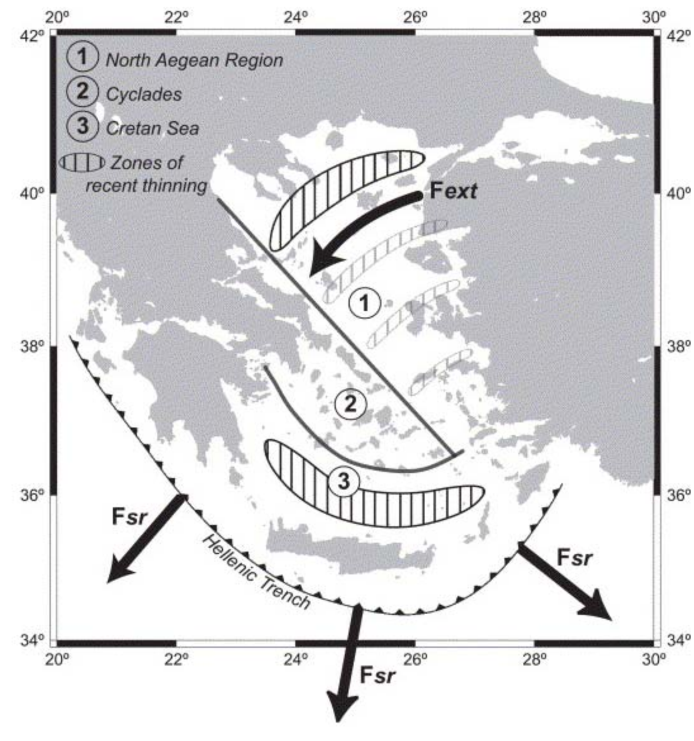

Fig. 97: Schematic map of the Aegean revealing three regions of different crustal thicknesses. (1) The North Aegean domain has a crustal thickness of <24 km showing NE-SW trending narrow zones of thinning caused by the extrusion of Anatolia (F_{ext}). (2) The Cyclades rest upon a flat Moho at 25 km. (3) The Cretan Sea reveals a crustal thickness of 22-23 km. Thick lines correspond to the volcanic arc and the boundary between the NE-SW trending zones of thinning and the area where extension is mostly due to the slab retreat (Fsr) (Tirel et al. 2004)

It is assumed that before post-orogenic extension, the crustal thickness of the Aegean domain was about 50 km, by comparison with Greece and Anatolia. The present mean crustal thickness of ca. 25 km was almost entirely caused by extension due to the southward retreat of the African slab during Oligocene to middle Miocene times (Makris & Vees 1977; Makris 1975, Tirel et al. 2004). Extension in the Aegean domain since the upper Miocene led to variations in crustal thickness, giving three different domains (fig. 97; Tirel et al. 2004):

(1) The North Aegean reveals a NE-SW trending thinning with a crustal thickness of <24 km that was caused by the westward extrusion of Anatolia since upper Miocene times (details are given below).

(2) The Cyclades rest upon a relatively flat Moho at ca. 25 km (Tirel et al.). This acted as a rigid block translated toward the SW without significant internal deformation (Walcott & White 1998).

(3) The Cretan Sea shows a thin crust of 22-23 km that formed due to the southward retreat of the African plate. The concave shape of the of the extended area in the Cretan Sea contours the arcuate Hellenic trench which reveals extension in SW, S and SE direction caused by slab retreat (Tirel et al. 2004). Further, the islands of the Cyclades as well as Peloponnese, Crete and Rhodes are tracing the shape of the Hellenic trench.

Since the high-angled fault system on Kea developed in the early Miocene (discussed below) and Aegean extension from the Oligocene to middle Miocene was only caused by roll back, one could argue that the "chocolate tablet boudinage" developed as a consequence of concave shape of the retreating slab as it is the case in the Cretan sea since upper Miocene.

However, the high-angle fault systems developed coevally with the low-angle detachment with a top-to-SW movement, with no evidence of ductile extension in a NW-SE-direction. Further, Jolivet et al. (1998) stated that Oligocene-Miocene extension has proceeded from north to south due to slab retreat which would explain the major orientation of deformation to the SW. The SW-kinematic oriented mineral direction seen on Kea can be attributed to block rotations in the Aegean.

Research on block rotations in the Aegean region show two blocks with opposite sense of rotation (Walcott & White 1998; Kondopoulou 2000; Van Hinsbergen et al. 2005). Whilst the western Aegean region, reaching from northern Albania to at least the northern part of Peloponnese and Evia in the east, shows clockwise rotation, the eastern block underwent counterclockwise rotation. The boundary between these blocks forms the Mid-Cycladic lineament (fig. 11). Kea forms part of the western block and was therefore submitted to clockwise rotation with an overall rotation of 50° since 15-13 Ma (Van Hinsbergen et al. 2005).

Thus the NE-SW and NW-SE striking fault systems cannot be linked to the present arcuate Hellenic trench.

Tectonic reconstructions of the subduction zone in the eastern Mediterranean indicate that the Hellenic trench did not form a distinctly curved shape during progressive subduction until late Eocene (Brun and Faccenna 2008). At 30-35 Ma, the absolute northward motion of Africa decreased and initiated fast slab retreat which led to the opening of the Aegean sea basin (Jolivet & Faccenna 2000). The spatially restricted slab rollback increased the curvature of the Hellenic margin which may have caused fractures to form (De Boorder et al. 1998) resulting in the development of NNE-SSW trending transform faults on both sides of the retreating slab (fig. 13). The transform faults would not have allowed much extension in the NW-SE direction.

2) Since extensional deformation in the Aegean domain was affected by the westward extrusion of the Anatolian plate, it was proposed (Grasemann, pers. comm.) that the origin of high-angled faults observed on Kea might be attributed to this event.

Since Miocene times, the Arabian plate has moved towards Eurasia (the Blitis suture traces the border between these plates) which led to the westward escape of Anatolia along the North (NAF) and East Anatolian Fault (EAF) (Armijo et al. 2003). The dextral NAF propagated in the Aegean domain no earlier than 2-3 Ma ago (Le Pichon et al. 1995; Dinter 1998) and caused extension in, for example, the Gulf of Corinth, by the so called “wing crack-mechanism” (fig. 12).

Kea is almost in line with the Corinth Rift and it was therefore suggested that brittle deformation on Kea might be related to its opening. On Kea, both the high- and the low-angle fault systems are kinematically linked and show evidence for origin at the brittle-ductile transition zone. Ar-Ar white mica data of greenschists suggest these fault systems initially formed during the early Miocene (ca. 16 – 20 Ma). Consequently, the high-angle faulting cannot be associated with the Corinth Rift, since the North Anatolian Fault responsible for the opening of the Gulf of Corinth did not propagate into the Aegean region before 2 – 3 Ma (Pichon et al., 1995; Dinter, 1998).

3) The high- and low-angle fault systems on Kea clearly show a coeval development: The NW-SE and NE-SW fracture system partly transect and partly root into low-angle faults with top-to-SW kinematics. At one locality it was also observed that the high-angle faults were cut by low-angle faults. All fault systems show evidence of a formation at the brittle-ductile transition zone. Subvertical extension veins related to the low-angle detachment with SW kinematics reveal a vertical maximum principal stress direction with extension to the SW. Both high-angle fault systems are conjugate, with the same orientation of the maximum principal stress direction. Both the linkages of the fault systems as well as the same stress field orientation indicate a synchronous development.

a) Buck (1988) proposed a model for low-angle normal fault (LANF) development that shows initiation of high-angle faults that rotate during extension into gentler dips. In the case of Kea, this assumption can be excluded due to evidence of synchronous development of the high- and low- angle fault systems.

b) However, there are some similarities with observations on fault development on Tinos (north-eastern Cyclades), which is a flat-lying extensional shear zone with a top-to-NE movement. The detachment shows a continuum from ductile to brittle low-angle fault development and is cut through by steeply dipping normal faults in the latest stage of deformation (Mehl et al. 2004). The inversion of fault slip data shows a direction of the minimum stress axis in NE-SW direction which is exactly parallel to the NE-SW stretching lineation direction. The stress field on Kea is similar with that on Tinos. The high-angle faults on Tinos also show evidence for development related to the low-angle detachment and reveal the last stages of brittle deformation. This also excludes the possibility of a rotation of high-angle faults to low-angle dips. High-angle normal faults on Kea are occasionally seen to have been cut by low-angle faulting. This has not been observed on Tinos (Mehl et al. 2004).

4) Micro-analysis on faults showed polyphase evolution with high fluid-activity. The cements mainly consist of quartz, calcite, ankerite and dolomite. Crystallised fluids show further ductile to brittle overprints that also reveal a development of the high-angle faults at the brittle-ductile transition zone.

A conceptual model links the development of veins with fluid pressure cycling as a consequence of fault-valve behaviour where the fault transects a suprahydrostatic gradient in fluid pressure (Sibson 1990). Therefore, failure on faults is strongly influenced by fluid pressure decreasing the critical level for tectonic shear stress.

6. CONCLUSIONS

- The lithologies in the research area consist of mylonitc, partly cataclastic chlorite-carbonate schists with layers of blue-grey calcitic marbles. The mineral assemblages comprise calcite, quartz, white mica, feldspar (albite), chlorite, and occasionally apatite and are characteristic for greenschist facies metamorphic conditions.

- Foliation planes dip shallowly in all directions, forming a gently elongate dome structure over the whole area.

- Stretching lineations of all lithologies plunge rather shallowly either to the NNE or SSW. Low-angle deformation occurred from ductile (e.g. sheath folds, isoclinal folds) to brittle deformation (e.g. cracked quartz minerals) with top-to-SSW kinematics shown by delta- and sigma clasts and SCC' fabrics.

- Penetrative subhorizontal ductile deformation associated with movement on the LANF occurred at around 300 – 450 °C; this indicates a depth of ca. 10 km.

- On Kea, both to the north and south of Pisses, well-developed high-angled normal fault systems show two dominant conjugate directions; NE-SW and NW-SE. From the north of Pisses southwards, the angle between these two directions changes gradually from a rhombohedral (ca. 50°/130° angle between faults, with the acute angle facing westwards) to an orthogonal geometry.

- The two high-angle fault systems developed coevally and show transitions from brittle to ductile deformation mechanisms, and vice-versa, indicating development within the brittle-ductile transition zone.

- The high-angled fault systems are kinematically linked to the SSW-directed low angle detachment. The conjugate pattern of the high-angle fault system and subvertical extension veins reveal a formation with an overall vertical maximum principal stress direction and suggest that the detachment was weak.

- SSW-directed extension of the high-angle fault system accommodates no more than estimated 2 - 3 %.

- The high-angle fault systems developed with a highly polyphase evolution and show interaction with quartzitic and carbonate-rich fluids.

- Ar/Ar-data of both fault systems reveal a deformation age of the early Miocene.

REFERENCES

Altherr R, Siebel W 2007. I-type plutonism in a continental back-arc setting. Miocene granitoids and monzonites from the central Aegean Sea, Greece. Contrib Mineral Petrol 35:287-288

Anders MH, Schlische RW 1994. Overlapping faults, intrabasin highs, and the growth of normal faults. J Geol 102:165-180

Armijo R, Lyon-Caen H, Papanikolaou D. 1992. East-West extension and Holocene normal fault scarps in the Hellenic arc, Geology 20:491-494

Armijo R, Flerit F, King G, Meyer B 2003. Linear elastic fracture mechanics explains the past and present evolution of the Aegean. Earth Planet Sci Lett 217:85-95. doi:10.1016/S0012-821X(03)00590-9

Barnett JAM, Mortimer J, Rippon JH, Walsh JJ, Watterson J 1987. Displacement geometry in the volume containing a single normal fault. American Ass Petrol Geol Bull 71, 925-937

Briole P, Rigo A, Lyon-Caen H, Ruegg JC, Papazissi K, Mitsataki C, Badolimou A, Veis G, Hatzfeld D, Deschamps A 2000. Active deformation of the Corinth rift, Greece: results from repeated global positioning system surveys between 1990 and 1995. J. Geophys. Res. 105 25605-25626

Brun J-P, Faccenna C 2008. Exhumation of high-pressure rocks driven by slab rollback. Earth Planet. Sci. Lett. 272:1-7

Buck W. R. 1988. Flexural rotation of normal faults. Tectonics 7:959-973.

Buick IS 1991a. Mylonite fabric development on Naxos, Greece. J Struct Geol 13:643-655. doi:10.1016/0191-8141(91)90027-G

Buick IS 1991b. The late alpine evolution of an extensional shear zone, Naxos, Greece. J Geol Soc 148:93-103.doi:10.1144/gsjgs.148.1.0093

Burchfiel BC, Zhiliang C, Hodges KV, Yuping L, Royden LH, Changrong D, Jiene X 1992. The south Tibetan detachment system, Himalayan orogen: Extension contemporaneous with and parallel to shortening in a collisional mountain belt: Geol Soc America Spec Paper 269:41

Burkhard M 1993. Calcite twins, their geometry, appearance and significance as stress-strain markers and indicators of tectonic regime: a review. J Struct Geol 13:351-368

Cartwright JA, Trudgill BD, Mansfield CS 1995. Fault growth by segment linkage: an explanation for scatter in maximum displacement and trace length data from the Canyon-lands Grabens of SE Utah. J Struc Geol. 17:1319-1326

Channell JET, Kozur HW 1997. How many oceans? Meliata, Vardar and Pindos oceans in Mesozoic Alpine paleogeography. Geology 25: 183-186

Chase CG 1979. Subduction, the geoid, and lower mantle convection. Nature 282:464-68

Chase CG 1980. Extension behind island arcs and motions relative to hot spots. J. Geophys. Res. 83:5358-87

Cherry JF, Davis JL, Mantzourani E 1991. Landscape Archaeology as Long-Term History. Northern Keos in the Cycladic Islands, from Earliest Settlements until Modern Times. Monumenta Archaeologica (University of California, Los Angeles, Institute of Archaeology) 16:57-67

Cowie PA, Scholz CH 1992a. Physical explanation for the displacement-length relationship for faults using a post-yield fracture mechanics model. J Struc Geol 14:1133-1148

Cowie PA, Scholz CH 1992b. Displacement-length scaling relationship for faults: data synthesis and discussion. J Struc Geol 14:1149-1156

Davis EN 1972. Geological structure of Kea Island. Bull Geol Soc Greece 9(2):252-256

Dawers NH, Anders MH, Scholz CH 1993. Growth of normal faults: displacement-length scaling. Geology 21:1107-1110

Dawers NH, Anders MH 1995. Displacement-length scaling and fault linkage. J Struct Geol 17:607-614

De Boorder H, Spakman W, White SH, Wortel MJR 1998). Late Cenozoic mineralization, orogenic collapse and slab detachment in the European Alpine Belt. Earth Planet Sci Lett 164:569-575

Dewey JF, Bird JM 1970. Mountain belts and new global tectonics. J Geophys Res 75:2625-47

Dinter DA 1998. Late Cenozoic extension of the Alpine collisional orogen, northeastern Greece: origin of the north Aegean basin. Geol Soc Am Bull 110:1208-1230.

Dürr S, Altherr R, Keller J, Odrusch M, Seidel E 1978. The median Aegean crystalline belt: stratigraphy, structure, metamorphism, magmatism. Alps, Apennines, Hellenides: Geodynamic Investigation along Geotraverses by an International Group of Geoscientists, ed. Closs H., Roeder D. Schmidt K. IUCG Sci Rep 38:537-64. Stuttgart: Schweizerbart

Edwards M, Grasemann B 2009. Mediterranean snapshots of accelerated slab retreat; subduction instability in stalled continental collision. In: van Hinsbergen, D., Edwards, M. A., and Govers, R. (eds.), Collision and collapse at the Africa-Arabia-Eurasia subduction zone. Geological Society, London, Special Publication 311, 155-192.

Ellis MA, Dunlap WJ 1988. Displacement variations along thrust faults: implications for the development of large faults. J Struc Geol 10:183-192

Engel M, Reischmann T 1997. Geochronological data on granitoid gneiss from Paros, Greece, obtained by single zircon Pb evaporation. Terra Nova 9:463

Facenna C, Jolivet L, Piromallo C, Morelli A 2003. Subduction and the depth of convection in the Mediterranean mantle. J. Geophys. Res. 108(B2):2099, doi:10.1029/2001JB001690

Faure M, Bonneau M 1988. Données nouvelles sur l'extension néogène de l'Egée: la deformation ductile du granite miocène de Mykonos (Cyclades, Grèce). C R Acad Sci Paris 307:1553-1559

Faure M, Bonneau M, Pons J 1991. Ductile deformation and syntectonic granite emplacement during the late Miocene extension of the Aegean (Greece). Bull Soc Geol Fr 162:3-12

Filbrandt JM, Richard PD, Franssen RCMW 1994. Growth and coalescence of faults: numerical simulations and sand-box experiments. TSG Special Meeting on Fault Populations, Edinburgh, U.K., Extended Abstract, Tectonic Studies Group, 57-59

Flerit F, Armijo R, King G, Meyer B 2004. The mechanical interaction between the propagating North Anatolian Fault and the Back-arc extension in the Aegean. Earth Planet Sci Lett 224:347-362. doi:10.1016/j.epsl.2004.05.028

Fytikas M, Innocenti F, Manetti P, Mazuoli R, Peccerilo A, Villari L 1984. Tertiary to Quaternary evolution of volcanism in the Aegean region. In "The Geological Evolution of the Eastern Mediterranean", ed. J. E. Dixon, A. H. Robertson. Geol. Soc. London, Spec. Publ. 17:687-700

Garfunkel Z., Anderson C. A. Schubert G. 1986. Mantle circulation and the lateral migration of subducted slabs. J. Geophys. Res. 91:7205-23

Gautier P, Brun JP, Jolivet L 1993. Structure and kinematics of upper Cenozoic extensional detachment on Naxos and Paros (Cyclades Islands, Greece). Tectonics 12:1180-1194. doi:10.1029/2002TC001406

Gautier P, Brun JP, Moriceau R, Sokoutis D, Martinod J, Jolivet L 2001. Timing, kinematics and cause of Aegean extension: a scenario based on a comparison with simple analogue experiments. Earth Planet Sci Lett 187:95-104

Götze J 2002. Potential of cathodoluminescence (CL) microscopy and spectroscopy for the analysis of minerals and materials. Anal Bioanal Chem 374:703-708

Grasemann B, Schneider DA, Stöckli D, Iglseder C. Miocene bivergent crustal extension in the Cyclades (Greece). Lithosphere – submitted

Grasemann B, Petrakakis K 2007. Evolution of the Serifos metamorphic core complex. In Inside the Aegean Metamorphic Core Complexes, ed. G Lister, M Forster, U Ring. J. Virtual Explor. 27(2), doi:10.3809/jvirtex.2007.00170

Groshong JrRH 1988. Low temperature deformation mechanisms and their interpretation. Bull Geol Soc Am 100:1329-1360

Harrison TM, Célérier J, Aikman AB, Hermann J, Heizler MT 2009. Diffusion of ^{40}Ar in muscovite. Geochimica et Cosmochemica Acta 4. pp 1039-1051. doi:10.1016/j.gca.2008.09.038

Huet B, Labrousse L, Jolivet L 2009. Thrust or detachment? Exhumation processes in the Aegean: insight from a field study on Ios (Cyclades, Greece). Tectonics, doi :10.1029/2008TC002397.

Iglseder C, Grasemann B, Rice AHN, Petrakakis K, Schneider DA 2011. Miocene S-directed low-angle normal fault evolution on Kea Island (West Cycladic Detachment System, Greece). Tectonics, in press

Isacks B, Molnar P 1969. Mantle earthquake mechanisms and sinking of lithosphere. Nature 223:1121-24

Jackson J 1994. Active tectonics of the Aegean region. Annu Rev Earth Planet Sci 22:239-271. doi:10.1146/annurev.ea.22.050194.0013

Jacobshagen V 1986. Geologie von Griechenland. Gebrüder Borntraeger, Berlin 363

Jolivet L 2001. A comparison of geodetic and finite strain pattern in the Aegean, geodynamic implications. Earth Planet Sci Lett 187: 95-104

Jolivet L, Brun J-P 2010. Cenozoic geodynamic evolution of the Aegean. Int J Earth Sci 99:109-138

Jolivet L, Brun JP, Gautier P, Lallemant S, Patriat M 1994a. 3-D kinematics of extension in the Aegean from the Early Miocene to the Present, insight from the ductile crust. Bull Soc Geol Fr 165L195-209

Jolivet L, Faccenna C 2000. Mediterranean extension and the Africa-Eurasia collision. Tectonics 19(6):1095-1106

Jolivet L, Faccenna C, Goffé B, Burov E, Agard P 2003. Subduction tectonics and exhumation of high-pressure metamorphic rocks in the Mediterranean orogens. Am J Sci 303:353-409, doi:10.2475/ajs.303.5.353

Jolivet L, Faccenna C, Goffé B, Mattei M, Rossetti F, Brunet C, Stroti F, Funiciello R, Cadet JP, Para R 1998. Mid-crustal shear zones in post-orogenic extension: the northern Tyrrhenian Sea case. J Geophys Res 103:12123-12160

Jolivet L, Lecomte E, et al. 2010. The North Cycladic Detachment System. Earth Planet Sci Lett 289:87-104.

Kim Y-S, Andrews JR, Sanderson DJ 2000. Damage zones around strike-slip fault evolution, Crackington Haven, southwest England. Geosci J 4:53-72

Kim Y.-S., Sanderson D. J. 2005. The relationship between displacement and length of faults: a review, Science Direct, Earth-Sci Rev 68:317-334

Kissel C, Speranza F, Milicevic V 1995. Paleomagnetism of external southern Dinarides and northern Albanides: implications for the Cenozoic evolution of the Eastern Mediterranean. Tectonophysics 362:199-217

Kondopoulou D. 2000. Paleomagnetism in Greece: Cenozoic and Mesozoic components and their geodynamic implications. Tectonophysics 326, 131-151

Laner G 2009. Fluid-rock interaction in a low-angle normal fault (Kythnos, Western Cyclades, Greece). Master's Thesis, Universitiy of Vienna

Lenauer I 2009. Structural and petrological investigations along a low-angle normal fault on Kythnos, Greece. Master's Thesis, University of Vienna

Le Pichon X, Angelier J 1981b. The Hellenic arc and trench system: a key to the neotectonic evolution of the eastern Mediterranean sea. Philos Trans R Soc London 300:357-372, doi:10.1098/rsta.1981.0069

Le Pichon X, Chamot-Rooke N, Lallemant SL, Noomen R, Veis G 1995. Geodetic determination of the kinematics of Central Greece with respect to Europe: implications for eastern Mediterranean tectonics. J Geophys Res 100:12675-12690.

Lister GS; Davis GA 1989. "The origin of metamorphic core complexes and detachment faults formed during Tertiary continental extension in the northern Colorado River region, J Struct Geol 11:65-94

Lister GS, Banga G, Feenstra A 1984. Metamorphic core complexes of Cordilleran type in the Cyclades, Aegean Sea, Greece. Geology 12:221-225

Lonergan L, White N 1997. Origin of the Betic-Rif mountain belt. Tectonics 16:504-22

Lyon-Caen H, Armijo R, Drakopoulos J, Baskoutass J, Delibassis N, Gaulon R, Kouskouna V, Latoussakis K, Makropoulos K, Papadimitriou P, Papanastassiou D, Pedotti G 1988. The 1986 Kalamata (South Peloponnesus) earthquake: detailed study of a normal fault, evidences for E-W extension in the Hellenic Arc. J Geophys Res 93:14967-15000.

Makris J 1975. Crustal structure of the Aegean Sea and the Hellenides obtained from geophysical surveys. J Geohpys 41:441-443

Makris J, Vees R 1977. Crustal structure of the Central Aegean Sea and the islands of Evia and Crete, Greece, obtained by refractional seismic experiments. J Geophys 42:329-341

Malavieille J 1993. Late orogenic extension in mountain belts: insights from the Basin and Range and the late Paleozoic Variscan belt. Tectonics 12:1115-1130.

Marrett R, Allmendinger RW 1991. Estimates of strain due to brittle faulting: sampling of fault populations. J Struct Geol 13:735-738

Martel SJ, Pollard DD, Segall P 1988. Development of simple strike-slip fault zones, Mount Abbot quadrangle, Sierra Nevada, California. Geol Soc Am Bull 100:1451-1465

Mc Clusky S, Balassanian S, Barka A, Demir C, Ergintav S, Georgiev I, Grukan O, Hamburger M, Hurst K, Kahle H, Kasens K, Kekelidze G, King R, Kotzev V, Lenk O, Mahmoud S, Mishin A, Nadariya M, Ouzonis A, Paradissis D, Peter Y, Prilepin M, Teilinger R, Danli I, Seeger H, Tealeb A, Toksöz MN, Veis G 2000. Global positioning system constraints on plate kinematics and dynamics in the eastern Mediterranean and Caucasus. J Geophys Res 105:5695-5720.

McDougall I, Harrison TM 1999. Geochronology and Thermochronology by the $^{40}Ar/^{39}Ar$ Method. Oxford University Press 3-43.

Mehl C, Jolivet L, Lacombe O 2005. From ductile to brittle: Evolution and localization of deformation below a crustal detachment (Tinos, Cyclades, Greece). Tectonics 24, TC4017, doi:10.1029/2004TC001767

Okrusch M, Bröcker M 1990. Eclogites associated with high-grade blueschists in the Cyclades archipelago, Greece: A review. Eur J Mineral. 2:451-478

Passchier CW, Trouw RAJ 2005. Mictrotectonics. Springer, Berlin, 366p

Peacock DCP, Sanderson DJ 1991. Displacement and segment linkage and relay ramps in normal fault zones. J Struc Geol 13:721-733

Peacock DCP, Sanderson DJ 1996. Effects of propagation rate on displacement variations along faults. J Struct Geol 18:311-320

Pe-Piper G., Piper D. J. W. 2007. Neogene back-arc volcanism of the Aegean: new insights into the relationship between magmatism and tectonics. In: Beccaluva L., Bianchini G. (eds) Cenozoic volcanism in the Mediterranean area. doi:10.1130/2007.2418(1102), Geol Soc Am 17-31

Ramsay J. G. 1980. The crack-seal mechanism of rock deformation. Nature. 284:135-139, doi:10.1038/284135a0

Reischmann T. 1997. Single zircon Pb/Pb dating of tectonic units from the metamorphic core complex of Naxos TERRA Abstr 9:496

Rice, A. H. N., C. Iglseder, B. Grasemann, P. I. Tsombos, K. G. Nikolakopoulos, M. Müller, K. Voit, A. Zámolyi, E. Draganits, M. Rockenschaub, and D. Mitropoulos 2010. Geological Map of Greece, Kea Island, Institute of Geology and Mineral Exploration, Athens.

Ring U, Glodny J, Will T, Thompson S 2010. The Hellenic Subduction System: High-Pressure Metamorphism, Exhumation, Normal Faulting, and Large-Scale Extension. Annu Rev Earth Planet Sci 38:45-76

Ring U, Layer PW 2003. High-pressure metamorphism in the Aegean, eastern Mediterranean: underplating and exhumation from the Late Cretaceous until the Miocene to recent above the retreating Hellenic subduction zone. Tectonics 22(3):1022, doi:10.1029/2001TC001350

Ring U, Will T, Glodny J, Kumerics C, Gessner K 2007b. Early exhumation of high-pressure rocks in extrusion wedges: Cycladic blueschist unit in the eastern Aegean, Greece, and Turkey. Tectonics 26:TC2001, doi: 10.1029/2005TC001872

Royden LH 1993. Evolution of retreating subduction boundaries formed during continental collision. Tectonics 12:629-38

Royden LH, Husson L 2006. Trench motion, slab geometry and viscous stresses in subduction systems. Geophys J Int 167:881-905

Schellart WP 2005. Influence of the subducting plate velocity on the geometry of the slab and migration of the subduction hinge. Earth Planet Sci Lett 231:197-219

Segall P, Pollard DD 1980. Mechanics of discontinuous faults. J Geophys Res 85:4337-4350

Selverstone J 1988. Evidence for east-west crustal extension in the eastern Alps: Implications for the unroofing history of the Tauern window. Tectonics 7:87-105.

Sibson RH 1990. Conditions for fault-valve behaviour. Geol Soc London 54:15-28

Stampfli GM, Borel GD 2002. A plate tectonic model for the Paleozoic and Mesozoic constrained by dynamic plate boundaries and restored synthetic oceanic isochrones. Earth Planet Sci Lett 196:17-33

Stern RJ 2002. Subduction zones. Rev Geophy 40:1012. doi:10.1029/2001RG000108

Tirel C, Gueydan F, Tiberi C, Brun J-P. Aegean crustal thickness inferred from gravity inversion. Geodynamical implications. Earth Planet Sci Lett 228:267-280

Trotet F, Jolivet L, Vidal O 2001a. Tectono-metamorphic evolution of Syros and Sifnos islands (Cyclades, Greece). Tectonophysics 338:179-206. doi:10.1016/S0040-1951(01)00138-X

Trotet F, Vidal O, Jolivet L 2001b. Exhumation of Syros and Sifnos metamorphic rocks (Cyclades, Greece). New constraints on the P-T paths. Eur J Mineral 13:901-920. doi:10.1127/0935-1221/2001/0013/0901

Tucholke B E, Lin L 1998. Megamullions and mullion structures defining oceanic metamorphic core complexes on the Mid-Atlantic Ridge: J Geophys Res. 103:9857-9866, doi: 10.1029/98JB00167

Uyeda S 1982. Subduction zones: an introduction to comparative subductology. Tectonophysics 81:133-59

Van Hinsbergen DJJ, Hafkenscheid E, Spakman W, Meulenkamp JE, Wortel R 2005a. Nappe stacking resulting from subduction of oceaic and continental lithosphere below Greece. Geology 33:325-28

Van Hinsbergen DJJ, Langereis CG, Meulenkamp JE 2005. Revision of timing, magnitude and distribution of Neogene rotations in the western Aegean region. Tectonophysics 396:1-34

Vannay J-C, Grasemann B, Rahn M, Frank W, Carter A, Baudraz V, Cosca M 2004. Miocene to Holocene exhumation of metamorphic crustal wedges in the NW Himalaya: evidence for tectonic extrusion coupled to fluvial erosion. Tectonics 23, TC1014 doi: 10.1029/2002TC001429.

Voit K 2008. Structural Geology and Geomorphology of Northern Kea – A crustal scale Viscous-frictional Shear Zone, Cyclades, Greece. Diploma thesis, University of Vienna

Walcott CR, White SH 1998. Constraints on the kinematics of post-orogenic extension imposed by stretching lineations in the Aegean area. Tectonophysics 298(1-3):155-175.

Walsh JJ, Nicol A, Childs C 2002. An alternative model for the growth of faults. J Struct Geol 24:1669-1675

Walsh JJ, Watterson J 1987. Distributions of cumulative displacement and seismic slip on a single normal fault surface. J Struc Geol 9:1039-1046

Walsh JJ, Watterson J 1988. Analysis of the relationship between the displacements and dimensions of faults. J Struc Geol 10:239-247

Watterson J 1986. Fault dimensions, displacements and growth. Pure and Applied Geophysics 124:365-373

Wawrzenitz N, Krohe A 1998. Exhumation and doming of the Thasos metamorphic core complex (S Rhodope, Greece). Structural and geochronological constraints. Tectonophysics 285:301-32

Wells DL, Coppersmith KJ 1994. New empirical relationships among magnitude, rupture length, rupture area, and surface displacement. Bull Seismolog Soc Am 84:974-1002

Wernicke B 1981. Low-angle normal faults in Basin and Range province: Nappe tectonics in an extending orogen. Nature 291:645-648, doi: 10.1038/291645a0

APPENDIX I – Mapping area with outcrop numbers

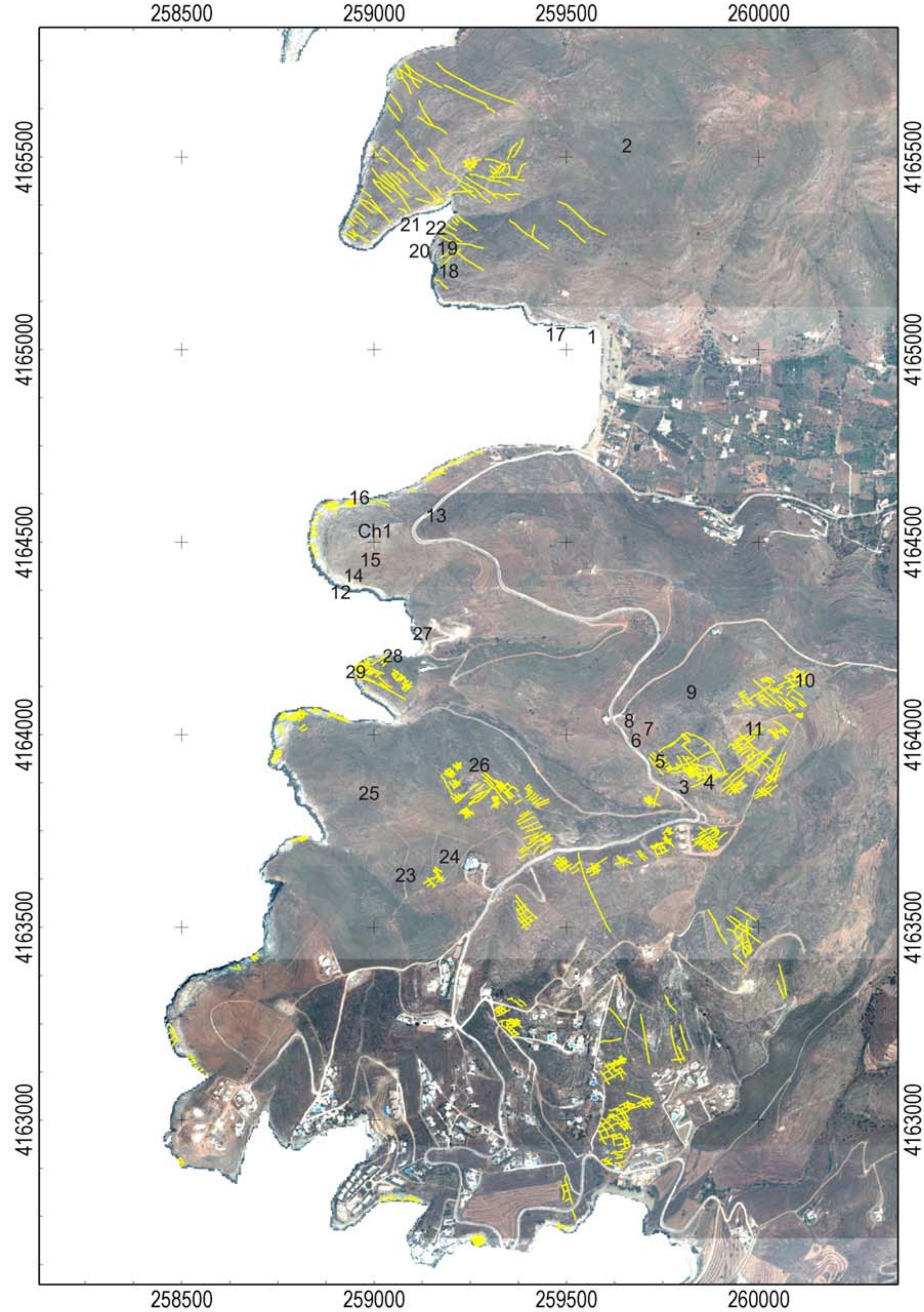

Combined outcrop-numbers of the map above for the stereo plots shown in chapter 4.2.2:

A: 1
B: 18 – 22
C: 1, 17
D: 12 – 16
E: Ch 1 (marble)
F: 9 – 11
G: 3 – 8
H: 27 – 29
I: 25, 26
J: 23, 24

APPENDIX III – EDAX, chemical mapping

Calcite (light grey)

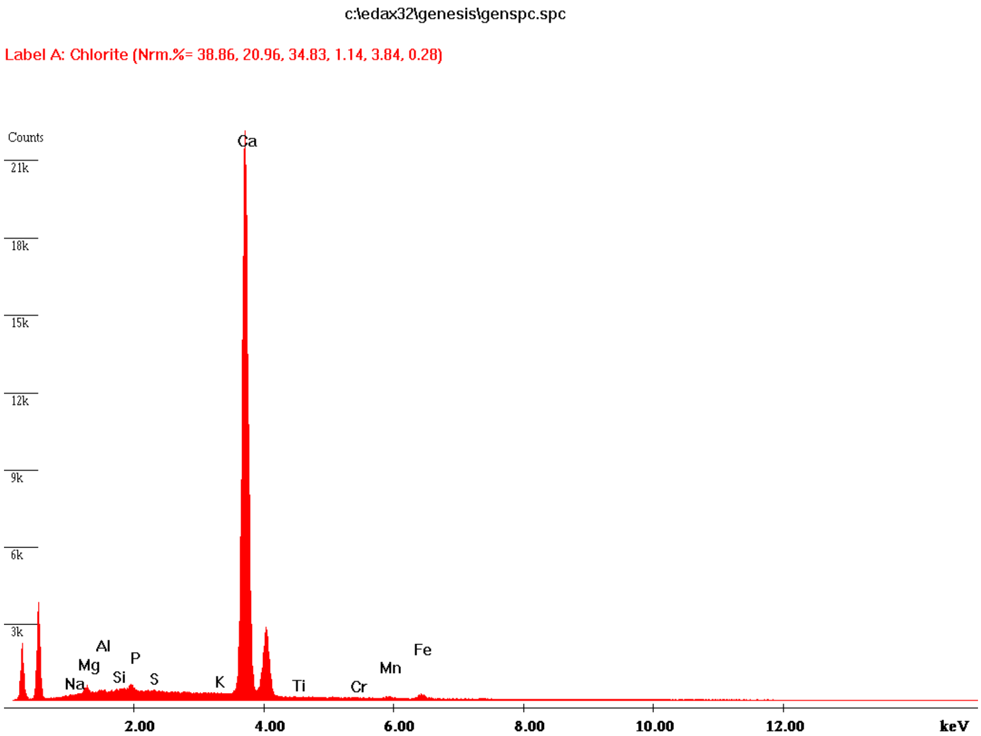

Calcite (dark grey)

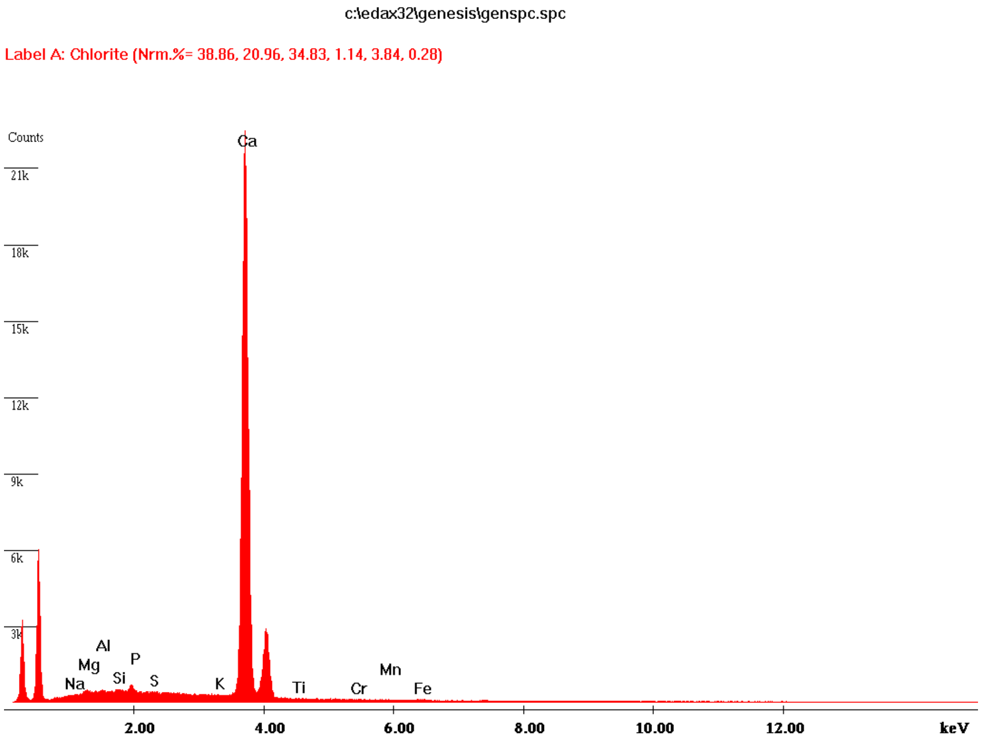

Quartz

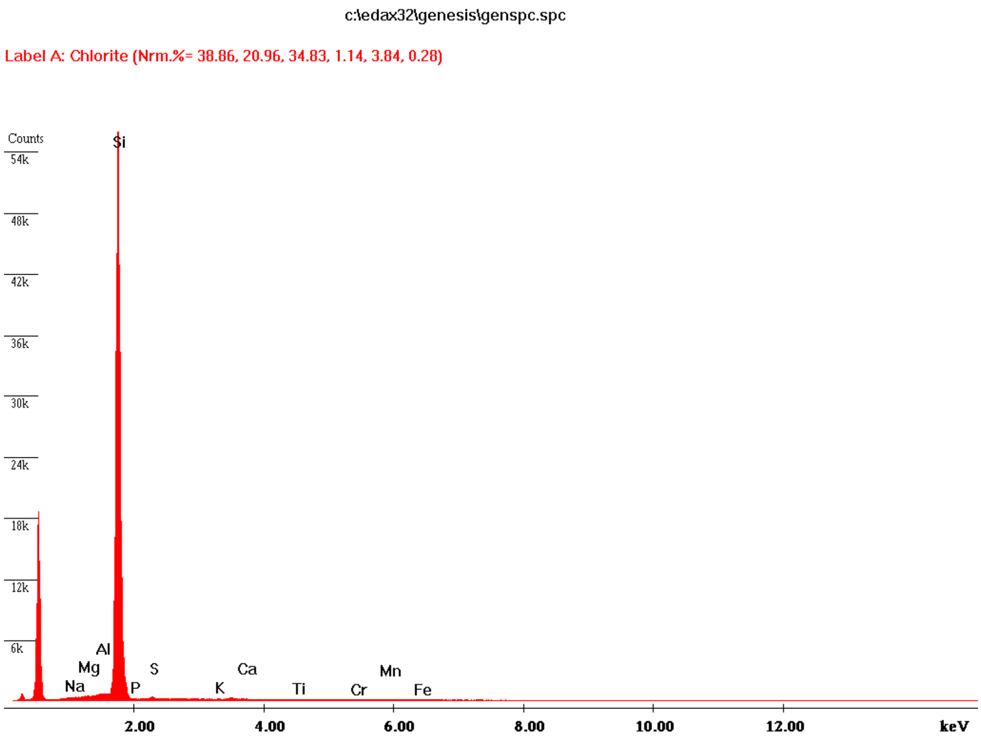

Chlorite

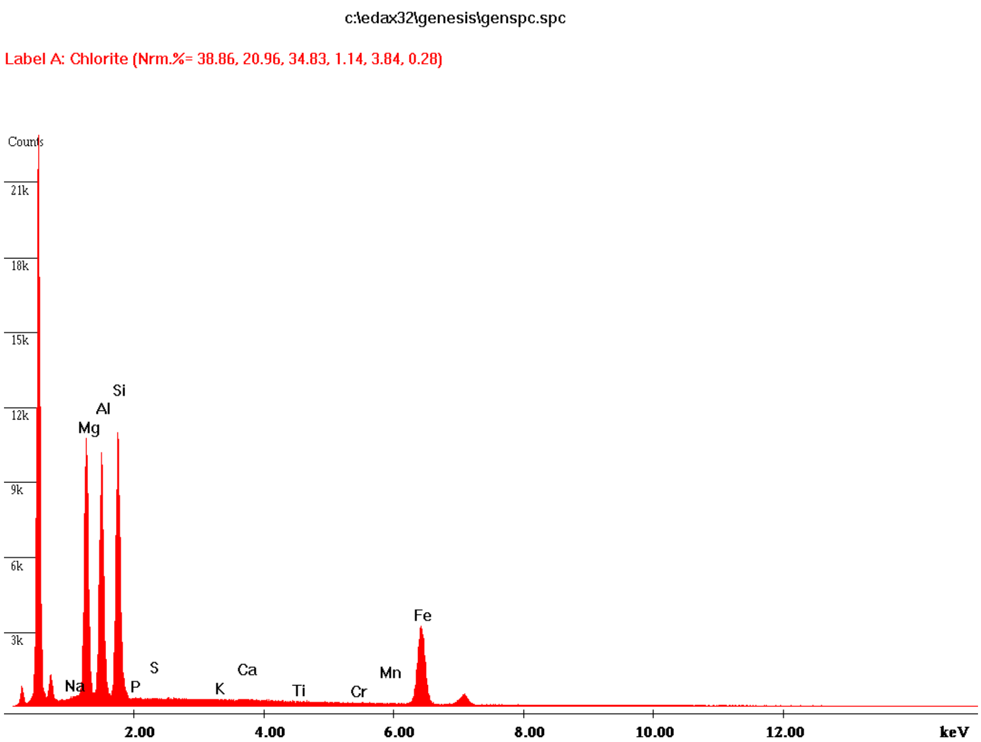

Muscovite

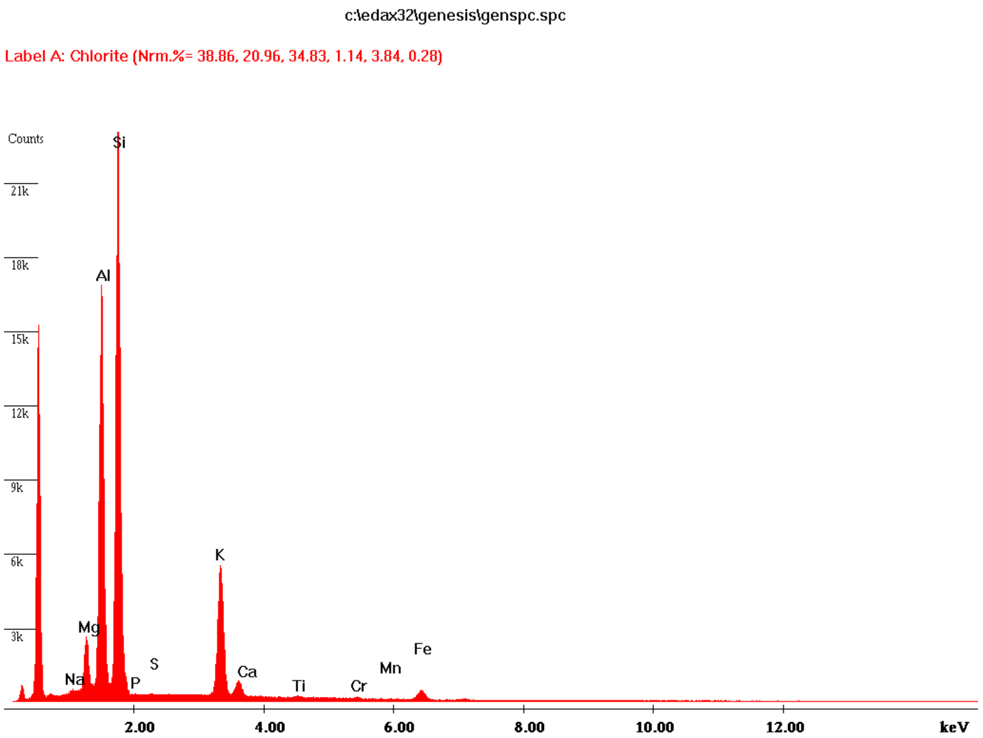

Orthoclase

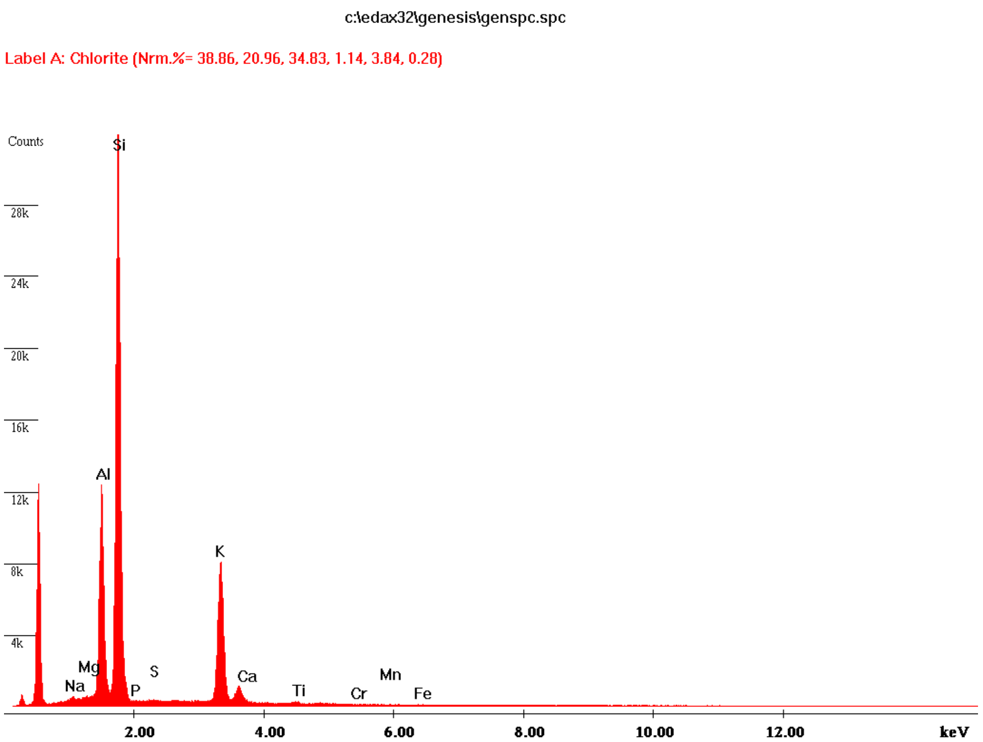

Albite

c:\edax32\genesis\genspc.spc

Label A: Chlorite (Nrm.%= 38.86, 20.96, 34.83, 1.14, 3.84, 0.28)

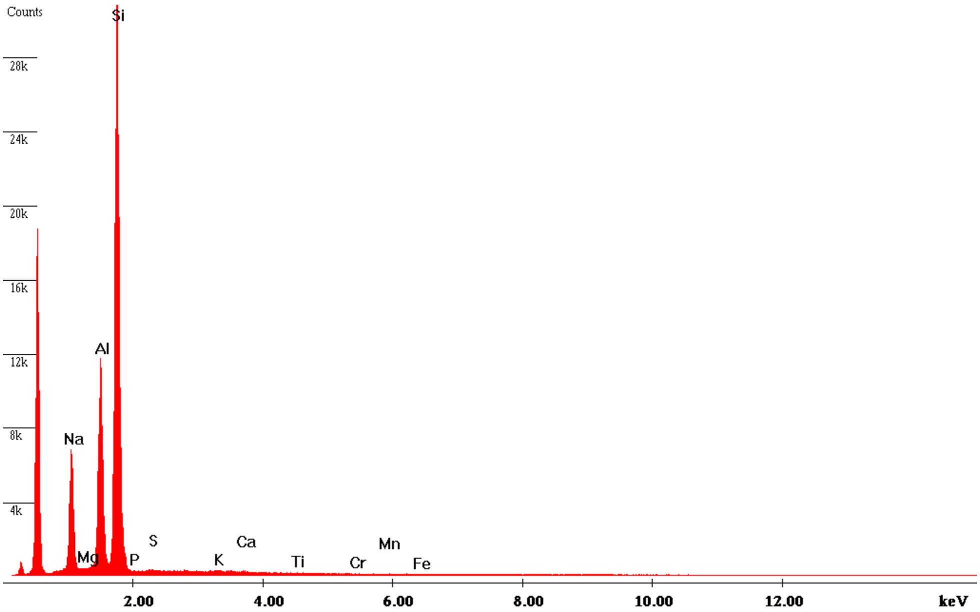

Apatite

c:\edax32\genesis\genspc.spc

Label A: Chlorite (Nrm.%= 38.86, 20.96, 34.83, 1.14, 3.84, 0.28)

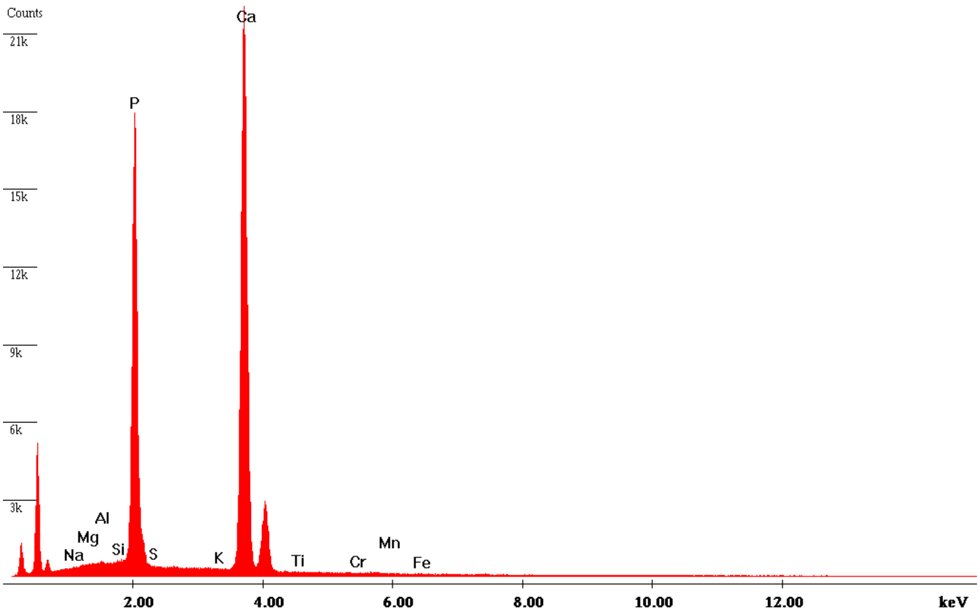

Rutile

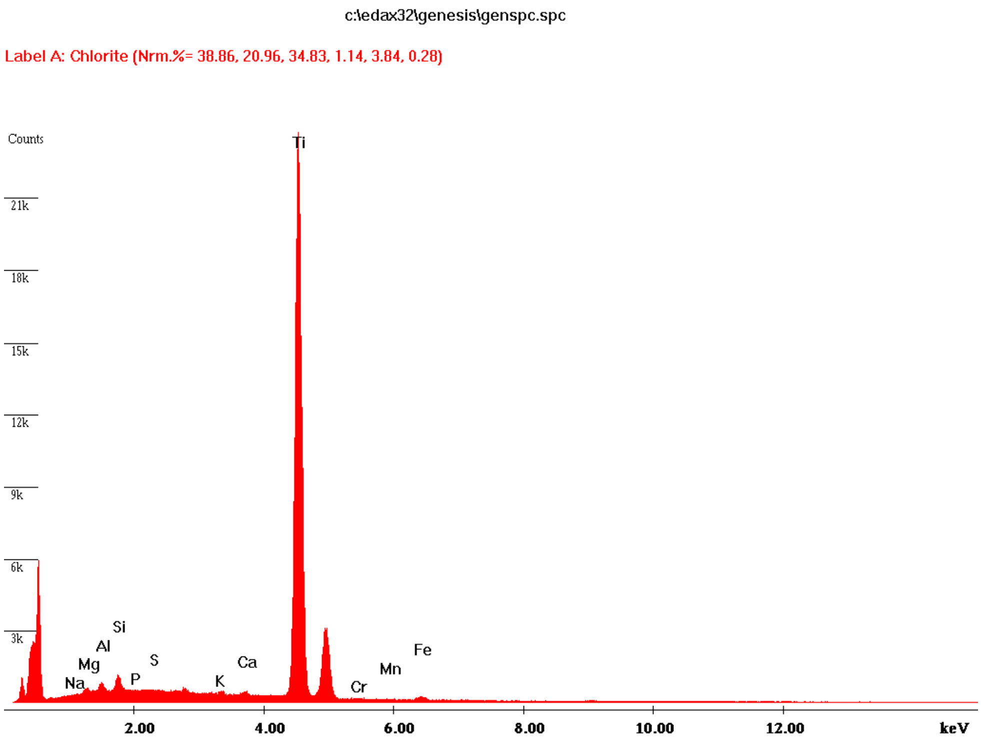

Pyrite

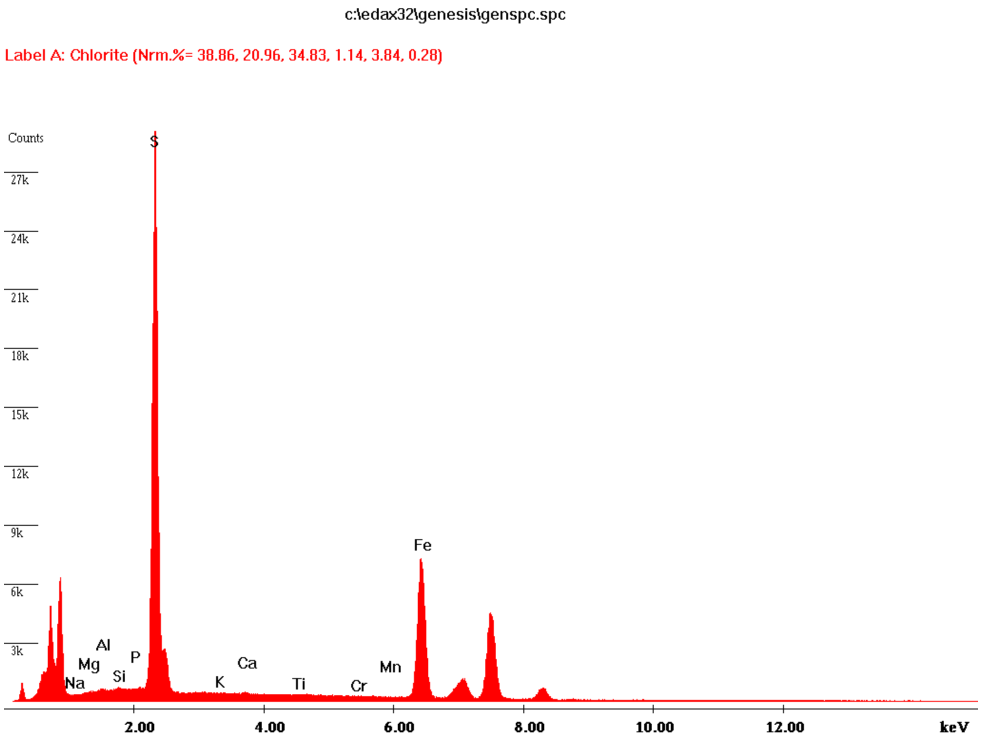

ACKNOWLEDGEMENTS

Primarily, I thank Bernhard Grasemann very sincerely for giving me the opportunity to work on this project and for his careful supervision. I am very glad that the topic and the wide-ranging methodologies of this thesis allowed me to gain a much better understanding of structural geology. I thank him for all his very helpful suggestions, explanations, discussions and his enormous patience - again.

Many thanks for support go to:

- Christoph Iglseder for helping me during the first days in the field.
- Andras Zamolyi for his patience with introducing me to GIS-applications and for spending hours creating rose-plots!
- Helga Zeitlhofer for assistance in thin-section analysis.
- Mrs. Hrabe, Mrs. Beybel and Mr. Slavek for producing very good thin-sections.
- Hugh Rice and Gerlinde Habler for help at the SEM.
- Dieter Mader for help with using the CL-microscope.

The biggest hug goes to Hugh Rice for making my thesis readable and for answering very stupid questions that I never would dare to ask Bernhard!

Great thanks go to all of my colleges – I'm not able to name all of them – for spending a wonderful time together during my studies!

Very special thanks go to my family for supporting me during my studies as well as to "Family Engler" who encouraged me to study at a university.

Finally, the warmest thanks go to my very closest friends Astrid Lengauer and Susanne Lukeneder who accompanied me during my studies – what would I do without you?

Thank you all very much!

Lebenslauf

Persönliche Daten

Name	Monika Rockenschaub
Anschrift	Pelzgasse 19/17 1150 Wien
Geburtsdatum	17. 06. 1981
Familienstand	ledig
Staatsangehörigkeit	Österreich

Ausbildung

2000	**Matura**, HBLA Freistadt (OÖ)
2000 – 2001	**Studium Völkerkunde** und **Französisch**, Universität Wien
Ab 2001	**Studium Erdwissenschaften** mit **Schwerpunkt Geologie**, Universität Wien **Bakk. rer. nat**. abgeschlossen Jänner 2010; Titel der Bakkalaureatsarbeit: *3D-Modellierung eines Erzganges im Arzberg (Steiermark)* Voraussichtlicher Abschluss des **Masterstudiums**: September 2011 Titel der Masterarbeit*: A brittle-ductile high- and low-angle fault system related to the Kea extensional detachment*

Berufserfahrung

Wissenschaftliche Projektmitarbeit	**Department für Geodynamik und Sedimentologie** Universität Wien	November 2008 – Februar 2009, geringfügig **Projekt: „Ägäische Kernkomplexe“** Aufbereitung von Gesteinsproben und Mineralseparation für Ar-Ar-Altersdatierung (Muskovit) Oktober 2009, freie Mitarbeit **OMV F&E Project FA536004 „Gosau Inventory“,** Kartendigitalisierung November 2010 – Juli 2011, geringfügig **Projekt: „Yemen Microtectonics“** Aufbereitung von Gesteinsproben und Mineralseparation für

		Rb-Sr- und U-Pb-Altersdatierung (Biotit, Zirkone)
Wissenschaftliche Projektmitarbeit	**Department für Anthropologie** Universität Wien	März 2009 – Oktober 2010, geringfügig **Projekt: „Early Australopithecine"** Aufbereitung von Gesteinsproben und Mineralseparation für Ar-Ar-Altersdatierung (u. a. Feldspäte, Gläser)
	Department für Paläontologie Universität Wien	2007 – 2009, freie Mitarbeit **Projekt: Lokale Diversität und Raubdruck: Eozän bis rezent** Separation und Archivierung von Molluskenproben
	Geologisch-Paläontologische Abteilung Naturhistorisches Museum Wien	Jänner bis März 2011, freie Mitarbeit **FWF-Projekt „Karnische Krise"** Aussuchen von Schlemmproben nach triassischen Mikrofossilien (Conodonten, Foraminiferen etc.)
	Joanneum Research Leoben	Juli 2010, freie Mitarbeit **Projekt der Wiender Linien: U1-Verlängerung,** Seichtseismik Rothneusiedl (Wien),
Tutorien	**Department für Geodynamik und Sedimentologie** Universität Wien	Sommersemester 2009 **Kartenkunde und Profilerstellen** Wintersemester 2010 **Geologische Kartierung im Bergbau** Sommersemester 2010 **Strukturgeologische Geländeübungen**

Weitere Qualifikationen

Sprachen

- Deutsch (Muttersprache)
- Englisch (fließend)
- Französisch (Grundkenntnisse)

Software

Sicherer Umgang:

- MS Office
- Corel Draw
- ArcGIS
- GoCAD

Grundkenntnisse:

- MatLab
- PhreeqC

Wien, 14.07.2011